University of Groningen

MRI of the kidney.

Strake, Lambertus te

IMPORTANT NOTE: You are advised to consult the publisher's version (publisher's PDF) if you wish to cite from it. Please check the document version below.

Document Version
Publisher's PDF, also known as Version of record

Publication date:
1987

Link to publication in University of Groningen/UMCG research database

Citation for published version (APA):
Strake, L. T. (1987). *MRI of the kidney.* [s.n.].

Copyright
Other than for strictly personal use, it is not permitted to download or to forward/distribute the text or part of it without the consent of the author(s) and/or copyright holder(s), unless the work is under an open content license (like Creative Commons).

The publication may also be distributed here under the terms of Article 25fa of the Dutch Copyright Act, indicated by the “Taverne” license. More information can be found on the University of Groningen website: https://www.rug.nl/library/open-access/self-archiving-pure/taverne-amendment.

Take-down policy
If you believe that this document breaches copyright please contact us providing details, and we will remove access to the work immediately and investigate your claim.

Downloaded from the University of Groningen/UMCG research database (Pure): http://www.rug.nl/research/portal. For technical reasons the number of authors shown on this cover page is limited to 10 maximum.

Download date: 04-06-2022

MRI

OF THE KIDNEY

L. TE STRAKE

MAGNETIC RESONANCE IMAGING
-MRI-
OF THE KIDNEY

Stellingen

behorende bij het proefschrift 'MRI of the Kidney', L. te Strake

1. Het vaststellen van de MRI opnametechniek zal altijd een compromis zijn tussen het bereiken van het gewenste contrast tussen weefsels, de beeldkwaliteit zoals het cosmetisch aspect van de opnamen (signaal-ruis verhouding en ruimtelijk oplossend vermogen) en de onderzoekstijd (dit proefschrift).

2. Nieuwe 'fast imaging' technieken geven een verbetering van de beeldkwaliteit van MRI niet alleen door verkorting van de opname tijd maar ook door een beter contrast oplossend vermogen (dit proefschrift).

3. MRI biedt bij een veldsterkte van 0.5 T en toepassing van conventionele spin echo puls sequenties weinig voordelen boven bestaande, goedkopere methoden bij de diagnostiek van nierafwijkingen (dit proefschrift).

4. Het gebruik van combinatieversterkingsschermen bij mammografie moet op grond van absorptie in het primaire scherm afgeraden worden.

5. Endo-ultrasonografie (EUS) is een belangrijke aanwinst voor de diagnostiek en stagering van maligniteiten van distale oesophagus, maag en pancreas.

6. Bij een onverklaarde mono-arthritis van een vinger of polsgewricht dient het osteoid osteoom uitgesloten te worden.

7. Isotopen cisternografie is het onderzoek van keuze voor de diagnostiek van nasale liquorroe.
   (Flynn B.M. et al. Med J Aust 1987;146:82-84)

8. Het gebruik van condooms bij safe sex schakelt het risico van AIDS besmetting niet uit.
   (Goedert J.J. N Engl J Med 1987; 317: 1339-1341).

9. Een kaakgewrichtsafwijking komt voort uit een afwijkende belangstelling voor het kaakgewricht.

10. De endoscopie van de tractus digestivus dient, als onderdeel van medical imaging en complementaire techniek aan het conventionele röntgenonderzoek, aan het takenpakket van de radiodiagnost te worden toegevoegd.

11. Juist doceren is veelal een kwestie van juist doseren.

12. Al is de NMR nog zo snel, de waarheid achterhaalt hem wel.

RIJKSUNIVERSITEIT GRONINGEN

MRI OF THE KIDNEY

Proefschrift

ter verkrijging van het doctoraat
in de Geneeskunde
aan de Rijksuniversiteit Groningen
op gezag van de Rector Magnificus Dr. E. Bleumink
in het openbaar te verdedigen op woensdag 30 september 1987
des namiddags te 2.45 uur precies
door

LAMBERTUS TE STRAKE

geboren te Melbourne (AUS)

1987
DRUKKERIJ VAN DENDEREN B.V.
GRONINGEN

Eerste promotor: Prof.Dr. J.R. Blickman
Tweede promotor: Prof.Dr. G.K. van der Hem
Derde promotor: Prof.Dr. A.E. van Voorthuisen

μηδεν αγαν

Aan

Rose-Marie
Stijn, Titus, Jesse

VOORWOORD

De evaluatie van een nieuwe techniek zoals MRI, vanaf het moment dat deze de klinicus als premature boreling in de schoot geworpen wordt tot op het moment dat de techniek als adolescent zelfstandig rondstapt in het ziekenhuis, is niet mogelijk zonder de actieve steun van meerdere geïnteresseerden. Dit geldt temeer voor het onderhavige onderzoek, dat op 4 verschillende locaties (Academische Ziekenhuizen van Groningen, Leiden en Amsterdam (VU); Philips MSD, Best) uitgevoerd werd.

Prof. Dr. J.R. Blickman. Zeer geachte promotor.
U was mijn opleider in de radiodiagnostiek. In die jaren en daarna was U de kapitein op het schip die met wijsheid een duidelijke, veelal rechtlijnige koers uitzette en voor zijn bemanning voldoende ruimte bood om, waar nodig, binnen het vakgebied te passagieren. Daarnaast hebt U zich zowel ten tijde van de geboorte van MRI als in de laatste fase van het promotieonderzoek een bekwaam verloskundige getoond, waarmede het proefschrift op een spontane en weinig traumatiserende wijze het levenslicht heeft kunnen aanschouwen. Ik dank U voor dit alles.
Prof.Dr. G.K. van der Hem. Zeer geachte tweede promotor.
U stond mede aan de wieg van dit onderzoek en was van oordeel dat het gerechtvaardigd was de Groningse neonaat voor verdere evaluatie over te plaatsen naar het AZL. Uw loyale steun en belangstelling gedurende het onderzoek en het tot stand komen van het proefschrift heb ik ten zeerste gewaardeerd.
Prof.Dr. A.E. van Voorthuisen. Zeer geachte derde promotor.
Uw afdeling heeft het Groninger stiefkind liefdevol opgenomen en in den beginne gefungeerd als peuterspeelzaal. Later heeft het onderzoek met de verbeterde MR technologie kunnen gedijen dankzij de bijzondere, binnen de afdeling aanwezige, wetenschappelijke ambiance. Voor de geboden faciliteiten voor het onderzoek, het hierin gestelde vertrouwen en de adviezen ben ik U zeer erkentelijk.
Het is onmogelijk de vele personen, die op enigerlei wijze en tijdstip hun medewerking aan het onderzoek hebben verleend persoonlijk in dit voorwoord te bedanken. De volgende afdelingen en personen wil ik echter met name vermelden onder dankzegging voor de geïnvesteerde tijd, de inzet en het geduld en met de verzekering dat de geleverde inspanningen voor mij een leerzame bron van inspiratie zijn geweest.

AZG	- Afd. Nephrologie	: A.M. Tegzess en collegae.
	Afd. Urologie	: Dr. J.A.P. Hooykaas en collegae.
RUG	- Path. Anat. Laboratorium	: Dr. S. Poppema en collegae.
	Afd. Physische Chemie	: Dr. R.L. Kamman.
AZL	- Afd. Nephrologie	: Dr. L.C. Paul, S. Lobatto en collegae.
	Afd. Urologie	: J. Langeveld, Prof.Dr. U. Jonas en collegae.
	Afd. Radiodiagnostiek	: L.J. Schultze Kool, Dr. J. Doornbos, J.L. Bloem, T.H.M. Falke, R.D. Bluemm en collegae. Laboranten MRI Afdeling
	Afd. Medische Statistiek	: Dr. J. Hermans.
	Path. Anat.Laboratorium	: Dr. J.J. Weening, Prof.Dr. D.J. Ruiter.
AZVU	- Afd. Nephrologie	: Dr. L.P. Oe, Prof.Dr. A.J. Donker, H. van Bronswijk.
	Afd. Radiodiagnostiek	: Prof.Dr. J. Valk, M. Sperber.
Philips MSD	- Afd. Applicatie	: A.A. Brouwer- van Herwijnen en collegae.

Prof.Dr. A.J. Donker, Prof.Dr. C.J.P. Thijn, Prof.Dr. J. Valk, U ben ik dank verschuldigd voor de wijze waarop U als leden van de promotiecommissie hebt willen fungeren.
De collegae van de afdeling Radiodiagnostiek AZG dank ik voor de geboden gelegenheid om het promotieonderzoek vanuit Groningen af te ronden.
Zonder de onnavolgbare wijze waarop Mevr. G. Weltevrede het manuscript heeft weten te hanteren, zou dit proefschrift zeker niet binnen de gestelde termijn gereed zijn geweest. De Heren C. Minnis en H. van der Zwaag ben ik dank verschuldigd voor het bewerken van het fotografisch materiaal en laatstgenoemde bovendien voor het verzorgen van de omslag en deel van de lay out.
Het verschijnen van dit proefschrift is mede mogelijk geworden door de financiële steun van BYK Nederland, Cablon Medical, CGR Nederland, G. E. Medical Systems, Nycomed, Schering Nederland en Agfa Gevaert.

Contents

Chapter 1

INTRODUCTION

1.1 Historical Perspective

A very concise description of the principle of Nuclear Magnetic Resonance (NMR) was first given in 1946 by Bloch et al (1). Even today it applies to NMR in medical practice: 'By superimposing on the constant field (z direction) an oscillating magnetic field in the x direction, the polarization, originally parallel to the constant field, will be forced to precess about that field with a latitude which decreases as the frequency of the oscillating field approaches the Larmor frequency. For frequencies near this magnetic resonance frequency one can, therefore, expect an oscillating induced voltage in a pick-up coil with axis parallel to the y direction'.

Independently and only a few weeks earlier Purcell et al. reported on resonance absorption by nuclear magnetic movements in paraffin (2). Bloch and Purcell were awarded the Nobelprize in 1952.

Many terms now familiar to anyone working in the medical field of NMR were defined and used during the initial period of basic NMR research.

Paramagnetic properties of certain substances were mentioned by Bloch et al. in their very first paper (1). Now, the use of paramagnetic contrast agents in Magnetic Resonance Imaging (MRI) is widely explored and accepted. T1 and T2 relaxation times were studied and defined by Bloch in 1946 (3). The properties and underlying principles of spin echo signals were discussed by Hahn in 1950 (4). The MR studies presented in this thesis were performed using mainly spin echo pulse sequences. Currently chemical shift imaging is a relatively new technique in MRI. The dependence of the nuclear magnetic resonance frequency upon chemical compound is known since 1949 (5,6). Despite the fact that the prerequisites for medical applications of NMR spectroscopy were present during the initial stages of its development, it was not until more than 2 decades later that Damadian first reported in 1971 on NMR properties of human tissues (7). He mentioned that spin echo NMR measurements may be used as a method to discriminate between malignant tumors and normal tissues, based on the differences in T1 and T2 relaxation times.

The first NMR studies in vivo, without any obvious harm to the live animal, were reported by Weisman et al. in 1972 (8). A malignant transplanted melanoma located on the mouse tail showed a spin-lattice (T1) relaxation time of

700 msec as opposed to the shorter T1 (300 msec) of normal tail tissue. In 1973 Lauterbur described a method of image formation ('zeugmatography') by induced local interactions employing NMR (9). In the following years the ability of NMR to differentiate between normal and malignant tumors was further studied as well as the factors influencing the differences in T1 and T2 between benign and malignant tissues. Kiricuta et al. (1975) observed that the main cause of these differences in T1 and T2 was a higher water content of neoplasms (10). T1 proved to be more sensitive than T2 to variations of tissue water content. At the same time he concluded that if only water content would be the principal cause, NMR would be much less promising for the detection of cancerous tissue than was originally thought.

Eggleston et al. (1975) furthermore stressed the nonspecific nature of prolongation of T1 in abnormal tissue (11). He found that T1 of abnormal non neoplastic tissue was in many instances longer than T1 of malignant tumors. Variable components of malignant tumors, e.g. vascularisation, amount of supporting stroma, number of accompanying inflammatory cells, hemorrhage and necrosis were considered to be important factors causing the lack of specificity of T1 measurements for cancer diagnosis. Bovée et al. (1978) also found, contrary to previously published reports, an overlap of T1 values measured in malignant, benign and normal breast tissues corrected for fat (12).

The first more detailed images obtained with NMR were presented in 1977. Images of a finger were recorded by Mansfield et al. using a two cm small bore magnet system (13). A thin-section image of the human wrist by Hinshaw et al. allowed a clear differentiation between fat, bone marrow, cortical bone, tendons and the motion of blood in the veins and arteries (14). Similar imaging experiments were carried out with normal rats and rabbits (15,16). Bottomley in 1979 demonstrated the detection and development of a hepatoma in a live rat (17).

Discrimination of the tumor from surrounding tissue was possible by the differences in signal intensity. Hansen et al. in 1980 showed that selective contrast enhancement for tissue discrimination was possible by manipulating data acquisition parameters rather than by injection of contrast agents (18). Important advantages of MRI over CT were reported by Cooks et al.: no ionizing radiation, imaging along any plane in the subject, no artefacts introduced by bone and air, superior soft tissue contrast and ability to perform flow studies without the need for contrast agents (19).

The first human whole-body MR images, showing the normal anatomy of the major blood vessels and organs, were published in early 1981 (20,21). Vizualization of the renal collecting system in the normal abdomen was reported later in 1981 (22). Pathological conditions in the human body were first demonstrated by means of NMR tomography in the brain in 1980 (23). One year later

in 1981 reports appeared in the literature on MRI in liver and kidney disease (24,25). Smith et al. showed that the differentiation between a renal cyst and tumor was possible as a result of the sensitivity of MRI for discriminating between different tissues by measuring the T1 relaxation time. Further studies by Smith et al. in 1982 in 30 patients with various renal diseases indicated the possible applications of MRI not only in the diagnosis of kidney tumors but also in the diagnosis of parenchymal disease and in renal transplants (26). It appeared that MRI was as accurate as ultrasound in the differentiation of renal cysts from tumors and that it would be superior to ultrasound and intravenous urography (IVU) in the management of patients with either acute reversible kidney failure or acute allograft rejection.

Inversion-recovery images of the kidney obtained by Young et al. in 1982 showed excellent intrarenal detail, allowing the distinction between cortex and medulla (27). Crooks et al. in 1982 also demonstrated the cortico-medullary junction and hilar structures in the normal kidney using spin echo technique (28). At this stage our interest in the application of MRI in the diagnosis of kidney disease was raised and a pilot study using a prototype resistive MR scanner (0.15 T) was started in late 1982.

The results of this pilot study were promising and appeared to justify further research in a clinical setting (29,30). These conclusions were supported by further reports in the literature during 1983 (31,32,33).

I.2 Purpose of the study

The objective of the study was to determine the value of MRI in 1. the diagnosis of diffuse parenchymal renal disease, 2. the diagnosis and staging of kidney tumors and 3. the evaluation of transplanted kidneys. In order to attain this goal three protocols were started in October 1984 and carried out until February 1986 at the University Hospital Leiden in cooperation with the Departments of Radiology and Nephrology, Free University Hospital Amsterdam (protocol on diffuse renal disease), and the Department of Nephrology, University Hospital Groningen (protocol on kidney transplantation).

I.3 References

1. Bloch F, Hansen WW, Packard M. Nuclear induction. Phys Rev 1946; 69:127.
2. Purcell EM, Torrey HC, Pound RV. Resonance absorption by nuclear magnetic moments in a solid. Phys Rev 1946; 69: 37-38.
3. Bloch F. Nuclear Induction. Phys Rev 1946; 70: 460-474.
4. Hahn EL. Spin echoes. Phys Rev 1950; 80: 580-594.
5. Knight WD. Nuclear magnetic resonance shift in metals. Phys Rev 1949; 76: 1259-1260.

6. Proctor WG. Yu FC. The dependence of a nuclear magnetic resonance frequency upon chemical compound. Phys Rev 1950; 77: 717.
7. Damadian R. Tumor detection by nuclear magnetic resonance. Science 1971; 171: 1151-1153.
8. Weisman ID, Bennett LH. Recognition of cancer in vivo by nuclear magnetic resonance. Science 1972; 178: 1288-1290.
9. Lauterbur PC. Image formation by induced local interactions: examples employing nuclear magnetic resonance. Nature 1973; 242: 190-191.
10. Kiricuta Jr. I, Simplaceanu V. Tissue water content and nuclear magnetic resonance in normal and tumor tissues. Cancer Research 1975; 35: 1164-1167.
11. Eggleston JC. Saryan LA, Hollis DP. Nuclear Magnetic Resonance investigations of human neoplastic and abnormal nonneoplastic tissues. Cancer Research 1975; 35: 1326-1332.
12. Bovée WMMJ, Getreuer KW, Smidt J, Lindeman J. Nuclear magnetic resonance and detection of human breast tumors. J. Natl. Cancer Inst 1978; 61: 53-55.
13. Mansfield P, Maudsley AA. Medical imaging by NMR. Br J Radiol 1977; 50: 188-194.
14. Hinshaw WS, Bottomley PA, Holland GN. Radiographic thin-section image of the human wrist by nuclear magnetic resonance. Nature 1977; 270: 722-723.
15. Crooks LE, Grover TP, Kaufman L, Singer JR. Tomographic imaging with nuclear magnetic resonance. Invest Radiol 1978; 13: 63-66.
16. Hinshaw WS, Andrew ER, Bottomley PA, Holland GN, Moore WS. Display of cross sectional anatomy by nuclear magnetic resonance imaging. Br J Radiol 1978; 51: 273-280.
17. Bottomley PA. In vivo tumor discrimination in a rat by proton nuclear magnetic resonance imaging. Cancer Research 1979; 39: 468-470.
18. Hansen G, Crooks L, Davis P, De Groot J, Herfkens R, Margulis AR, Gooding C, Kaufman L, Hoenninger J, Arawaka M, McRee R, Watts J. In vivo imaging of the rat anatomy with nuclear magnetic resonance. Radiology 1980; 136: 695-700.
19. Crooks L, Hoenniger J, Arawaka M, Kaufman L, McRee R, Watts J, Singer JH. Tomography of hydrogen with nuclear magnetic resonance. Radiology 1980; 136: 701-706.
20. Edelstein WA, Hutchison JMS, Smith FW, Mallard J, Johnson G, Redpath TW. Human whole-body NMR tomographic imaging: normal sections.Br J Radiol 1981; 54: 149-151.
21. Bangert V, Mansfield P. Whole-body tomographic imaging by NMR. Br J Radiol 1981; 54: 152-154.
22. Hawkes RC, Holland GN, Moore WS, Roebuck EJ, Worthington BS. Nuclear magnetic resonance (NMR) tomography of the normal abdomen. J Comput Assist Tomogr 1981; 5: 613-618.
23. Hawkes RC, Holland GN, Moore WS, Worthington BS. Nuclear magnetic resonance (NMR) tomography of the brain: a preliminary clinical assessment with demonstration of pathology. J Comput Assist Tomogr 1980; 4: 577-586.
24. Smith FW, Mallard JR, Reid A, Hutchison JMS. Nuclear magnetic resonance tomographic imaging in liver disease. Lancet 1981; i: 963-966.
25. Smith FW, Hutchison JM, Mallard JR, Reid A, Johnson G, Redpath TW, Selbic RD. Renal cyst or tumour? Differentiation by whole-body nuclear magnetic resonance imaging. Diagn Imag 1981; 50: 61-65.
26. Smith FW, Reid A. Mallard JR. Hutchison JM, Power DA, Catto GR. Nuclear magnetic resonance tomographic imaging in renal disease. Diagn Imag 1982; 51: 209-213.
27. Young IR, Bailes DR, Burl M, Collins AG, Smith DT, McDonnell MJ, Orr JS, Banks LM, Bydder GM, Greenspan RH, Steiner RE. Initial clinical evaluation of a whole-body nuclear magnetic resonance (NMR) tomograph. J Comput Assist Tomogr 1982; 6: 1-18.

28. Crooks L, Arawaka M, Hoenninger J, Watts J, McRee R, Kaufman L, Davis PL, Margulis AR, De Groot J. Nuclear magnetic resonance whole-body imager operating at 3,5 K Gauss. Radiology 1982; 143: 169-174.
29. te Strake L, Blickman JR, van der Hem GK, Hooykaas JA, Poppema S, Brouwer-van Herwijnen AA. Imagerie RMN du rein. J Radiol 1984; 65: 631-635.
30. te Strake L, van der Hem GK, Hooykaas JA, Poppema S, Brouwer-van Herwijnen AA. Nuclear magnetic resonance imaging of the kidney. Diagn Imag Clin Med 1984; 53: 198-202.
31. Hricak H, Crooks L, Sheldon P, Kaufman L. Nuclear magnetic resonance imaging of the kidney. Radiology 1983; 146: 425-432.
32. Hricak H, Williams RD, Moon KL, Moss AA, Alpers C, Crooks LE, Kaufman L. Nuclear magnetic resonance imaging of the kidney: renal masses. Radiology 1983; 147: 765-772.
33. Kressel HY, Axel L, Thickman D, Alavi A, Pollack H, Arger P, Edelstein W, Bottomley P, Redington R, Baum S. NMR imaging of the abdomen at 0.12 T: initial clinical experience with a resistive magnet. AJR 1983; 141: 1179-1186.

Chapter II

IMAGERIE RMN DU REIN

L. te Strake[1], J.R. Blickman[1], G.K. van der Hem[2], J.A.P. Hooykaas[3], S. Poppema[4], A.A. Brouwer-van Herwijnen[5].

Departments of Radiology[1], Nephrology[2], Urology[3], and Pathology[4], University Hospital Groningen, The Netherlands.
Philips Medical Systems Division[5], Best, The Netherlands.

II.1 Résumé

Une imagerie a été obtenue chez 18 malades présentant différentes affections rénales. On a utilisé deux scanners, un système prototype résistif de 0.14T et le Gyroscan S5 superconducteur. L'imagerie RMN s'est avérée être une technique très sensible.
On peut détecter des tumeurs ne dépassant pas 5-10 mm, et on peut faire la distinction entre tumeurs solides et kystes.
Grâce à une excellente résolution des contrastes et à la différenciation des tissus, l'imagerie RMN semble être très précise pour établir le stade d'un cancer rénal. Les vaisseaux au sein de la tumeur peuvent se voir sous forme de petites taches noires.
Du fait de leur bref T1, les kystes hémorragiques peuvent être différenciés de simple kystes. D'autres études prospectives de surveillance seront nécessaires pour se prononcer définitivement sur l'intérêt de l'imagerie RMN dans les affections diffuses du parenchyme rénal. On n'a pas trouvé de calcifications. Il ne semble pas que l'imagerie RMN soit plus spécifique pour la caractérisation des tissus que d'autres modalités d'imagerie.

II.1 Summary

NMR imaging was performed in 18 patients suffering from various renal disorders. 2 scanners were used, a 0.14 T resistive prototype system and the superconducting Gyroscan S5. NMR imaging proved to be a very sensitive technique.

J Radiol 1984; 65: 631-635
(with permission of Masson SA, Paris)

Tumours as small as 5-10 mm were detected. Solid tumours and cysts could be distinguished. As a result of the excellent contrast resolution and tissue differentiation, NMR imaging appears to be very accurate in the staging of renal cell carcinoma.
Blood vessels within a tumour may be visible as little black dots.
Because of their T1 hemorrhagic cysts can be differentiated from simple cysts. Further prospective follow-up studies are required before a definite statement can be made as to the value of NMR imaging in diffuse parenchymal disease. Calcifications were not detected. NMR imaging does not seem to be any more specific as to tissue characterisation than other imaging modalities.

II.2 Introduction

Bien que l'essentiel des traveaux réalisés jusqu'à présent en imagerie RMN médicale se soient focalisés sur le cerveau (3,4,12), il est devenu évident que cette technique pouvait être en même temps appliquée pour l'examen du thorax et de l'abdomen (1). Gr*ace à leur caractéristique T1 (11), on peut faire le diagnostic différentiel entre cancer du rein et kyste.

L'imagerie RMN des voies urinaires est apparue être une technique prometteuse (9). Devant la rareté des données de la littérature, on a mis en oeuvre un essai visant à étudier l'intérêt de l'imagerie RMN du rein. Dans ce travail, l'imagerie RMN sera désignée par l'abréviation IRM (Imagerie par Résonnance Magnétique) (8).

II.3 Matériel d'Étude et Méthodologie

L'imagerie par résonnance magnétique a été pratiquée avec deux scanners et, au début, on a utilis ún scanner prototype résistif 0.14T. On trouvera ailleurs la description de cet appareil. Au début de l'été 1983, on a pu disposer du Gyroscan S5 0.5T superconducteur en clinique. On a appliqué des séquences pulsées 'Spin Echo' (SE) et 'Inversion Recovery' (IR). Le TR poul l'imagerie SE a été de 500 msec, le TE de 50 msec (matrice 128 x 128) ou de 75 msec (matrice 256 x 256). Le TR en imagerie IR a été 1000 msec (scanner prototype) ou de 500 msec (Gyroscan S5) et le TD de 400 msec. On a obtenu des coupes distinctes dans les plans transverse et vertical.
L'épaisseur des coupes a été de 5, 10 ou 15 mm. Ultérieurement,
au cours de cette étude, on a disposé de données de volume entier 3-D.
L'examen a porté sur 18 malades présentant différentes affections
rénales (tableau I).

Tableau 1 Matériel d'étude: 18 malades
Table 1 Material: 18 patients

Tumeur	Cancer du rein	6
	Cancer du rein récidivant	1
	Angiomyolipome	1
	Adénome	1
Maladie polykystique		2
Maladie parenchymateuse diffuse		5
Reins transplantés		3

II.4 Résultats

C'est l'image IR qui, normalement, permet de mieux de distinguer cortex et médullaire (Fig. 1a). Du fait de son T1 plus long, la médullaire apparaît en noir. Le cortex qui contient moins d'eau a une densité supérieure du fait d'un T1 plus bref. On note très peu de détails à l'intérieur du rein sur l'image SE lorsqu'on utilise un TR long de 1000 msec (Fig. 1b). Mais, avec un TR plus bref (200 msec), on obtient plus d'information T1 sur l'image SE, et on peut ainsi distinguer dans une certaine mesure cortex et médullaire (Fig. 1c). La graisse périrénal et hilaire a une densité élevée. On peut identifier certaines structures du hile telles que le système collecteur et les vaisseaux.

Nos critères d'appréciation pour les tumeurs rénales, ont été la taille, la consistance, la vascularisation et l'extension locale. Il n'y a pas eu de difficulté à détecter des tumeurs kystiques ou solides mesurant 5-10 mm (Fig. 2).

Du fait de son long T1, un kyste simple a une faible densité et apparaît en noir. L'intensité d'un angiomyolipome est analogue à celle de la graisse périrénale. Dans notre groupe de patients, les cancers rénaux ont été d'une intensité relativement élevée sur l'image SE (Fig. 3a) et d'une faible densité, si l'on utilisait la séquence pulsée IR. Du fait d'un T1 long, les portions nécrotiques d'une tumeur ont une faible intensité sur l'image IR (Fig. 3c). En fonction des constituants et du TR, une nécrose est éventuellement invisible sur l'image SE ou se dessine sous la forme d'une zone de faible intensité.

Un courant sanguin rapide ne permet de recevoir que très peu de signaux. Les petites artères au sein d'une tumeur se distinguent ainsi visiblement sous forme de petites taches noires (Fig. 3a,b). L'IRM s'est avérée exacte dans tous les cas de cancer du rein, quant à l'extension périrénale de la tumeur.
Dans la maladie polykystique et multikystique du rein, l'intensité des kystes varie en fonction de leur contenu (Fig. 4a). La corrélation avec le fragment de

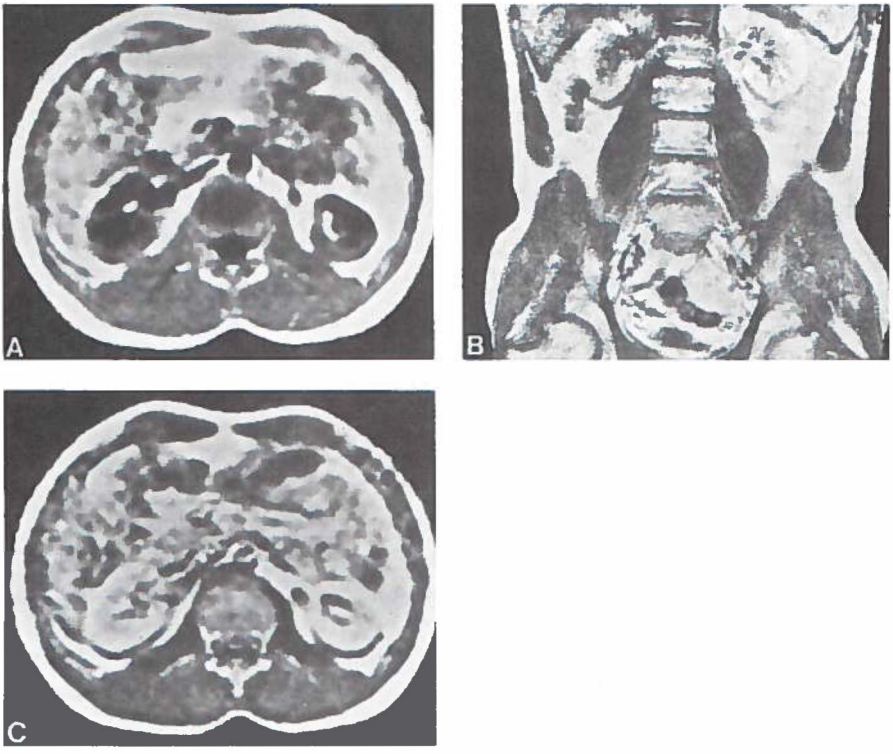

Fig. 1 a) IR 1000/400: Bonne différenciation de la médullaire en noir par rapport au cortex environnant.
b) SE 1000/50: Peu de dfails dans l'intérieur du rein en dehors des structures hilaires.
c) SE 500/50: Ligne de démarcation cortico-médullaire esquissée, noter les vaisseaux hilaires et le système collecteur.

Fig. 1 a) IR 1000/400: good differentiation of dark medulla from surrounding cortex.
b) SE 1000/50: except of hilar structures little intrarenal detail.
c) SE 500/50: some cortex-medulla demarcation. Note the hilar vessels and collecting system.

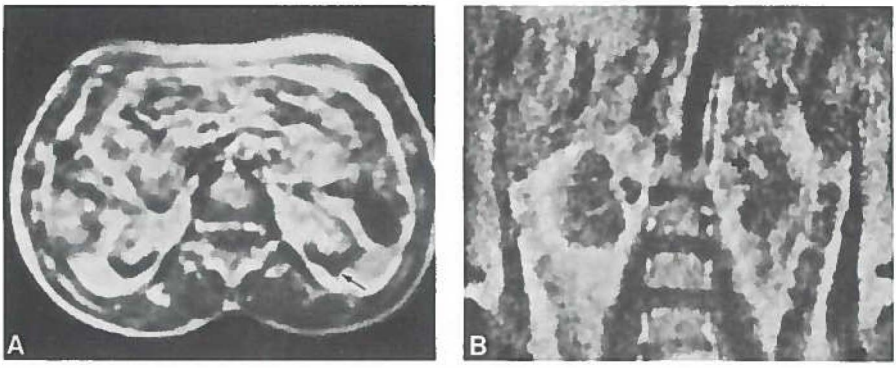

Fig. 2 a) SE 1000/50: Glomérulosclérose. Minceur du cortex de faible intensité. Petit kyste de faible intensité sur la face postérieure du rein gauche (flèche).
b) IR 1000/400: Angiomyolipome du pôle supérieure du rein gauche (flèche).

Fig. 2 a) SE 1000/50: glomerulosclerosis. Thin cortex of low intensity. Small cyst of low intensity on posterior aspect of left kidney (arrow).
b) IR 1000/400: angiomyolipoma in the upper pole left kidney (arrow).

néphrectomie obtenu dans un cas, a révélé qu'une valeur brève de T1 correspond à un liquide hémorragique (Fig. 4b).

Dans les affections parenchymateuses diffuses, le cortex est apparu avoir une intensité relativement faible, et on a noté la perte de la ligne de démarcation cortico-médullaire (Fig. 5). Un rejet aigu d'un rein transplanté fait disparaître également cette ligne de démarcation.

L'oedème de ces reins augmentés de volume entraîne une faible densité du parenchyme. En cas de rejet chronique, nous avons observé des plages d'altération de faible intensité, du fait d'un infarctus antérieur et de la fibrose et nécrose secondaires. Présentes dans un cas, des calcifications ont été détectées par tomodensitométrie informatisée, mais ne l'ont pas été par IRM. On a comparé les aspects des altérations bénignes et des altérations malignes du rein, mais on n'a pas pu mettre en évidence des caractéristiques nettes en faveur de la malignité.

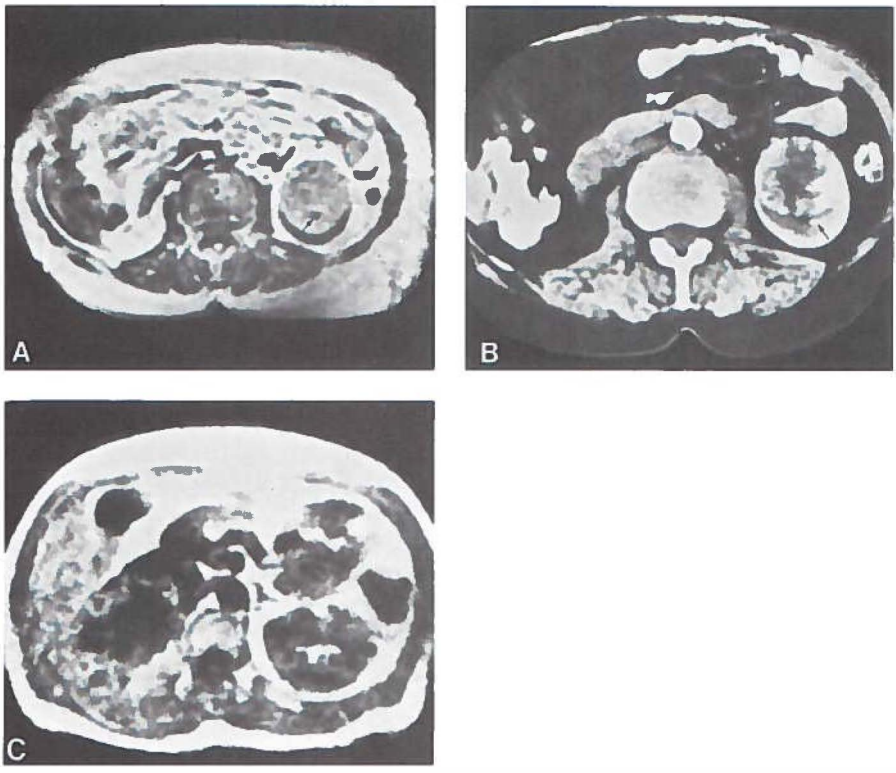

Fig. 3 a) SE 1000/50: Cancer du rein gauche, une petite artère vascularisant la tumeur se présente sous la forme d'une petite tache noire (flèche).
b) Tomodensitométrie informatisée dynamique à ce niveau. Noter la déviation vers le haut de la même artère intra-rénale.
c) IR 1000/400: Récidive de cancer rénal dans la fosse rénale droite. Remarquer la nécrose centrale noir.

Fig. 3 a) SE 1000/50: renal cell carcinoma left kidney. A small artery feeding the tumor is represented as a little black dot (arrow).
b) Dynamic X-ray CT scan at the corresponding level. Note the enhancement of the same intrarenal artery.
c) IR 1000/400: recurrent renal cell carcinoma right renal fossa. Note dark central necrosis.

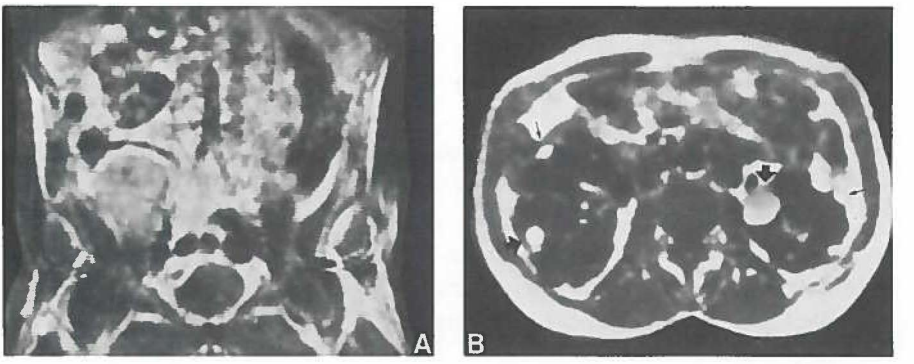

Fig. 4 a) SE 500/50: Reins multikystiques chez un malade en hémodialyse depuis 16 ans. Greffe rénale augmentée de volume dans la fosse hilaire gauche. Perte de la démarcation entre cortex et médullaire, du fait du rejet aigu.
b) IR 1000/400: Reins polydystiques de type adulte. Kystes hémorragiques bilatéraux multiples (flèches).

Fig. 4 a) SE 500/50: multicystic kidneys in a patient who has had hemodialysis for 16 years. Swollen transplant kidney in left iliac fossa. Loss of cortex-medulla differentiation due to acute rejection.
b) IR 1000/400: polycystic kidneys (adult-type), Multiple bilateral hemorrhagic cysts (arrows).

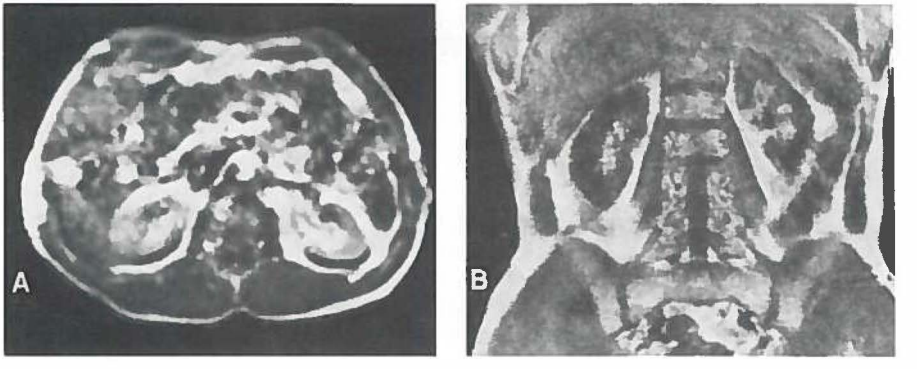

Fig. 5 Glomérulonéphrite membrano-proliférative.
a) SE 500/50: Reins de taille normale, aucun détail sur le parenchyme.
b) IR 1000/400: Disparition de la démarcation cortico-médullaire.

Fig. 5 Membranoproliferative glomerulonephritis.
a) SE 500/50: normal sized kidneys, no parenchymal detail.
b) IR 1000/400: loss of cortex-medulla differentiation.

II.5 Discussion

L'IRM présente plusieurs avantages sur les autres modalités d'imagerie. Il s'agit d'une méthode non sanglante et ne nécessitant pas le recours à des radiations ionisantes. La possibilité d'avoir une image anatomique dans le plan vertical est utile pour établir les relations anatomiques des différentes structures (7). Lorsque l'on compare IRM et tomodensitométrie informatisée, on se rend compte que la résolution des contrastes est supérieure. La tomodensitométrie informatisée ne peut donner qu'un paramètre, savoir l'absorption des rayons X. Avec l'IRM, en revanche, plusieurs paramètres concourent à la formation de l'image, la densité des protons, T1, T2 et le débit. Ainsi peut-on avoir une meilleure visualisation des parties molles (6).

Du fait de cette meilleure différenciation des tissus, l'IRM promet d'être une méthode très précise pour établir le stade des cancers du rein. Nos résultats concordent avec ce qui a été rapporté antérieurement (5,11), montrant que l'IRM est vraisemblablement un outil intéressant dans le diagnostic des affections parenchymateuses diffuses. Néanmoins, nous sommes d'avis qu'un plus grand nombre d'études prospectives suivies seront nécessaires avant de pouvoir se prononcer définitivement sur l'intérêt de l'IRM dans les affections parenchymateuses diffuses du rein.

L'inconvénient de l'IRM est qu'elle ne met pas en évidence les calcifications. Il semble, en outre, qu'elle ne soit pas plus spécifique pour la caractérisation des tissus que d'autres techniques d'imagerie.

Nous pouvons conclure, en résumé, que l'IRM est une exploration sensible dont l'intérêt, dans le diagnostic des affections rénales, demeure encore à préciser.

II.6 Bibliographie

1. Edelstein WA, Hutchison MS, Smith FW, Mallard J, Johnson G, Redpath TW. Human whole-body NMR tomographic imaging: normal sections. Br J Radiol 1981; 54: 149-151.
2. Go KG, van Dijk P, Luiten AL, Brouwer-van Herwijnen AA, van der Leeuw YCL, Kamman RL, Vencken LM, Wilmink J, Berendsen HJC. Interpretation of nuclear magnetic resonance tomograms of the brain. J Neurosurg 1983; 59: 574-584.
3. Hawkes RC, Holland GN, Moore WS, Worthington BS. Nuclear magnetic resonance (NMR) tomography of the brain: a preliminary clinical assessment with demonstration of pathology. J Comput Assist Tomograph 1980; 4: 577-586.
4. Holland GN, Hawkes RC, Moore WS. Nuclear magnetic resonance (NMR) tomography of the brain: coronal and sagittal sections. J Comput Assist Tomograph 1980; 4: 429-433.
5. Hricak H, Crooks L, Sheldon P, Kaufman L. Nuclear magnetic resonance imaging of the kidney. Radiology 1983; 146: 425-432.
6. James AE, Partain CL, Holland GN, Gore JC, Rollo FD, Hams SE, Price RR. Nuclear magnetic resonance imaging: The Current State. AJR 1981; 138: 201-210.

7. Kressel HY, Axel L, Glover G, Baum S. Coronal nuclear magnetic resonance (NMR) imaging of the abdomen at 0,5 Tesla. J Comput Assist Tomograph 1984; 8: 29-31.
8. Meaney TF. Magnetic resonance without nuclear. Radiology 1984; 150: 277.
9. Newhouse JH. Urinary Tract Imaging by Nuclear Magnetic Resonance. Urol Radiol 1982; 4: 171-175.
10. Steiner RE, Bydder GM. Nuclear magnetic resonance imaging of the abdomen. Diagn Imag Clin Med 1984; 53: 38-42.
11. Smith FW, Hutchison JMS, Mallard JR, Reid A, Johnson G, Redpath TW Selbie RD. Renal cyst or tumourdifferentiation of whole-body nuclear magnetic resonance imaging. Diagn Imaging 1981; 50: 61-65.
12. Young IR, Burl M, Clarke GJ, Hall AS, Pasmore T, Collins AG, Smith DT, Orr JS, Bydder GM, Doyle FH, Greenspan RH, Steiner RE. Magnetic resonance properties of hydrogen: Imaging the posterior fossa. AJR 1981; 137: 895-901.

Chapter III

TECHNICAL CONSIDERATIONS AND NORMAL ANATOMY

III.1 Introduction

The efficacy of any imaging technique depends on its ability to provide reliable qualitative and quantitative diagnostic information. Unlike X-ray CT, which displays the X-ray attenuation as the only tissue parameter, MR imaging is a much more complicated modality (1). A basic understanding of the information contained within an MR image and the way it is obtained, is necessary for a clear apprehension of the technique. In MRI image quality is largely determined by the signal intensity (SI) of individual tissues, the contrast between different tissues and the noise which negatively affects the overall image quality (2). Quantitative information allows the description of pathology in a more objective way. The ability to distinguish between benign and malignant tissues, the specificity, will greatly influence the impact on cancer diagnosis. A diagnostic test should be safe and without side-effects. In this chapter an attempt is made to discuss in a concise way the interactions between tissues, instrumental parameters and the diagnostic information obtained with MRI. The basic principles of NMR have been described extensively elsewhere and will not be discussed in detail (3,4,5,6,7).

III.2 Image quality

III.2.a *Signal intensity.*

Signal intensity (SI) is dependent on the nuclear spin density N [H], the spin-lattice relaxation time T1 and the spin-spin relaxation time T2 of the tissue (8). SI can be manipulated by changing the imaging technique, the pulse sequences used to acquire an image (1). The signal strength varies with the main static magnetic field and increases proportional to the square of the magnetic field strength (9).

III.2.b *Contrast.*

Since contrast between tissues is determined by differences in signal intensity, contrast accordingly depends on the intrinsic characteristics of tissues N

[H], T1 and T2, magnetic field strength and pulse sequences (10). T1 will be longer at higher magnetic field strength; T2 is relatively independent of the NMR frequency (11). An increase of the field strength will decrease T1 contrast while T2 contrast remains nearly constant (12). Display electronics, processing and noise will affect the observed contrast (13).

III.2.c *Signal-to-noise (S/N) ratio and contrast-to-noise (C/N)ratio.*

Noise is generated in the body as randomly fluctuating currents and is picked up by the receiver coil (14). The design of the radio-frequency (RF) coil and receiver chain furthermore determine the noise level. The image quality depends on the proportion of SI, contrast and noise, and can be expressed as the signal-to-noise (S/N) and contrast-to-noise (C/N) ratio. There are several options to improve the S/N ratio.

One way is to choose a high magnetic field strength (14,15,16). A second option is the use of surface coils (15). The receiving antenna is positioned closely to the area that is to be imaged. Thus, less noise from other parts of the body will be picked up by the receiver coil. Otherwise improvement of S/N ratio, using conventional Spin-Echo or Inversion-Recovery pulse sequences, will be at the expense of the total examination time or spatial resolution. In MRI, S/N ratio is proportional to the volume of the voxel (14). If spatial resolution is decreased by a factor 2, e.g. by choosing a matrix size of 128 x 128 instead of 256 x 256, the S/N ratio will be increased by a factor 4. A longer measurement time, that can be obtained by increasing the number of excitations or the repetition time (TR), will result in a higher signal strength and improved S/N ratio (14,16). The C/N ratio is determined by the signal received from different tissues, system noise and data acquisition time (17).

It has been stressed by several authors that C/N ratio not only depends on T1 and T2 relaxation times of tissues, but also to a large extent on differences in proton density (13,18). The MR imaging strategy will always be a compromise between the achievement of appropriate contrast between tissues, image quality such as the cosmetic appearance of the image (S/N ratio and spatial resolution), and examination time. At a given magnetic field strength the appropriate contrast should be achieved by optimizing the pulse sequences for the intrinsic characteristics, N [H], T1 and T2, of the tissues (10).

III.3 Pulse sequence optimalization

All examinations discussed in this thesis were performed with a 0.5 T superconducting MR scanner (Gyroscan S5, Philips). Initially in 1984 when the imaging protocols were set up, two pulse sequences were available: Inversion-Recovery (IR) and Spin Echo (SE). During 1985 a new pulse sequence, Fast Field

Echo (FFE), enabling fast imaging with an acquisition time of seconds was implemented (Chapter VII). IR imaging produces T1 contrast, the images may be referred to as T1 weighted images. The S/N ratio of IR is relatively low according to Hricak et al., resulting in a suboptimal overall resolution (19). Therefore, and because a T1 weighted SE sequence (TR = 400-900 msec) can be performed in a much shorter time than an IR sequence (TR=1400 msec), in this study only Spin Echo (SE) technique was used for imaging purposes. With SE, the TR will largely determine the T1 contrast (15). T2 contrast is obtained by increasing the echo time (TE). Generally a SE sequence with a short TR and TE will be T1 weighted, a long TR and TE will result in a T2 weighted image. The signal strength for SE is defined by the following equation (1,20): signal strength = K.N [H] exp (-TE/T2) 1 - 2 exp -(TR- TE/2)/T1 + exp (-TR/T1) (1). K is a specific constant for SE technique. The equation expresses the dependence of the signal intensity on the intrinsic tissue characteristics, N [H], T1 and T2, and the instrumental parameters TR and TE. Equation 1 can be used in several ways for pulse sequence optimization. As an example we will discuss the sequence, which optimizes the contrast between renal cortex and medulla.

The main difference between these tissues is the higher water content of the medulla as a result of the urine collected within the tubules and pyramids. The optimal pulse sequence will be a T1 weighted sequence since T1 is more sensitive to variations of tissue water than T2 (21). In order to obtain a T1 weighted image, TE should be chosen as short as possible, e.g. TE=30 msec. T1 and T2 measurements at 20 mHz on freshly excised human renal cortex and medulla yield the following results: T1(cortex)=540 msec, T1(medulla) =725msec, T2(cortex)=78 msec, T2(medulla)=86 msec; N [H] (cortex)=82 wt%, N [H] (medulla)=85 wt% (R.L. Kamman, unpublished data). By feeding the values of TE, T1, T2 and N [H] into equation 1, the signal intensity (SI) of cortex and medulla can be calculated for different values of TR (fig.1).

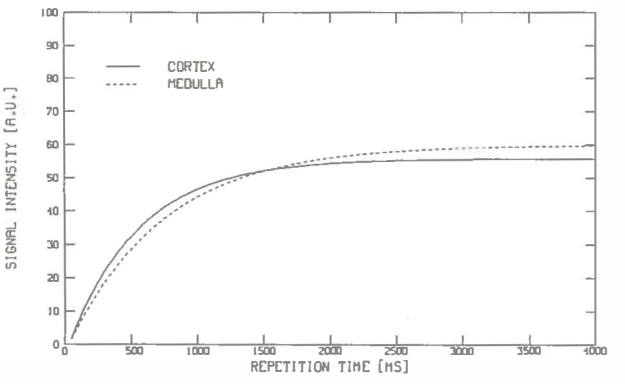

Fig. 1. Signal intensity of cortex and medulla plotted as a function of TR for TE = 30 msec.

From these curves it appears that the optimum TR to show maximum contrast between cortex and medulla ranges from 500-700 msec. Hendrick et al. have shown that the optimal TR for the highest S/N ratio for a single tissue can be calculated according to the following formula (22):
TR opt=1.27 T1 en 1.9 TE(min). These TR values (TR opt, cortex=742 msec; TR opt, medulla=977 msec) are slightly higher than the TR values calculated for optimal contrast between cortex and medulla.

In a similar way using equation 1 and a computer model, isosignal curves can be obtained as a function of T1 and T2 for a particular pulse sequence (1).

Alternatively isocontrast contour curves can be calculated as a function of TE and TR for different tissues (23,24). Advantages of these techniques are that at a glance one can choose the optimum pulse sequence for maximum contrast between tissues. In spite of all these theoretical considerations several authors have demonstrated that in clinical practice in most cases both T1 and T2 weighted pulse sequence are needed to show the full extent of disease(25, 26, 27). A nice demonstration of the need for both T1 and T2 contrast is a set of synthetic images calculated from images obtained in a patient with a renal cell carcinoma in the right kidney (Fig.2). Optimum contrast between the tumor and the high signal intensity of the perirenal fat is present on the short TR and TE T1 weighted image. The T2 weighted image with a long TR and TE shows the better differentiation between tumor and liver.

Synthetic images are generated by the computer via calculation from previously acquired calculated T1, T2 and proton density images (10, 24, 28). For this purpose, we used a combination of SE (TR=1000 msec, TE=50 msec, 4 echoes) and IR (TR=1400 msec, TE=50 msec, TI=400 msec) pulse sequence. After the patient examination contrast can be manipulated and optimized for certain tissues without actually rescanning the patient. Despite its interesting concept up to now synthetic imaging has not found general acceptance in clinical practice, since basically all the contrast needed for an accurate diagnosis can be obtained if merely a T1 and a T2 weighted pulse sequence are applied.

111.4 Normal anatomy

The excellent contrast resolution and multiplanar imaging capability of MRI enable both the display of the intrarenal anatomy and of the relationship between the kidneys and surrounding structures in an exquisite way (19, 29, 30). The kidneys are located in the retroperitoneal space and are surrounded by perirenal fat. Fat appears bright on both T1 and T2 weighted images because of its short T1 and long T2. Fat is a valuable reference tissue for MR studies and relatively uninfluenced by variations of age, sex or obesity (31). Only T2 was

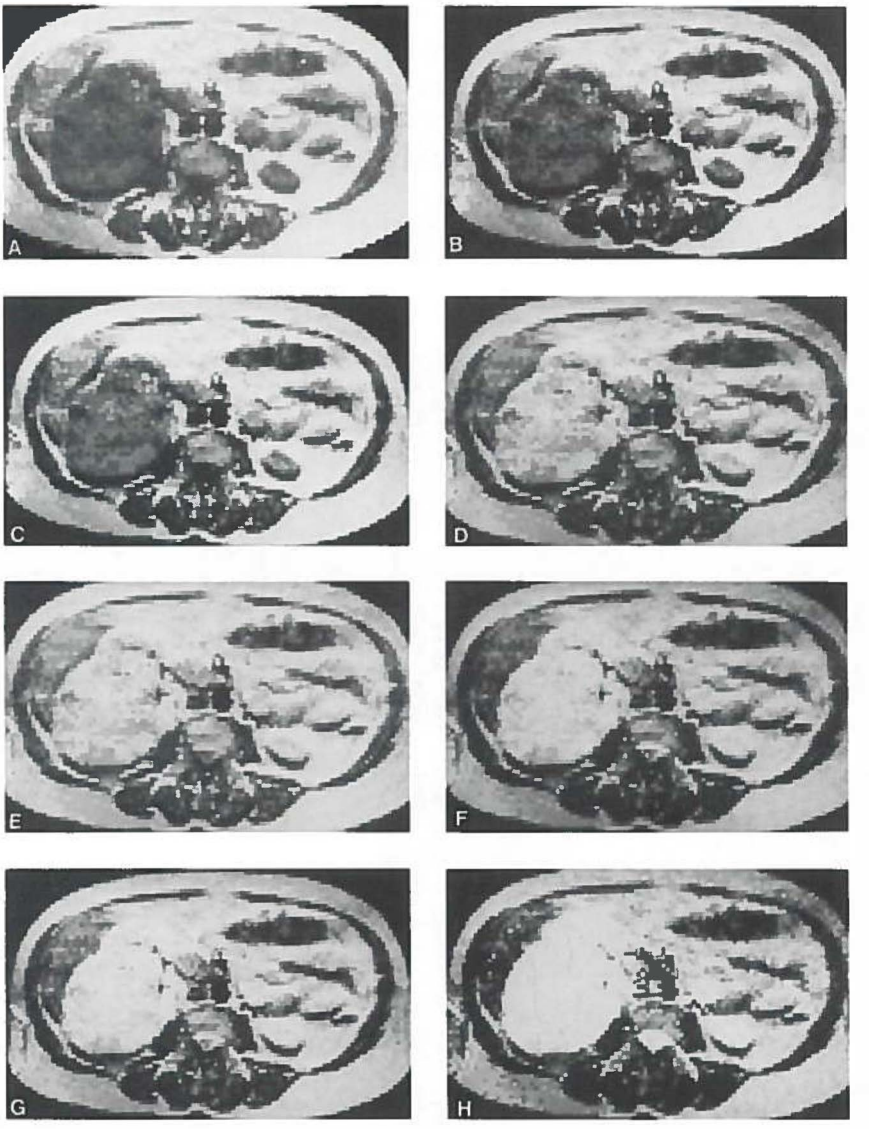

Fig. 2. Large renal cell carcinoma right kidney. Synthetic SE images.

a. TR=100 msec, TE=10 msec.
b. TR=450 msec, TE=20 msec.
c. TR=450 msec, TE=30 msec.
d. TR=900 msec, TE=30 msec.
e. TR=2000 msec, TE=30 msec.
f. TR=2000 msec, TE=50 msec.
g. TR=2000 msec, TE=100 msec.
h. TR=2000 msec, TE=200 msec

found to be decreased in patients older than 65 years and in cachectic patients (31). Within the perirenal space, the upper pole of each kidney is in close relation with the adrenal gland (Fig. 3a). The right liver lobe adjoins the right kidney (Fig. 3a and 4b). The relation between the left kidney, splenic pedicle, pancreas and spleen is particularly well outlined on a sagittal scan (Fig. 3a and 3b).

In the normal kidney the cortex and medulla are identified as separate structures on the T1 weighted image (Fig. 3b). No cortex-medulla demarcation

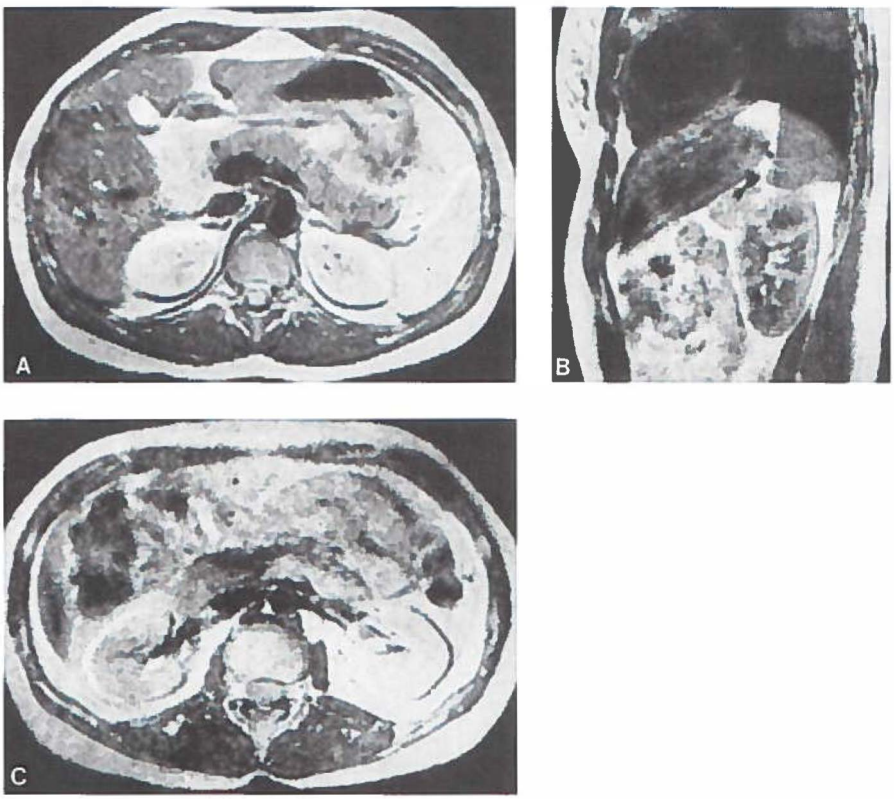

Fig. 3. Normal renal anatomy SE images.

a. TR=2000 msec, TE=100 msec. Transverse section showing the relation of kidneys and adrenals, liver, spleen and pancreas. No CMD on this T2 weighted image.

b. TR=500 msec, TE=30 msec. Sagittal section showing the left kidney, spleen, splenic pedicle and pancreas. Anterior to the pancreas is the fluid filled stomach and left liver lobe. Excellent intrarenal anatomy with clear CMD, renal sinus fat and blood vessels.

c. TR=1500 msec, TE=50 msec. Note the chemical shift artefact and inhomogeneous brightness artefact.

(CMD) is noted on the T2 weighted images in the native kidney (Fig.3a). The CMD varies with the state of hydration (19). In rats CMD was not affected by overhydration, but a decrease of T1 in the inner medulla was observed after 24 hours of dehydration (32). The renal cortex-to-medulla contrast (CMC) can be calculated and a decrease or absence of CMC appears to be a sensitive but non-specific sign of kidney disease (33). The renal sinus fat and both the intra- and extrarenal blood vessels are well shown at MRI (Fig. 3b and 3c). In normal subjects using a conventional SE pulse sequence, flowing blood appears dark. The rapidly flowing protons have left the imaging plane before the SE sequence has been completed and therefore no echo is received (34, 35, 36). However, signal may be perceived due to paradoxical enhancement in case of slowly flowing blood or if turbulent flow is present. The urine within the renal pelvis will be of low or high signal intensity, depending on the pulse sequence used (Fig. 3c).

III.5 Artefacts

MR image quality is prone to degradation due to artefacts. Artefacts are generated by the patient and related to technical factors. In fact up to now the abundance of motion artefacts has significantly hampered the impact of MR imaging in the upper abdomen. Motion artefacts result from respiratory and intestinal movements as well as from pulsatile blood flow. Motion artefacts cause a blurring of the moving structures and subsequently a loss of both spatial and contrast resolution (Fig.4a). Furthermore ghost images may appear (Fig. 3c and 4a). Ghost images are image harmonics which appear in the direction of the phase encoding gradient (37,38,39,40). Usually only the subcutaneous fat is visible in the ghost images(41).

Ghosting may occur locally close to an artery due to pulsatile flow and is seen as a bright spot outside the vessels (38).

Several techniques have been developed to reduce motion artefacts due to respiratory movements. Respiratory gating has not become a routine procedure since it prolongs the acquisition time with a factor 2-4 (42). Respiratory ordered phase encoding (ROPE) controls the respiratory movement artefacts without prolongation of the examination time by using the respiratory signal to determine the order in which the data are collected (43). An alternative is the short TI inversion recovery sequence (STIR), which reduces the signal intensity of the anterior abdominal wall fat to zero and therefore not only reduces ghosting but also the chemical shift artefact (44). ROPE and STIR can be applied simultaneously in order to further reduce respiratory artefacts (45). The chemical shift artefact occurs along the frequency encoding axis and is due to

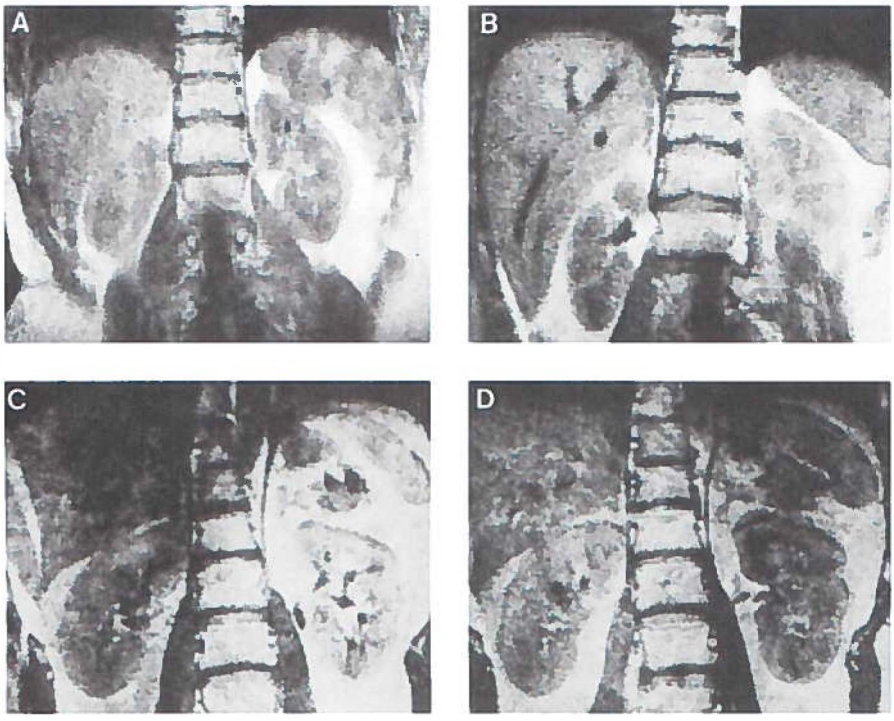

Fig. 1. Normal anatomy, SE images.

a. TR=500 msec, TE=30 msec. Coronal section, blurring of the image due to respiratory artefacts.

b. TR=500 msec, TE=30 msec. Respiratory gating improves both spatial and contrast resolution.

c. and d. Two contiguous sections of multiple slice sequences (TR=700 msec, TE=50 msec), showing asymmetric brightness and inversed signal intensity of kidneys and spleen on the two images.

the 4 ppm lower resonance frequency of lipid protons compared to water protons (29,40,46, 47). The images arising from the fat and water containing structures are shifted 1 pixel relative to each other. This results in a dark or bright rim on either side of the kidney (Fig. 3a and 3c). The chemical shift artefact is easily recognized and does not pose a diagnostic problem.

Erroneous interpretation of the MR findings, however, may occur if the diagnosis is based solely on the signal intensity of a lesion or organ. The signal intensity may be falsely low or high without relation to the real properties of the tissue.

Asymmetric brightness (Fig.3c) may be due to filtering problems or nonuniform slice thickness (40). Inhomogeneous brightness is caused by an incorrect RF tip angle, RF inhomogeneity or asymmetric patient positioning (40,48). Furthermore when images of contiguous slices are acquired with a multiple slice sequence, that first excites the even slices (2,4,6 etc.) and after that the uneven slices (1,3,5 etc), saturation effects due to imperfect slice selection may cause variations in signal intensity between adjacent slices within one organ (Fig. 4c and 4d). Absolute signal intensity values cannot generally be compared from section to section (48).

Magnetic field inhomogeneity may result in spatial distortion towards the periphery of an image (49). Truncation artefacts, are not as apparent as motion artefacts in the upper abdomen. These artefacts are observed as a property of the Fourier transformation used in the image reconstruction as multiple duplications of interfaces between two structures with abrupt transition of signal intensity (40, 50). One could compare the appearance of this artefact with the well-known reverberation artefact in ultrasound. The aliasing artefact (Fig. 4a) will occur in the direction of the phase encoding gradient if the field of view is smaller than the object diameter (40).

Metallic implants both with and without measurable ferromagnetic properties may cause local distortion of the magnetic field and subsequently lead to artefacts (51). Artefacts may be produced by prosthetic heart valves and other metallic implants such as surgical clips, central nervous shunting and orthopedic devices (52,53). The presentation of the artefact is dependent on composition, mass, orientation and position in the body. The ferromagnetic material can be small, e.g. an iron splinter, and still cause considerable artefacts (54). Even minute particles, that are left behind after a surgical procedure using bone drills, may cause detectable distortion of the magnetic field, while they remain undetected by X-ray CT (55).

III.6 Quantitative MR data

Quantitative information is useful to describe pathology in a more objective way and ideally should be specific enough to allow differentiation between different tissue types. In MRI the T1 and T2 relaxation times can be calculated and interpreted as properties of a tissue.

III.6.a *T1 and T2 relaxation times.*

The time required for a spin to return to its equilibrium position parallel to the static magnetic field after the RF pulse has been switched off, can be characterized by two time constants, the spin-lattice (T1) and spin-spin (T2) relaxation

time. T1 describes the loss of energy of protons to their environment (lattice), whereas T2 is a parameter for the interchange of energy between spinning nuclei (8). T1 and T2 are determined by biological, physical and instrumental parameters (56). Temperature and pH of the tissue as well as the total water content, the distribution and state (bound or free) of water will affect T1 and T2 (56,57). Environmental factors, e.g. diet and age, have been found to change T1 and T2 (58). Both T1 and T2 are dependent on tissue type (11).
As opposed to T2, T1 is strongly dependent on the resonance frequency, which in turn is determined by the main magnetic field strength (11,12). Unlike T1, T2 will often show a complex multi-exponential behaviour, resulting in multiple different T2 values arising from various components within a tissue (11).
For a multitude of reasons T1 and T2 have proven not to be specific tissue parameters, due to both the overlap of T1 and T2 for various pathological conditions and the limitations involved with in vivo calculations of T1 and T2.

III.6.b *Calculated T1 and T2 values.*
T1 and T2 relaxation times can be calculated in various ways from conventional pulse sequences. The Gyroscan S5 (Philips) uses a combination of an IR (TR=1400 msec; TE=50 msec; TI=400 msec) and SE (TR=1000 msec; TE=50 msec) multi echo pulse sequence for in vivo T1 and T2 calculations.
In vitro T1 and T2 measurements on freshly excised tissue samples provide accurate and reproducible values within the first 24-48 hours after excision of most tissues (59,60).
Exceptions observed in the rat, are T1 of liver and spleen (stable for 6 hours), T2 of muscle and T1 and T2 of intestine (unstable within 1 hour). The multiexponential behaviour of particularly T2 is readily assessed in this way and the NMR experiments are free of motion artefacts. Early results of in vitro relaxation time measurements already showed the nonspecific nature of the prolongation of T1 (61). In vivo experiments in animals show that T1 and T2 are not specific for individual pathologic conditions (62,63). A definite overlap of T1 and T2 for malignant tumors, abcesses and hematomas has been observed in the rat (25). In vivo calculated T1 and T2 values of pathological conditions in the human brain do not correlate with the histologic changes (64,65). Also in the abdomen an overlap of T1 and T2 between different tumors has been noted (27).
T1 and T2 calculations are subject to errors both related to the object and instrumental imperfections (15,66,67,68,69,70). First there is the tissue heterogeneity and multi-exponential behaviour of tissues. The T1 and T2 values obtained will be the average values over a certain volume. Partial volume effects also play a role in the inaccuracies due to patient motion and flow. The pulse sequences may be suboptimal and not suited to record the multiexponential

behaviour of tissues. A poor S/N ratio will result in large standard errors of the data obtained. Further instrumental parameters which may affect T1 and T2 are RF inhomogeneity and errors in the pulse flip angle.
For all these reasons in vivo calculated T1 and T2 values have been of little value in the diagnosis and characterization of pathological conditions.

III.7 Safety

Possible side-effects of MRI and danger to the patient may result on the one hand from the imaging procedure itself and on the other hand from metallic objects within the patient or examination room. MRI as it is used today, is a safe procedure. In 1948 Purcell and Ramsey exposed their heads to a 2 T magnetic field and a powerful RF field. During the following decades these scientists have not shown any signs of side-effects of this magnetic adventure (71).

Early reports on the follow-up of several hundreds of patients did not mention any ill-effects (72,73). Long-term exposures that greatly exceed those used in MRI, have failed to cause any detectable genetic or cytogenic damage (74,75,76). No chromosomal aberrations or inhibition of DNA synthesis have been demonstrated (77). Sixty six hours of continuous exposure of spermatogenic cells to a 0.3 T magnetic field did not show any significant cytotoxicity (78). There is no evidence of short or long term behavioral changes or effects on spatial memory processes in rats (79,80). One hour of exposure to a 1.5T static magnetic field does not cause any change of human body temperature (81). When describing the effects of magnetic fields on the human body, distinction should be made between the effects of the static magnetic field, time-varying magnetic field effects and the effects of the RF field (82,83).

Possible changes due to the static magnetic field include: macromolecular orientation, resulting in changes in chemical shift kinetics and membrane permeability; enzyme kynetics; reduced nerve conduction; changes in the T wave of the EKG as a result of superposition of low potentials (82). Time-varying magnetic fields may induce visual light flashes, known as magnetic phosphenes. Energy absorption from the RF field will result in a rise of body temperature. Furthermore disturbances of the blood-brain barrier and of nerve conduction have been observed in rats at GHz frequencies. In order to reduce or obviate these possible side-effects, guidelines have been set by the British National Radiological Protection Board and the American Food and Drug Administration (84,85); the static magnetic field should not exceed 2.5 and 2T, respectively.

Time-varying magnetic field (dB/dt) exposures should be limited to 3T/sec (85). RF exposures should not result in a rise of body temperature of more than

1°C (the basic metabolic rate during sleep) by limiting the specific absorption rate (SAR) as averaged over the whole body to 0.4W/kg or to 2W/kg as averaged over any one gram of tissue (84,85). Danger from metallic objects within the examination room needs no further elucidation. These objects can be attracted by the magnet and become dangerous missiles for the patient in the MR scanner. Definite contraindications for MR imaging are pacemakers and certain ferromagnetic clips, particularly in the head (51,86).

Otherwise metallic implants including prosthetic heart valves may cause serious disturbances of the local magnetic field and therefore give rise to artefacts, but these are not a contra indication for MRI (52,53,87). It is wise to check patients known to have metallic material within the body with either a metal detector or a magnetometer (more sensitive) (88).

III.8 References

1. Kurtz D, Dwyer A. Isosignal contours and signal gradients as an aid to choosing MR imaging techniques. J Comput Assist Tomogr 1984; 8: 819-828.
2. Hart HR, Bottomley PA, Edelstein WA, Karr SG, Leue WM, Mueller O, Redington RW, Schenck JF, Smith LS, Vitas D. Nuclear magnetic resonance imaging: contrast-to-noise ratio as a function of strength of magnetic field. AJR 1983; 141: 1195-1201.
3. Mansfield P, Pykett JL. Biological and medical imaging by NMR. J Magn Resonance 1978; 29: 355-373.
4. Mallard J. The noes have it! Do they? Br J Radiol 1981; 54: 831-849.
5. James AE, Partain CL, Holland GN, Gore JC, Rollo FD, Harms SE, Price RR. Nuclear magnetic resonance imaging: the current state. AJR 1981; 138: 201-210.
6. Fullerton GD. Basic concepts for nuclear magnetic resonance imaging. Magn Reson Imaging 1982; 1: 39-55.
7. Moore WS. Basic physics and relaxation mechanisms. Br Med Bull 1984; 40: 120-124.
8. Pykett IL, Newhouse JH, Buonanno FS, Brady TJ, Goldman MR, Kistler JP, Pokost GM. Principles of nuclear magnetic resonance imaging. Radiology 1982; 143: 157-168.
9. Crooks LE, Arawaka M, Hoenninger J, McCarten B, Watts J, Kaufman L. Magnetic resonance imaging: effects of magnetic field strength. Radiology 1984; 151: 127-133.
10. Bobman SA, Riederer SJ, Lee JN, Suddarth SA, Wang HZ, MacFall JR. Synthesized MR images: comparison with acquired images. Radiology 1985; 155: 731-738.
11. Bottomley PA, Foster TH, Argersinger RE, Pfeifer LM. A review of normal tissue hydrogen NMR relaxation times and relaxation mechanisms from 1-100 MHz: dependence on tissue type, NMR frequency, temperature, species, excision and age. Med Phys 1984; 11: 425-448.
12. Kroeker RM, McVeigh ER, Hardy P, Bronskill MJ, Henkelman RM. In vivo measurements of NMR relaxation times. Magn Reson in Med 1985; 2: 1-13.
13. Wehrli FW, MacFall JR, Glover GH, Grigsby N, Haughton V, Johanson J. The dependence of nuclear magnetic resonance (NMR) image contrast on intrinsic and pulse sequence timing parameters. Magn Reson Imaging 1984; 2: 3-16.
14. Edelstein WA, Glover GH, Hardy CJ, Redington RW. The intrinsic signal-to-noise ratio in NMR imaging. Magn Reson in Med 1986; 3: 604-618.

15. Budinger TF, Canterbur PC. Nuclear magnetic resonance technology for medical studies. Science 1984; 226: 288-298.
16. Loeffler W. Oppelt A. Physical principles of NMR tomography. Europ J Radiol 1981; 1: 338-344.
17. Hendrick RE, Nelson TR, Hendee WR. Optimizing tissue contrast in magnetic resonance imaging. Magn Reson Imaging 1984; 2: 193-204.
18. Nelson TR, Hendrick RE, Hendee WR. Selection of pulse sequences producing maximum tissue contrast in magnetic resonance imaging. Magn Reson Imag 1984; 2: 285-294.
19. Hricak H, Crooks L, Sheldon P, Kaufman L. Nuclear magnetic resonance imaging of the kidney. Radiology 1983; 146: 425-432.
20. Go KG, van Dijk P. Luiten AL, Brouwer-van Herwijnen AA, Van der Leeuw YCL, Kamman RL, Vencken LM, Wilmink JT, Berendsen HJC. Interpretation of nuclear magnetic resonance tomograms of the brain. J. Neurosurg 1983; 59: 574-584.
21. Kiricuta Jr. I, Simplaceanu V. Tissue water content and nuclear magnetic resonance in normal and tumor tissues. Cancer research 1975; 35: 1164-1167.
22. Hendrick RE, Newman FD, Hendee WR. MR imaging technology: maximizing the signal-to-noise ratio from a single tissue. Radiology 1985; 156: 749-752.
23. Richardson ML, Amparo EG, Gillespy T, Helms CA, Demas BE, Genant HK. Theoretical considerations for optimizing intensity differences between primary musculoskeletal tumors and normal tissue with spin-echo magnetic resonance imaging. Invest Radiol 1985; 20: 492-497.
24. Orthendahl DA, Hylton N, Kaufman L, Watts J, Crooks LE, Mills CM, Stark DD. Analytical tools for magnetic resonance imaging. Radiology 1984; 153: 479-488.
25. Herfkens R, Davis P, Crooks L, Kaufman L, Price D, Miller T, Margulis AR, Watts J, Hoenninger J, Arawaka M, McRee R. Nuclear magnetic resonance imaging of the abnormal live rat and correlations with tissue characteristics. Radiology 1981; 141: 211-218.
26. Koenig SH, Brown RD, Adams D, Emerson D, Harris CG. Magnetic field dependence of 1/T1 of protons in tissue. Invest Radiol 1984; 19: 76-81.
27. Schmidt HC, Tscholakoff D, Hricak H, Higgins CB. MR image contrast and relaxation times of solid tumors in the chest, abdomen and pelvis. J Comput Assist Tomogr 1985; 9: 738-748.
28. Schöpflin RE, Bosiger P, Meier D. Critical evaluation of the quality of synthetic MR images. Magn Reson Imaging 1986; 4: 435-436.
29. Newhouse JH, Markisz JA, Kazam E. Magnetic resonance imaging of the kidneys. Cardiovasc Intervent Radiol 1986; 8: 351-366.
30. Kressel HY, Axel L, Glover G, Baum S. Coronal nuclear magnetic resonance(NMR) imaging of the abdomen at 0.5T. J Comput Assist Tomogr 1984; 8: 29-31.
31. Dooms GC, Hricak H, Margulis AR, de Geer G. MR imaging of fat. Radiology 1986; 158: 51-54.
32. Kundel HL, Schlakman B, Joseph PM, Fishman JE, Summers R. Water content and NMR relaxation time gradients in the rabbit kidney. Invest Radiol 1986; 21: 12-17.
33. Terrier F, Hricak H, Justich E, Dooms GC, Grodd W. The diagnostic value of renal cortex-to-medulla contrast on magnetic resonance images. Europ J Radiol 1986; 6: 121-126.
34. Axel L. Blood flow effects in magnetic resonance imaging. AJR 1984; 143: 1157-1166.
35. Crooks LE, Kaufman L. NMR imaging of blood flow. Br Med Bull 1984; 40: 167-169.
36. Bradley WG, Waluch V. Blood flow: magnetic resonance imaging. Radiology 1985; 154: 443-450.
37. Aisen AM, Glazer GM, Carson PL, Hearshen DO. Motion artefacts on quantitative magnetic resonance imaging. Magn Reson Imaging 1986; 4: 207-213.

38. Perman WH. Moran PR, Moran RA, Bernstein MA. Artefacts from pulsatile flow in MR imaging. J Comput Assist Tomogr 1986; 10: 473-483.
39. Haacke EM, Patrick JL. Reducing motion artefacts in two-dimensional fourier transform imaging. Magn Reson Imag 1986; 4: 359-376.
40. Pusey E, Lufkin RB, Brown RKJ, Solomon MA, Stark DD, Tarr RW, Hanafee WN. Magnetic resonance imaging artefacts: mechanism and clinical significance. Radiographics 1986; 6: 891-911.
41. Wood ML, Henkelman RM, The magnetic field dependence of the breathing artifact. Magn Reson Imag 1986; 4: 387-392.
42. Ehman RL, McNamara MT, Pallack M, Hricak H, Higgins CB. Magnetic resonance imaging with respiratory gating: techniques and advantages. AJR 1984; 143: 1175-1182.
43. Bailes DR, Gilderdale DJ, Bydder GM, Collins AG, Firmin DN. Respiratory ordered phase encoding (ROPE): a method for reducing respiratory motion artefacts in MR imaging. J Comput Assist Tomogr 1985; 9: 835-838.
44. Bydder GM, Pennock JM, Steiner RE, Khenia S, Payne JA, Young IR. The short TI inversion recovery sequence an approach to MR imaging of the abdomen. Magn Reson Imag 1985; 3: 251-254.
45. Steiner RE. Present and future clinical position of magnetic resonance imaging. Magn Reson Med 1986; 3: 473-490.
46. Weinreb JC, Brateman L, Babcock EE, Maravilla KR, Cohen JM, Homer SD. Chemical shift artefact in clinical magnetic resonance images at 0.35T. AJR 1985; 145: 183-185.
47. Babcock EE. Brateman L, Weinreb JC, Horner SD, Nunnally RL. Edge artefacts in MR images: chemical shift effect. J Comput Assist Tomogr 1985; 9: 252-257.
48. Ehman RL, Kjos BO, Hricak H, Brash RC. Higgins CB. Relative intensity of abdominal organs in MR images. J Comput Assist Tomogr 1985; 9: 315-319.
49. Zhu XP, Checkley DR, Hickey DS, Isherwood I. Accuracy of area measurements made from MR images compared with computed tomography. J Comput Assist Tomogr 1986; 10: 96-102.
50. Smith MR, Nichols ST, Henkelman RM, Wood ML. Application of autoregressive modelling in magnetic resonance imaging to remove noise and truncation artefacts. Magn Reson Imaging 1986; 4: 257-261.
51. New PFJ, Rosen BR, Brady TJ, Buonanno FS, Kistler JP, Burt CT, Hinshaw WS, Newhouse JH, Pohost GM, Taveras JM. Potential hazards and artefacts of ferromagnetic and nonferromagnetic surgical and dental materials and devices in nuclear magnetic resonance imaging. Radiology 147; 1983: 139-148.
52. Soulen RL, Budinger TF, Higgins CB. Magnetic Resonance imaging of prosthetic heart valves. Radiology 1985; 154: 705-707.
53. Laakman RW, Kaufman B, Han JS, Nelson AD, Clampitt M, O'Block AM, Haaga JR. Alfidi RJ. MR imaging in patients with metallic implants. Radiology 1985; 157: 711-714.
54. Go KG, van Dijk P, Luiten AL, Koster WG, Piers A, Kingma LM, van Woerden H, te Strake L, Vermey J. First experiences with proton spin tomography (NMR). Clin Neur Neurosurg 1982; 84: 81-90.
55. Heindel W, Friedman G, Bunke J, Thomas B, Firsching R, Ernestus RI. Artefacts in MR imaging after surgical intervention. J Comput Assist Tomogr 1986; 10: 596-599.
56. Mathur-de Vré R. Biomedical implications of the relaxation behaviour of water related to NMR imaging. Br J Radiol 1984; 57: 955-976.
57. Fullerton GD, Cameron IL, Ord VA. Frequency dependence of magnetic resonance spin-lattice relaxation of protons in biological materials. Radiology 1984; 151: 135-138.
58. Mardini IA, McCarter RJM, Fullerton GD. NMR relaxation times of skeletal muscle: dependence on fiber type and diet. Magn Reson Imaging 1986; 4: 393-398.

59. Thickman DI, Kundel HL, Wolf G. Nuclear magnetic resonance characteristics of fresh and fixed tissue: the effect of elapsed time. Radiology 1983; 148: 183-185.
60. Kamman RL, Go KG, Stomp GP, Hulstaert CE, Berendsen HJC. Changes of relaxation times T1 and T2 in rat tissues after biopsy and fixation. Magn Reson Imag 1985; 3: 245-250.
61. Eggleston JC, Saryan LA, Hollis DP. Nuclear Magnetic Resonance Investigations of human neoplastic and abnormal nonneoplastic tissues. Cancer Research 1975; 35: 1326-1332.
62. Moon KL, Davis PL, Kaufman L, Crooks LE, Sheldon PE, Miller T, Brito AC, Watts JC. Nuclear magnetic resonance imaging of a fibrosarcoma tumor implanted in the rat. Radiology 1983; 148: 177-181.
63. Brant-Zawadski M, Bartkowski HM, Orthendahl DA, Pitts LH, Hylton NM, Nishimura MC, Crooks LE. NMR in experimental cerebral edema: value of T1 and T2 calculations. AJNR 1984; 5: 125-129.
64. Araki T, Inouye T, Suzuki H, Machida T, Iio M. Magnetic resonance imaging of brain tumors: measurements of T1. Radiology 1984; 150: 95-98.
65. Mills CM, Crooks LE, Kaufman L, Brant-Zawadzki M. Cerebral abnormalities: use of calculated T1 and T2 magnetic resonance images for diagnosis. Radiology 1984; 150: 87-94.
66. Pykett IL, Rosen BR, Buonanno FS, Brady TJ. Measurement of spin-lattice relaxation times in nuclear magnetic resonance imaging. Phys Med Biol 1983; 28: 723-729.
67. Kjos BO, Ehman RL, Brant-Zawadzki M. Reproducibility of T1 and T2 relaxation times calculated from routine MR imaging sequences: phantom study. AJR 1985; 144: 1157-1163.
68. Smith MA, Taylor DG. The absence of tissue specificity in MRI using in vivo T1 or T2 determination: true-biological variation or technical artefact? Br J Radiol 1986; 59: 82-83.
69. Majumdar S, Orphanoudakis SC, Gmitro A, O'Donnell M, Gore JC. Errors in the measurements of T2 using multiple-echo MRI techniques. II. Effects of static field inhomogeneity. Magn Reson Med 1986; 3: 562-574.
70. Young IR. Considerations affecting signal and contrast in NMR imaging. Br Med Bull 1984; 40: 139-147.
71. Andrew ER. A historical review of NMR and its clinical applications. Br Med Bull 1984; 40: 115-119.
72. Smith FW. Safety of NMR imaging. Lancet 1982; 974.
73. Reid A, Smith FW, Hutchison JMS. Nuclear magnetic resonance imaging and its safety implications: follow-up of 181 patients. Br J Radiol 1982; 55: 784-786.
74. Schwartz JL, Crooks LE. NMR imaging produces no observable mutations or cytotoxicity in mammalian cells. AJR 1982; 139: 583-585.
75. Wolff S, James TL, Young GB, Margulis AR, Bodycote J, Afzal V. Magnetic resonance imaging: absence of in vitro cytogenic damage. Radiology 1985; 155: 163-165.
76. Cooke P, Morris PG. The effects of NMR exposure on living organisms. II. A genetic study of human lymphocytes. Br J Radiol 1981; 54: 622-625.
77. Wolff S, Crooks LE, Brown P, Howard R, Painter RB. Tests for DNA and chromosomal damage induced by nuclear magnetic resonance imaging. Radiology 1980; 136: 707-710.
78. Withers HR, Mason KA, Davis CA. MR effect on murine spermatogenesis. Radiology 1985; 156: 741-742.
79. Ossenkopp KP, Innis NK, Prato FS, Sestini E. Behavioral effects of exposure to nuclear magnetic resonance imaging: 1. Open-field behavior and passive avoidance learning in rats. Magn Res Imag 1986; 4: 275-280.
80. Innis NK, Ossenkopp KP, Prato FS, Sestini E. Behavioral effects of exposure to nuclear magnetic resonance imaging: II spatial memory tests. Magn Reson Imag 1986; 4: 281-284.
81. Shellock FG, Schaeffer DJ, Gordon CJ. Effects of a 1.5 T static magnetic field on body temperature of man. Magn Res Med 1986; 3: 644-647.

82. Budinger TF. Nuclear magnetic resonance (NMR) in vivo studies: known thresholds for health effects. J Comput Assist Tomogr 1981; 5: 800-811.
83. Saunders RD, Smith H. Safety aspects of NMR clinical imaging. Br Med Bull 1984; 40: 148-154.
84. The National Radiological Protection Board ad hoc Advisory Group on nuclear magnetic resonance clinical imaging. Revised guidance on acceptable limits of exposure during nuclear magnetic resonance clinical imaging. Br J Radiol 1983; 56: 974-977.
85. Public Health Service. Food and Drug Administration USA. Guidelines for evaluating electromagnetic risk for trials of clinical NMR systems. Feb. 25, 1982.
86. Pavlicek W, Geisinger M, Castle L, Borkowski GP, Meany TF, Bream BL, Gallagher JH. The effects of nuclear magnetic resonance on patients with cardiac pacemakers. Radiology 147; 1983: 149-153.
87. Davis PL, Crooks L, Arakawa M, McRee R, Kaufman L, Margulis AR. Potential hazards in NMR imaging: heating effects of changing magnetic fields and RF fields on small metallic implants. AJR 1981; 137: 857-860.
88. Finn EJ, Di Chiro G, Brooks RA, Sato S. Ferromagnetic materials in patients: detection before MR imaging. Radiology 1985; 156: 139-141.

Chapter IV

MAGNETIC RESONANCE IMAGING (MRI) IN THE DIAGNOSIS OF DIFFUSE RENAL DISEASES

L. te Strake[1], LP. Oe[2], S. Lobatto[3], M. Sperber[4], J.J. Weening[5], J.J. Hermans[6], A.J. Donker[2], J. Doornbos[1], H. van Bronswijk[2], J.R. Blickman[7], J. Valk[4].

Dept. of Radiology[1], University Hospital Leiden. Dept. of Medicine[2], Free University Hospital Amsterdam. Dept. of Nephrology[3], University Hospital Leiden. Dept. of Radiology[4], Free University Hospital Amsterdam. Dept. of Pathology[5], University Hospital Leiden. Dept. of Medical Statistics[6], University Leiden. Dept. of Radiology[7], University Hospital Groningen. The Netherlands.

IV.1 Abstract

The purpose of this study was to investigate correlations between MRI and clinical- and histological findings in patients with diffuse renal parenchymal diseases, and to determine the possible application of MRI as an adjunct to renal biopsy. Ten healthy volunteers and 38 patients with acute or chronic renal failure were studied at 2 different institutions with 2 different (0.5 T and 0.6 T) MR scanners applying a T1 weighted spin echo pulse sequence. Patients were classified into 3 categories according to MR findings of a normal cortex-medulla demarcation (CMD)(group 1), decreased CMD (group 2) or absent CMD (group 3). Patients with a nephrotic syndrome due to minimal change disease were not found in group 3.

Although an abnormal CMD is highly indicative of the presence of diffuse renal disease and impaired renal function, MRI can not replace renal biopsy since the MR findings appear not to be conclusive for a particular renal disease. However, MRI might be a useful technique to select those cases with nephrotic syndrome and selective proteinuria that can be treated with corticosteroids without previous biopsy, particularly children and adults with a contra indication for percutaneous renal biopsy, e.g. the existence of a solitary kidney. Further experience in a larger group of patients with minimal change disease is needed before definite statements can be made.

Accepted for publication in Proceedings of the 2nd Int. Congress of noninvasive kidney disease. Vienna, 1986. Ed. G. Lubec, London.

IV.2 Introduction

During the initial stage of its clinical evaluation Magnetic Resonance Imaging (MRI) proved to be an excellent method to show normal renal anatomy (1,2). Cortex and medulla can be imaged as separate structures. The normal cortex-medulla demarcation (CMD) can be decreased or absent in the presence of renal parenchymal disease (3,4). It was expected that MRI could have a major role in the diagnosis of diffuse renal parenchymal diseases and could become an important adjunct to renal biopsy (5). Until now no specific studies have been reported on the correlation between MRI, renal function and histological changes in patients suffering from diffuse renal diseases. The purpose of this study was to investigate this correlation and to determine the possible role of MRI as an adjunct to renal biopsy.

IV.3 Material and methods

MRI was performed at 2 institutions (University Hospital Leiden - UHL and Free University Hospital Amsterdam - FUHA) using 2 different superconducting MR scanners (0.5 T Gyroscan S5, Philips, and 0.6 T Teslacon, Technicare, respectively). A T1 weighted Spin Echo (SE) pulse sequence was applied, TR=550 ms, TE=30 msec (Gyroscan) or TR=420-500 msec, TE=32 msec (Teslacon).

Multiple slices of both kidneys were obtained in the transverse plane. Slice thickness was 1 cm, matrix size 256x256 or 256x128. Scan time was approximately 4 minutes, total examination time including positioning of the patient was less than 15 minutes.

Ten normal volunteers, 3 females and 7 males aged 22-35 (mean age 25), without a history of renal disease or hypertension were studied with the Gyroscan S5. Furthermore, thirty eight patients suffering from acute or chronic renal failure, 20 females and 18 males aged 15-81 (mean age 47), were examined (Gyroscan n=13, Teslacon n=25). Twenty nine patients underwent renal biopsy, whereas in 9 patients the diagnosis was established on clinical data without biopsy. The histological examinations were performed according to standard techniques, using light- and immunofluorescence microscopy. If necessary, also electron microscopy was performed. The histological findings were classified according to the WHO classification (6). Twenty six patients had their biopsy taken at the UHL or FUHA. The histological findings in these 26 biopsies were reviewed and graded as normal, slightly abnormal or severely abnormal. The interval between biopsy and MRI varied from 1 week (n=11) up to 7 years (n=18). A longer interval was accepted if it was not to be expected that

histological findings would have changed and if renal function had not changed during this period.

The following clinical and laboratory data were obtained at the time of MRI: urine production, blood pressure, creatinine (μmol/l), creatinine clearance (ml/min), proteinuria (g/24h), erythrocyte sedimentation rate (ESR) and hemoglobin (Hb) content of blood.

Volunteers and patients were classified according to the MRI findings into 3 groups: normal CMD (group 1, fig. 1 and 2), decreased CMD (group 2, fig. 3), or absent CMD (group 3, fig 4).

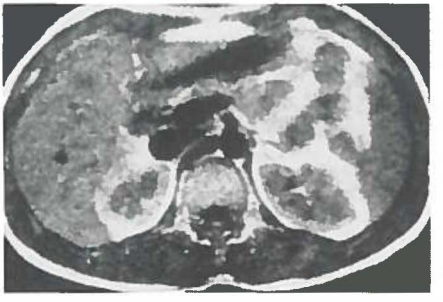

Fig. 1 SE (Gyroscan TR=550 msec, TE=30 msec). Normal cortex-medulla demarcation (CMD). Normal volunteer.

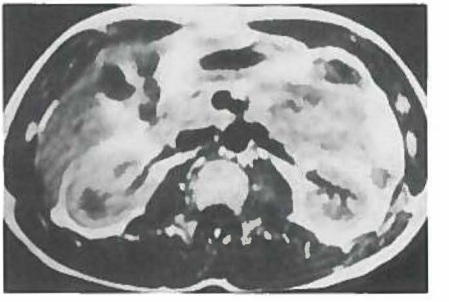

Fig. 2 SE (Teslacon TR=420 msec, TE=32 msec). Normal CMD (group 1). Minimal change disease.

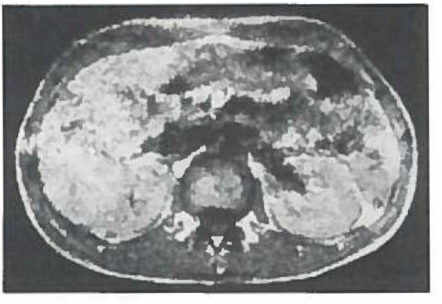

Fig. 3 SE (Gyroscan TR=550 msec, TE=30 msec). Decreased CMD (group 2). Proliferative lupus nephritis.

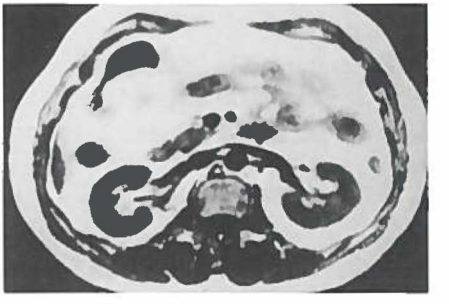

Fig. 4 SE (Teslacon TR=500 msec, TE=32 msec). Absent CMD (group 3). Membrano-proliferative glomerulonephritis.

Signal intensities (SI) of cortex and medulla were measured in each kidney and the corticomedullary contrast (CMC) was calculated as proposed by Thickman et al (7):

$$CMC = \frac{SI\ (cortex) - SI\ (medulla)}{SI\ (cortex) + SI\ (medulla)} \times 100\%$$

IV.4 Results

In all 10 volunteers the CMD was clearly visible (Fig. 1). The CMC in patients with a normal CMD (Gyroscan: mean 11.3% ± 4.3%, Teslacon 11.7% ± 4.5%) was not significantly different from the CMC in the normal volunteers (mean 12.9% ± 4.2%). CMC values obtained in group 3 were significantly different from those in group 1 and 2 (Kruskall-Wallis: $p < 0.01$). However, no

Table 1

Cortico-medullary contrast (CMC mean ± SD) in MRI group 1, 2 and 3

	Group 1 CMD normal	Group 2 CMD decreased	Group 3 CMD absent
Right kidney	12.2% ± 3.7%	14.2% ± 9.5%	5.7% ± 4.5%
Left kidney	14.1% ± 5.3%	13.1% ± 7.5%	8.7% ± 8.9%

----------n.s----------
---------- $p < 0.01$---
---------- $p < 0.01$----------

difference in CMC was found between group 1 and 2 (table 1). The MR findings in the 38 patients and their diagnosis based on histological and/or clinical findings are listed in table 2. Patients with minimal change disease were not found in group 3. Table 3 shows the histological findings in the 26 biopsies that were reviewed. In case of minimal change disease all histological parameters were normal. Severe histological changes were not found in patients with normal CMD. In this group, mild glomerular changes were found in one patient with IgA nephritis and in one case of focal and segmental mesangioproliferative glomerulonephritis. The biopsy specimen of another patient with vasculitis showed mild glomerular, vascular and fibrotic changes. The MR examination in this patient was suboptimal due to respiratory artefacts and could also

have been classified under group 2. When a decreased or absent CMD was found, one or more histological parameters were mildly or severely abnormal. In the total group of 38 patients CMD was abnormal (decreased or absent) in 31 cases (81%).

Table 2

Histological and clinical diagnosis in MRI group 1, 2, 3

	Group 1 CMD normal n = 7	Group 2 CMD decreased n = 15	Group 3 CMD absent n = 16
Minimal change disease	2*	2*	
Membranous glomerulonephritis		1*	
Membranoproliferative glomerulonephritis			5(* n=3)
Focal and segmental mesangioproliferative glomerulonephritis	1*		
Ig A nephritis	1*		
Mesangial glomerulonephritis (pre-eclamptic toxemia)		1*	
Tubulo-interstitial nephritis			1*
Extracapillary nephritis		1*	2*
Nephrosclerosis		1*	1*
Proliferative lupus nephritis		3*	
Vasculitis	1*	1*	1
Amyloidosis		1*	1*
Sarcoidosis		1*	
Diabetic nephropathy			2
Renovascular hypertension			1
Essential hypertension	2	3(* n=1)	
End-stage chronic renal failure			2

* = histology reviewed (26 biopsies)

Table 3

Histological findings in MRI Group 1, 2 and 3 (26 biopsies)

		Group 1 CMD normal n = 5	Group2 CMD decreased n = 13	Group 3 CMD absent n = 8
Glomerular changes	-absent	2	5	1
	-mild	3	3	2
	-severe	-	5	5
Vascular changes	-absent	4	7	4
	-mild	1	5	4
	-severe	-	1	-
Fibrosis	-absent	4	6	3
	-mild	1	7	2
	-severe	-	-	3
Edema	-absent	5	8	5
	-mild	-	3	-
	-severe	-	2	3
Inflammatory changes	-absent	5	6	2
	-mild	-	4	3
	-severe	-	3	3
Medullary changes	-absent	5	10	5
	-mild	-	3	2
	-severe	-	-	1

Regarding the correlation between a normal or abnormal CMD and the presence or absence of histological changes in the 26 biopsies that were reviewed, the following statistical values were found: sensitivity 86%, specificity 50%, positive predictive value 90%, negative predictive value 40%.

The following clinical variables were not significantly different between the 3 groups: urine production, blood pressure, proteinuria, ESR and Hb. Serum creatinine and creatinine clearance were not significantly different between group 1 and 2, but the values obtained in group 3 were significantly different from those in group 1 and group 2 (Kruskall-Wallis: $p < 0.01$, table 4).

Table 4

Serum creatinine and creatinine clearance (mean ± S.D.) in MRI group 1, 2, 3

	group 1 CMD normal	group 2 CMD decreased	group 3 CMD absent
Creatinine (μmol/l)	90 ± 28	133 ± 70	322 ± 192
Creatinine clearance (ml/min)	85 ± 16	64 ± 38	30 ± 21

-------- n.s ----------

---------- $p < 0.01$-----

---------- $p < 0.01$----------

IV.5 Discussion

MRI reliably shows normal renal anatomy. In our study all 10 normal volunteers had a normal CMD. LiPuma (8) observed in a series of 40 patients without signs of renal disease a normal cortico-medullary junction in 96%. Poor scan quality and respiratory artefacts were considered the main reasons for nonvisualization. CMD is also influenced by the hydration state of the patient (5). During forced diuresis following dehydration the medulla appears more prominent and CMD is more apparent.

In this study CMC values in normal volunteers were not significantly different from those in the patients with a normal CMD. These values were slightly lower than those reported by Terrier et al: i.e. 19% ± 2% (9). Our results are in agreement with the previous author in that a loss of CMC (5) or CMD is a sensitive but nonspecific finding. In some cases of significant parenchymal disease and a relatively good nephrogram and contrast excretion at IVU or contrast-enhanced CT, a loss of CMD has been observed as a sign of parenchymal disease (10).

When histological and MRI findings are compared it appears that a loss of CMD is due to one or a combination of multiple histologic changes. Therefore MRI cannot provide a specific histologic diagnosis and will not replace renal biopsy.

In many institutions a surgical biopsy is performed in case of a solitary kidney. In children a renal biopsy is a traumatic procedure that may require general anaesthesia of the patient. In these cases the clinician may feel reluctant to perform a renal biopsy. MRI in children appears to be superior to ultrasound

in the diagnosis of chronic renal failure, since it better shows small fibrotic kidneys and associated cortical cysts (11).

Our study indicates that MRI may be a useful method to select those patients with nephrotic syndrome due to minimal change disease, who may be treated initially with corticosteroids without previous biopsy. When CMD is found to be absent in a patient with a nephrotic syndrome, it is unlikely that the patient will have minimal change disease and therefore renal biopsy is strongly indicated. In case of a normal CMD at MRI and the presence of selective proteinuria, the patient is likely to suffer from minimal change disease and could be treated with corticosteroids initially without previous biopsy. In this respect MRI could be a useful diagnostic tool, providing relevant information to the clinician who has to decide on performing a renal biopsy. The number of patients with minimal change disease in our study is limited and therefore, further experience in a large group of patients is needed before definite statements can be made.

At present images obtained with a 0.5 or 0.6 T MR scanner and standard technique are subject to degradation due to instrumental imperfections. The relatively long scanning time of several minutes induces respiratory artefacts. Inhomogeneity of the static magnetic field and partial volume effects may lead to inaccurate measurements or T1 and T2 relaxation times and spin density resulting in incorrect display of tissues (12,13). A solution to reduce respiratory artefacts and partial volume effects could be the imaging of thinner slices in a shorter scanning time. This, however, at the same time will negatively affect the signal-to-noise ratio of the images since less signal is received.

Imaging at higher field strength, e.g. 1.5 T, will improve both the signal-to-noise ratio and the inhomogeneity of the static magnetic field. Furthermore, the application of surface coils will improve the signal-to-noise ratio, allowing the imaging of thinner slices with preservation of image quality. Recently, new pulse sequences have been introduced resulting in a scanning time of seconds rather than minutes (14).

Advantages of this technique are the freezing of respiratory and intestinal motion and the ability to perform dynamic perfusion studies of the kidney following i.v. administration of paramagnetic contrast agents. These latest developments in technology, currently under clinical evaluation, will certainly add to the sensitivity of MRI.

This, and the results of our present study seem to warrant further research as to the application of MRI as a diagnostic tool in the study of diffuse parenchymal renal diseases.

IV.6 References

1. Smith FW, Reid A, Mallard JR, Hutchison JMS, Power DA, Catto GRD. Nuclear magnetic resonance tomographic imaging in renal disease. Diagn Imaging 1982; 51: 209-213.
2. Young IR, Bailes DR, Burl M, etal. Initial clinical evaluation of a whole body nuclear magnetic resonance (NMR) tomograph. J Comput Assist Tomogr 1982; 6(1): 1-18.
3. Leung AWL, Bydder GM, Steiner RE, Bryant DJ, Young IR. Magnetic resonance imaging of the kidneys. AJR 1984; 143: 1215-1227.
4. te Strake L, Blickman JR, van der Hem GK, Hooykaas JAP, Poppema S, Brouwer-van Herwijnen AA. Imagerie RMN du rein. J Radiol 1984; 65: 631-635.
5. Hricak H, Crooks L, Sheldon P, Kaufman L. Nuclear magnetic resonance imaging of the kidney. Radiology 1983; 146: 425-432.
6. Renal disease: Classification and atlas of glomerular diseases. Churg J, Sobin LH. eds. Tokio Igaku - Shoin Ltd, 1982.
7. Thickman D, Kundel H, Biery D. Magnetic resonance evaluation of hydronephrosis in the dog. Radiology 1984; 152: 113-116.
8. Li Puma JP. Magnetic resonance imaging of the kidney. Radiol Clin North Am 1984; 22: 925-941.
9. Terrier F, Hricak H, Dooms GC, Justich E. Diagnostic value of the renal corticomedullary contrast on MR images (abstract). Radiology 1985; 157(P): 276.
10. Newhouse JH, Markisz JA, Kazam E. Magnetic Resonance Imaging of the kidneys. Cardiovasc Intervent Radiol 1986; 8: 351-366.
11. Dietrich RB, Kangarloo H. Kidneys in infants and children: evaluation with MR. Radiology 1986; 159: 215-221.
12. Young IR. Considerations affecting signal and contrast in NMR imaging. Brit Med Bull 1984; 40(2): 139-147.
13. Wehrli FW, MacFall JR, Glover GH, Grigsby N, Haughton V, Johanson J. The dependence of nuclear magnetic resonance (NMR) image contrast on intrinsic and pulse sequence timing parameters. J Magn Res. 1984; 2: 3-16.
14. van der Meulen P, Groen JP, Cuppen JJM. Very fast MR imaging by field echoes and small angle excitation. Magnetic Resonance Imaging 1985; 3: 297-299.

Chapter V

MAGNETIC RESONANCE IMAGING (MRI) IN THE DIAGNOSIS AND STAGING OF RENAL MASSES: A CRITICAL APPRAISAL AND COMPARISON WITH CT.

L. te Strake[1], J.L. Bloem,[1], T.H.M. Falke[1], J. Langeveld[2], J. Hermans[3], J. Doornbos[1], D.J. Ruiter[4], U. Jonas[2].

Departments of Radiology[1], Urology[2], Medical Statistics[3] and Pathology[4], University Hospital Leiden, Rijnsburgerweg 10, Leiden, The Netherlands

V.1 Abstract

The purpose of this prospective study was to compare the accuracy of MRI and CT in the diagnosis and staging of renal masses. MRI was performed with a 0.5 T superconducting MR scanner using conventional T1 and T2 weighted spin echo pulse sequences. The results of MRI and CT were compared in thirty one patients with a renal mass. In the diagnosis of benign tumors similar information was obtained by MRI and CT. Regarding malignant tumors one transitional cell carcinoma, imaged by CT, was not shown by MRI. CT appeared to be slightly more accurate in the determination of perinephric extension of renal cell carcinoma (Stage I v.s. Stage II). Comparable results were obtained in Stage III and Stage IV tumors. The main diagnostic limitations which may lead to inaccurate staging of renal cell carcinoma are encountered in MRI as well as CT. They are: the assessment of tumor extension into the intrarenal vein, the differentiation between lymphadenopathy due to reactive hyperplasia and metastatic involvement, and the differentiation between tumor extension into adjacent organs and adhesions without tumor spread outside the renal capsule. It is concluded that CT remains the method of choice in the diagnosis and staging of renal masses as long as no substantial improvements in MRI performance have been achieved.

World Journal of Urology, accepted for publication.

V.2 Introduction

In the past CT has largely replaced angiography in the preoperative staging of renal masses. CT is particularly more accurate and sensitive than angiography in the determination of peri- and pararenal extension and lymph node involvement (1-6). Initial reports indicated that MRI could become a useful and reliable modality in the staging of renal masses (7-9). A prospective study in 27 patients with renal cell carcinoma yielded an accuracy of 96% for MRI in the anatomic staging of renal cell carcinoma (10). The purpose of this prospective study was to compare the accuracy of MRI and CT in the diagnosis and staging of renal masses.

V.3 Materials and Methods

During a 14 months period 40 patients were referred for MRI because of clinically suspected renal mass.
After MRI and CT evaluation nine patients were excluded from this study for various reasons: extrarenal disease (n=5), normal MRI and CT scan (n=2; one pseudotumor and one patient with hematuria of unknown origin), no CT scan available for comparison (n=2; one angiomyolipoma and one Stage II renal cell carcinoma). In the remaining 31 patients with a renal mass, 15 women and 16 men (age 25-73 years), both MRI and CT scan were available for comparison. The diagnoses are listed in table 1. One patient had bilateral renal cell carcinoma with two masses in one kidney.

The patients with angiomyolipoma and simple cyst were treated conservatively. Twenty of the 23 patients with a renal cell carcinoma underwent nephrectomy. Three were considered to be inoperable because of histologically proven lung metastases (n=1), bone metastases (n=1) or advanced local spread de-

Table 1

Diagnosis in 31 patients referred for diagnosis and/or staging of renal masses

	n
Renal cell carcinoma	23
Transitional cell carcinoma	1
Oncocytoma	1
Angiomyolipoma	3
Simple cyst	3

monstrated by MRI and CT (n=1). The transitional carcinoma of the renal pelvis was confirmed at surgery and histological proof of the oncocytoma was available from a biopsy 18 years prior to MRI.
Tumor staging was performed to the classification described by Robson et al. (11):

Stage I : confined to kidney
Stage II : extension into perirenal fat, not beyond Gerota's fascia
Stage III A : extension into renal and/or inferior vena cava (IVC)
Stage III B : involvement of regional lymph nodes
Stage III C : combination of Stage III A and III B
Stage IV A : extension beyond Gerota's fascia into adjacent organs
Stage IV B : distant metastases

CT and MRI were evaluated prospectively and independently without knowledge of surgical and histological findings by two radiologists: observer 1 (O1), (L.t.S.), and observer 2 (O2), (J.L.B. or T.H.M.F.). The CT and MRI findings were compared with the surgical and histological reports, if available (n=21).

CT was performed using a Pfizer 0450 AS and A scanner with a scan-time of 4.8 seconds and 9 mm slice-thickness. Scans were obtained from the domes of diaphragm to the iliac crests before intravenous (i.v.) administration of contrast material. Scans through the area of interest were repeated after i.v. bolus injection of 50-100 cc meglumine ioxitalamate (Telebrix 30, Laboratoire Guerbet) during rapid sequential scanning.

MRI was carried out with a 0.5T superconducting MR scanner (Gyroscan S5, Philips). In all cases Spin Echo (SE) pulse sequences were applied. Slice thickness was 10 mm, acquisition and display matrix size 256x256. As a standard, initially five T1 weighted images (TR=550 msec, TE=30 msec), 10 mm apart, were acquired in the transverse plane at the level of both kidneys. Then a sagital T1 weighted scan (TR=900 msec, TE=30 msec) was performed with a 10 mm slice interval through the tumor and the IVC. The MR examination was completed with a set of T2 weighted contiguous transverse sections through the abdomen (TR=1800 msec or longer, TE=50 msec and 100 msec).

V.4 Results

Cysts: In 3 patients with a simple cyst a correct diagnosis was made by both observers on MRI and CT. The cysts appeared on the T1 weighted images as a well circumscribed mass of low signal intensity and as a bright mass on the T2 weighted images.

Angiomyolipoma: Three patients with angiomyolipoma were studied; one patient had bilateral angiomyolipomas. The diagnosis of angiomyolipoma was made correctly on MRI and CT by both observers in all patients. On MRI the angiomyolipomas appeared bright on both T1 and T2 weighted images. Areas of inhomogeneous signal intensity distribution were noted, which corresponded to areas of decreased or mixed density on CT (Fig. 1a,b).

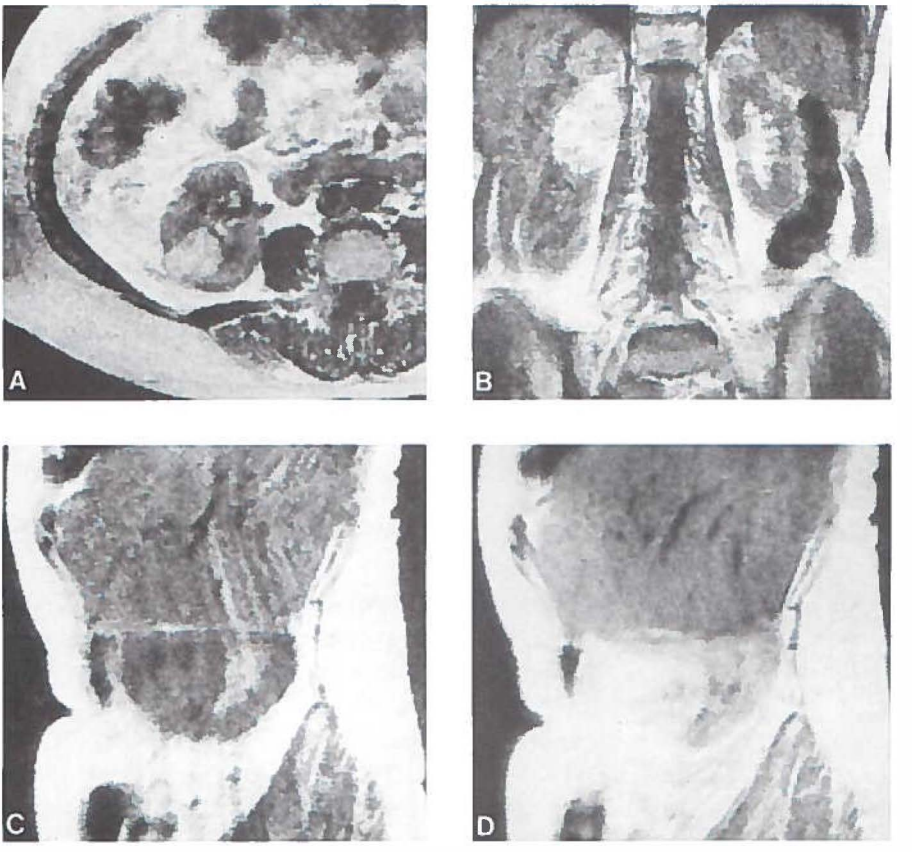

Fig. 1 a. Angiomyolipoma. Transverse section (SE TR=450 msec, TE=30 msec). Homogeneous bright fatty mass.
b. Angiomyolipoma. Coronal section (SE TR=350 msec, TE=30 msec). Inhomogeneous signal intensity consistent with a higher content of smooth muscle tissue and/or old hemorrhage.
c. Oncocytoma. Sagittal section (SE TR=250 msec, TE=30 msec). Tumor has well circumscribed borders; MR appearance is identical to Stage I renal cell carcinoma.
d. Same patient as 1c. Sagittal section (SE TR=1800 msec, TE=50 msec). T2 weighted image showing high signal intensity similar to perirenal fat.

Oncocytoma: The oncocytoma was diagnosed by both observers on MRI and CT as a Stage I renal cell carcinoma. The tumor showed a homogeneous distribution of signal intensities, which could not be differentiated from the signal intensity characteristics of a renal cell carcinoma (Fig 1c,d).
Transitional cell carcinoma: The transitional cell carcinoma was accurately diagnosed and staged with CT. However, this tumor was not detected at MRI (Fig. 2a,b).

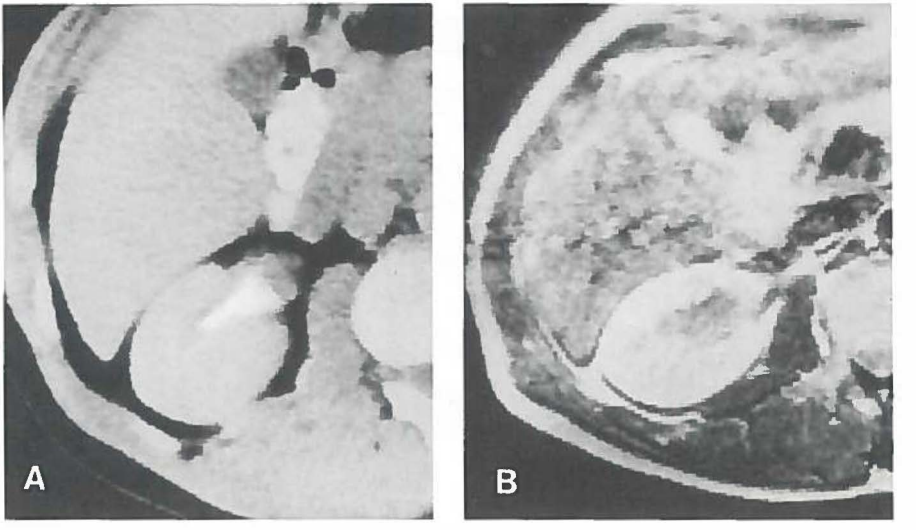

Fig. 2 a. Transitional cell carcinoma. Transverse CT section. Note small filling defect of transitional cell carcinoma in the renal pelvis.
b. Transitional cell carcinoma. Transverse section (SE TR=1850 msec, TE=50 msec). Transitional cell carcinoma was not detected at MRI.

Staging of renal cell carcinoma.

All twenty five renal cell carcinomas in 23 patients were shown on MRI and CT. The smallest tumor in this series measured 3 cm in diameter. The results obtained in the preoperative MRI and CT staging of twenty patients with renal cell carcinoma who underwent nephrectomy are first reported according to the accuracy for each stage separately (tables 2-5). Next is reported the agreement between observers with each technique as well as the agreement between MRI and CT for each observer (table 6).

a. *Extension into the perinephric space* (Stage I v.s.Stage II, table 2).
Extension into the perinephric fat was shown by the irregular contour of the tumor and in more advanced cases also by thickening of Gerota's fascia

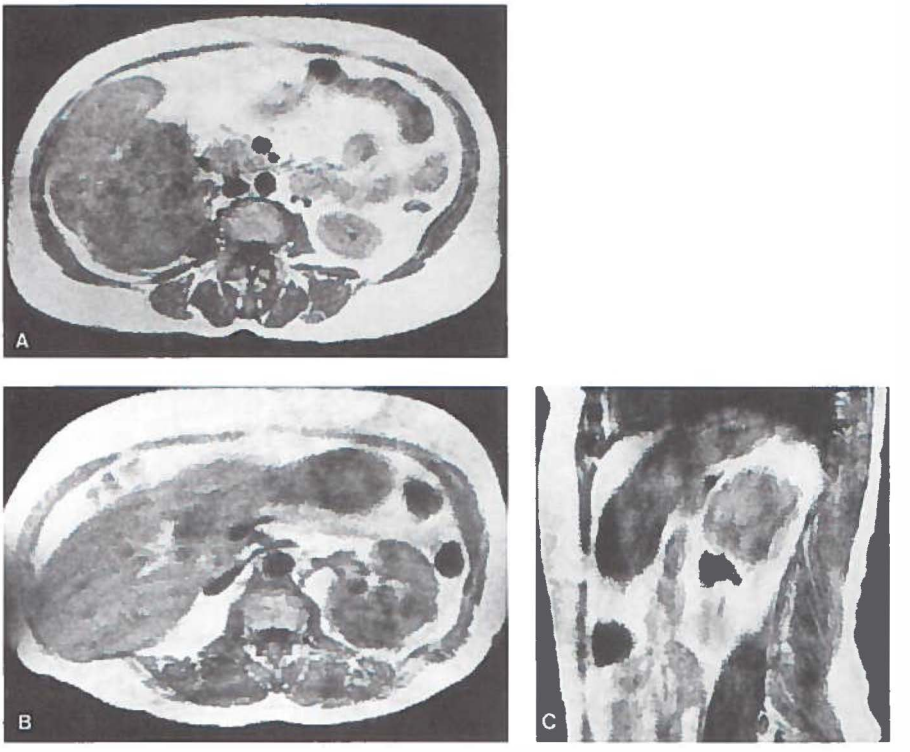

Fig. 3. a. Renal cell carcinoma. Stage III A. Transverse section (SE TR=550 msec, TE=30 msec.). Note irregular anterior contour and thickened Gerota's fascia due to perinephric extension. Intrarenal vein involvement was not detected.
b. Renal cell carcinoma. Stage I. Transverse section (SE TR=550 msec, TE=30 msec). Irregular margin of the tumor was interpreted as perinephric extension.
c. Same patient as 3b. Sagittal section (SE TR=800 msec, TE=30 msec). Note irregular tumor margin and blurring of the image due to respiratory motion.

(Fig. 3a). The number of false positive and false negative interpretations were slightly higher for MRI (25-30%) than for CT (15-25%). Unsharp and irregular borders accounted for a false positive diagnosis at MRI and could be partly explained in retrospect by the blurring of the MR image due to respiratory motion (Fig.3b,c).

b. *Extension into the renal vein and/or IVC* (Stage III A, table 3 and 4).
On MRI, extension into the intrarenal vein was not detected by both observers in the same two patients (Fig.3a). In a third patient, extension into the main renal vein was observed by O1 but missed by O2 (Fig.4a). At CT, O2 accurately established the presence of tumor thrombus in the intrarenal vein in one case which was not noted by O1.

Table 2

Stage II: extension into perinephric space (n= 20 nephrectomized patients)

	O_1		O_2	
	MRI n	CT n	MRI n	CT n
True positive	3	4	1	3
True negative	11	11	14	14
False positive	5	5	2	2
False negative	1	0	3	1
Accuracy	70%	75%	75%	85%

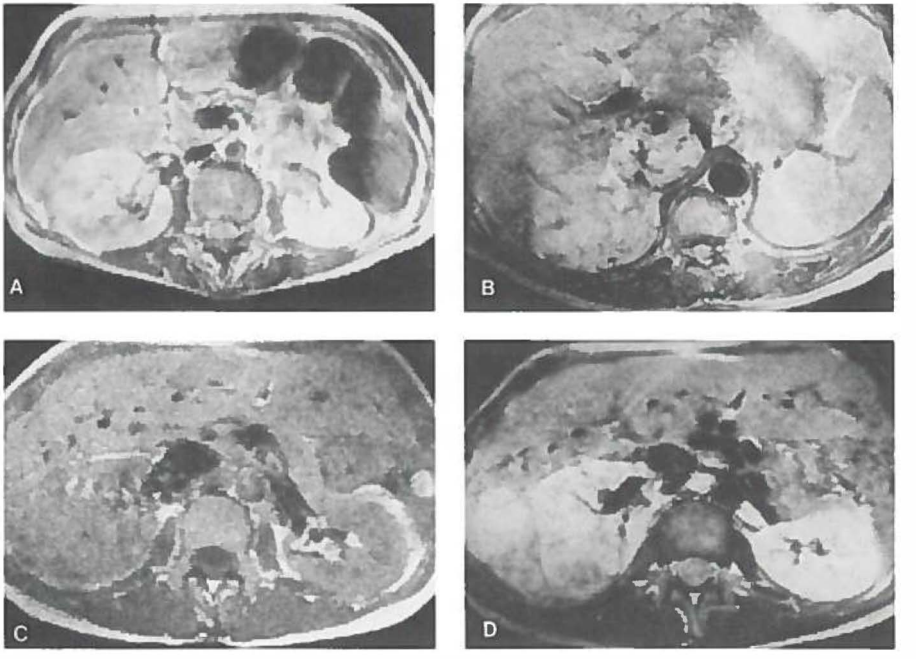

Fig. 4. a. Renal cell carcinoma, Stage III A. Transverse section (SE TR=2100 msec, TE=50 msec). Tumor extension into main renal vein.
b. Renal cell carcinoma, Stage III A. Transverse section (SE TR=2400 msec, TE=50 msec). Large tumor thrombus in IVC. Integrity of IVC wall difficult to assess.
c. Renal cell carcinoma. Stage IV A. Transverse section (SE TR=550 msec, TE=30 msec). Enlarged lymph node of low signal intensity in between IVC and aorta.
d. Same patient and section as 4c. (SE TR=2250 msec, TE=50 msec).
Lymph node of high signal intensity on T2 weighted image.
Histology revealed hyperplasia.

In one patient even in retrospect it was not possible to show tumor extension into the IVC on MRI or CT. Invasion of the IVC was found at nephrectomy two weeks following the MRI and CT examination. Prediction of invasion of the wall of the IVC was not possible in any of the 4 cases (Fig.4b).

Table 3

Stage IIIA: extension into renal vein (n=20 nephrectomized patients)

	O_1		O_2	
	MRI n	CT n	MRI n	CT n
True positive	4	3	3	4
True negative	14	14	14	13
False positive	0	0	0	1
False negative	2	3	3	2
Accuracy	90%	85%	85%	85%

Table 4

Stage IIIA: extension into inferior vena cava (n= 20 nephrectomized patients)

	O_1		O_2	
	MRI n	CT n	MRI n	CT n
True positive	3	3	3	3
True negative	16	16	16	16
False positive	0	0	0	0
False negative	1	1	1	1
Accuracy	95%	95%	95%	95%

c. *Lymph node involvement* (Stage III B, table 5).
The accuracy for the detection of metastatic lymph nodes is rather low. During laparotomy in 5 cases enlarged lymph nodes up to 3 cm in diameter were found. Histology revealed hyperplasia without metastatic disease in all 5 cases. Enlarged lymph nodes were of relatively low signal intensity on the T1 weighted image and high signal intensity on the T2 weighted MR image (Fig.4c,d).

The accuracy for anatomical staging regarding the presence of enlarged lymph nodes is considerably better than the accuracy for the detection of metastatic lymph nodes.

Table 5

Stage IIIB: Lymph node involvement (n= 20 nephrectomized patients).

	O_1		O_2	
	MRI n	CT n	MRI n	CT n
True positive	0	0	0	0
True negative	13	11	16	17
False positive	7(4*)	9(5*)	4(2*)	3(2*)
False negative	0	0	0	0
Accuracy	65%(85%**)	55%(80%**)	80%(90%**)	85%(95%**)

* enlarged lymph nodes at surgery, showing hyperplasia at histology
** accuracy for anatomic staging

d. *Extension into adjacent organs* (Stage IV A).
True extension into the liver was present in only one case and correctly diagnosed by O1 and O2 at MRI and CT (Fig. 5a). On MRI in one case and on CT in another case, O2 suspected invasion of the liver which was not confirmed at surgery. In one case O1 suspected extension of tumor on both MRI and CT scans. At surgery the tumor was found to be adherent to the liver but confined to the renal capsule (Fig. 5b). During nephrectomy in three other cases the tumor proved to be adherent to the liver (n=1), colon (n=2) or posterior abdominal wall (n=1; Fig.5c,d). None of these adhesions were suspected preoperatively on MRI and CT.

e. *Distant metastases* (Stage IV B).
One patient had bilateral renal cell carcinoma. All three tumors in this case, 4-8 cm in diameter, proved to be Stage I renal cell carcinomas at pathological examination. Clinically, there were no signs of distant spread and therefore all three tumors were considered to be most likely primary tumors. In one case on MRI only, O1 suspected a 2 cm metastatic lesion in the contralateral kidney, which was visible on CT in retrospect (Fig.6a,b). Preoperative fine needle biopsy was negative. No biopsy was performed during

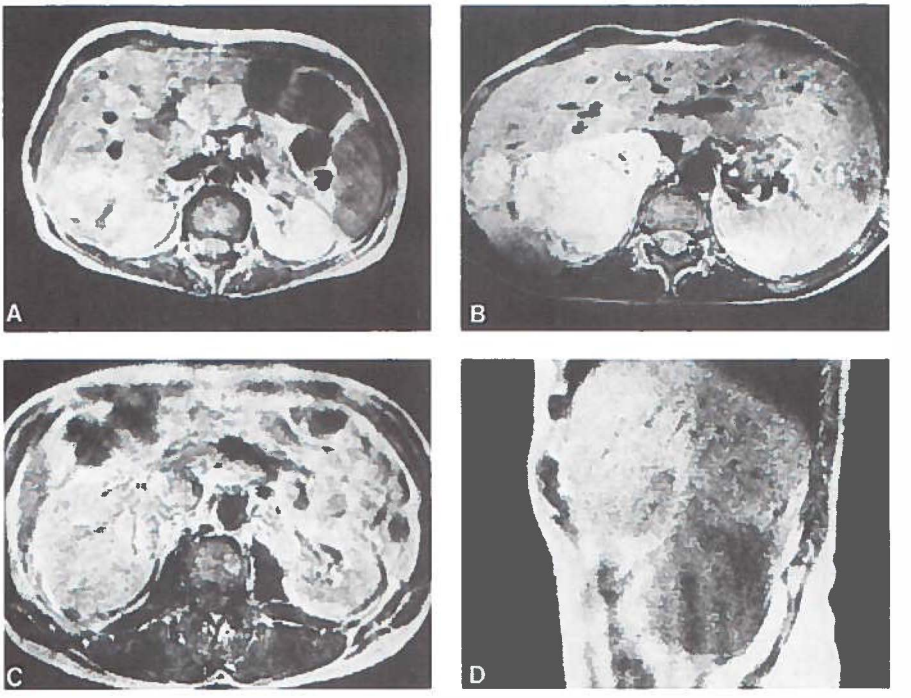

Fig. 5. a. Renal cell carcinoma. Stage III A. Transverse section (SE TR=2100 msec, TE=50msec). Indistinct border between liver and tumor. Adhesions were found at surgery.
b. Renal cell carcinoma, Stage IV A. Transverse section (SE TR=2250 msec, TE=50 msec). Indentation of indistinct tumor margin due to tumor extension into the liver.
c. Renal cell carcinoma, Stage III A. Transverse section (SE TR=2100 msec, TE=50 msec). Extension of tumor into IVC and perinephric fat with thickened Gerota's fascia.
d. Same patient and section as 5c. Sagittal section (SE TR=800 msec, TE=30msec). At surgery the tumor was adherent to posterior abdominal wall which was not suspected at MRI.

nephrectomy and the patient died from metastatic disease 7 months later. Autopsy was not performed. In two of the three patients who were inoperable, bone- and lung metastases were diagnosed at MRI and CT (Fig. 6c,d). A metastatic lesion in the rib was more apparent on the MR image than on CT because of higher contrast between the lesion and adjacent structures.

f. *Agreement between observers and between techniques* (Table 6a and 6b). Considerable disagreement between O1 and O2 for each technique and between MRI and CT for each observer was found for the assessment of perinephric extension and metastatic lymphnode involvement. Little variations

were noted for the determination of tumor extension into the renal vein and inferior vena cava. The percentage of variations were in the same range as the percentage of accuracy for staging of renal cell carcinoma (Table 2-5).

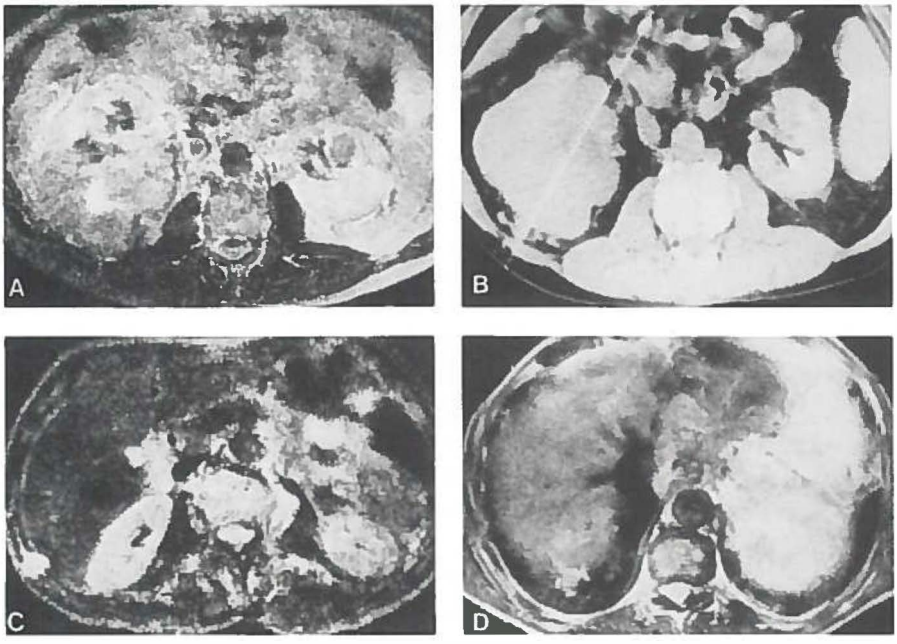

Fig. 6. a. Renal cell carcinoma, Stage III A. Transverse section (SE TR=2400 msec, TE=100 msec). Large tumor right kidney and small lesion of identical signal intensity, possibly metastasis, in contra-lateral kidney.
b. Identical section as 6a. CT scan in retrospect showed the same lesion.
c. Renal cell carcinoma, Stage IV B. Transverse section (SE TR=2100 msec, TE=100 msec). Note very bright metastasis to the rib.
d. Renal cell carcinoma, Stage IV B. Transverse section (SE TR=2250 msec, TE=50 msec). Metastasis to the right lung.

Table 6a

Staging of renal cell carcinoma: agreement between Observer 1 and Observer 2

Stage		MRI	CT
II:	perinephric extension	65 %	70 %
IIIA:	extension into renal vein	95 %	85 %
IIIA:	extension into inferior vena cava	100 %	95 %
IIIB:	metastatic lymph node involvement	85 %	70 %

Tabel 6b

Staging of renal cell carcinoma: agreement between MRI and CT

Stage		Observer 1	Observer 2
II:	perinephric extension	75 %	80 %
IIIA:	extension into renal vein	90 %	90 %
IIIA:	extension into inferior vena cava	95 %	100 %
IIIB:	metastatic lymph node involvement	80 %	80 %

V.5 Discussion

In this study MRI and CT provided similar diagnostic information concerning benign renal masses. All simple cysts were accurately diagnosed as such. The angiomyolipomas were characterized by their typical appearance on MRI and CT. The MR appearances varied from a homogeneous bright mass on the T1 and T2 weighted images to a more inhomogeneous mass of mixed signal intensity consistent with areas of a higher smooth muscle content or old hemorrhage within the tumor. These observations are in agreement with previous anecdotal reports (7,8, 12-15).
One patient underwent an excision biopsy in 1967 of a small tumor with the size of an hazelnut, which proved to be an oncocytoma. The mass recurred and was followed over a period of 18 years. At the time of MRI and CT, the mass was approximately 6 cm in diameter, well demarcated and could not be differentiated from a Stage I renal cell carcinoma.

Differentiation between oncocytoma and renal cell carcinoma is only possible histologically (16). Oncocytomas have shown a benign behaviour during a long period of follow up (17). Our patient was a 72 year old female without any signs of metastatic disease and no surgery was performed.

Contrast-enhanced CT appears to be more sensitive than MRI in the detection of a small transitional cell carcinoma within the renal pelvis. The transitional cell carcinoma in our series was not shown at MRI and an early report mentioned similar problems in differentiating the tumor from the urine within the renal pelvis (18).

The reported accuracy of CT in the staging of renal tumors ranges from 62-91% (table 7). In previous reports a number of causes for inaccurate staging have been described. Microscopic invasion of the perinephric fat may result in understaging of Stage II tumors (20). The lack of perirenal fat and/or the presence of edematous connective septa within the perirenal fat may cause overstaging of Stage I tumors at CT (2). For the same reasons inaccurate staging by

Table 7

Accuracy of CT for staging of malignant renal tumors

Author	Year	Number of cases studied	Accuracy %
Love(19)	1979	17	89
Karp(20)	1981	27	70
Cronan(5)	1982	23	91
Plainfosse(21)	1983	12	75
Elder(22)	1984	31	62

MRI of Stage I and Stage II tumors can be expected. Furthermore, respiratory movement artefacts, e.g. blurring of the MR image with subsequent loss of spatial resolution, appears to negatively affect the accuracy of MRI.

Respiratory artefacts at MRI may explain the slightly better accuracy of CT in the assessment of perinephric extension in our series.

Renal vein involvement cannot be diagnosed on CT in 9-13% of all renal cell carcinomas (2,19,23). Intrarenal vein involvement and the presence of tumor thrombus within the main right renal vein, which has an oblique course, may be difficult to assess. In our limited series MRI was not more sensitive than CT in detecting particularly intrarenal vein involvement.

Lymphadenopathy can be a further source of overstaging on MRI and CT. Not all lymphadenopathy noted at CT is due to metastatic involvement. Lymph node enlargement at surgery due to hyperplasia has been reported to be present in 3-17% of all patients (2,20,23). A prospective study in 27 patients yielded an accuracy of 96% for MRI in the anatomical staging of renal cell carcinoma (10). However, no comment was made on the histologic findings in the 10 cases of confirmed lymphadenopathy. In our own study 5 patients had lymphadenopathy, all due to hyperplasia. Similar to CT, MRI cannot differentiate between hyperplasia and lymphadenopathy due to metastatic involvement (24-26). Furthermore microscopic metastatic foci in lymph nodes of normal size will remain undetected by both MRI and CT.

Accurate determination of tumor extension into adjacent organs (Stage IV A) may be difficult with both MRI and CT. Previous studies have shown adhesions of tumor to adjacent organs without extension beyond the renal capsule (2,27). Adhesions in our series were found at surgery in 4 cases, causing in one case a false positive interpretation of Stage IV A at MRI.

We studied one patient with bilateral renal cell carcinoma. Based on the tumor Stage I of each carcinoma and the absence of distant metastases, all 3 tumors were probably primary tumors. Differentiation between concurrent bilateral Stage I renal cell carcinoma and a Stage IV B tumor was not possible with

MRI and is also clinically and histologically difficult (28). In one patient MRI demonstrated a lesion in the contralateral kidney which could not be verified by aspiration biopsy. Although not histologically proven, it seems not unlikely that this small lesion, which was only visible on the heavily T2 weighted MR image and primarily not noted on CT, did represent a metastasis.

Considerable inter- and intraobserver variations were found for the assessment of perinephric extension and metastatic lymph node involvement, being the principal causes of inaccurate staging.

The results in our study indicate that MRI at 0.5 T using conventional Spin Echo pulse sequences is not more accurate than CT in the characterization and staging of renal masses. Therefore, CT should be considered as the method of choice for staging renal cell carcinoma as long as no substantial improvements in MRI performance have been achieved.

V.6 References

1. Levine E, Lee KR, Weigel J. Preoperative determination of abdominal extent of renal cell carcinoma by computed tomography. Radiology 1979; 132: 395-398.
2. Weyman PJ, McClennan BL, Stanley RJ, Levitt RG, Sagel SS. Comparison of computed tomography and angiography in the evaluation of renal cell carcinoma. Radiology 1980; 137: 417-424.
3. Probst P, Hoogewoud HM, Haertel M, Zingg E, Fuchs WA. Computerized tomography versus angiography in the staging of malignant renal neoplasm. Br J Radiol 1981; 54: 744-753.
4. Mauro MA, Wadsworth DE, Stanley RJ, McClennan BL. Renal cell carcinoma: angiography in the CT era. AJR 1982; 139: 1135-1138.
5. Cronan JJ, Zeman RK, Rosenfield AT. Comparison of computerized tomography, ultrasound and angiography in staging renal cell carcinoma. J Urol 1982; 127: 712-714.
6. Richie JP, Garnick MB, Seltzer S, Bettm MA. Computerized tomography scan for diagnosis and staging of renal cell carcinoma. J Urol 1983; 129: 1114-1116.
7. Hricak H, Williams RD, Moon KL, Moss AA, Alpers C, Crooks LE, Kaufman L. Nuclear magnetic resonance imaging of the kidney: renal masses. Radiology 1983; 147: 765-772.
8. Choyke PL, Kressel HY, Pollack HM, Arger PM, Axel L, Mamourian AC. Focal renal masses: magnetic resonance imaging. Radiology 1984; 152: 471-477.
9. Herman SD, Friedman AC, Siegelbaum M, Ramchandani P, Radecki PD. Magnetic resonance imaging of papillary renal cell carcinoma. Urol Radiol 1985; 7: 168-171.
10. Hricak H, Demas BE, Williams RD, McNamara MT, Hedgcock MW, Ampara EG, Tanagho EA. Magnetic resonance imaging in the diagnosis and staging of renal and perirenal neoplasms. Radiology 1985; 154: 709-715.
11. Robson CJ, Churchill BM, Anderson W. The results of radical nephrectomy for renal cell carcinoma. J Urol 1969; 101: 297-301.
12. Leung AWL, Bydder GM, Steiner RE, Bryant DJ, Young IR. Magnetic resonance imaging of the kidneys. AJR 1984; 143: 1215-1227.
13. Kulkarni MV, Shaff MI, Sandler MP, Tishler J, Winfield AC, Patton JA, Wolfe O, Partain CL, James AE. Evaluation of renal masses by MR imaging. J Comput Assist Tomogr 1984; 8: 861-865.

14. Li Puma JP. Magnetic resonance imaging of the kidney. Radiol Clin North Am 1984; 22: 925-941.
15. Newhouse JH, Markisz JA, Kazam E. Magnetic resonance imaging of the kidneys. Cardiovasc Intervent Radiol 1986; 8: 351-366.
16. Lautin EM, Gordon PM, Friedman AC. McCormick JF, Fromowitz FB, Goldman MJ, Sugarman LA. Radionuclide imaging and computed tomography in renal oncocytoma. Radiology 1981; 138: 185-190.
17. Moura ACF, Nascimento AG. Renal oncocytoma: report of a case with unusual presentation. J Urol 1982; 127: 311-313.
18. Von Fiegler W, Felix R, Schörner W, Claussen C. Die Kernspintomographie bei raumfordernden Nierenprozessen. Fortschr Röntgenstr 1984; 141: 155-159.
19. Love L, Churchill R, Reynes C, Schuster GA, Moncada R, Berkow A. Computed tomography staging of renal carcinoma. Urol Radiol 1979; 1: 3-10.
20. Karp W, Ekelund L, Olafsson G, Olsson A. Computed tomography, angiography and ultrasound in staging of renal cell carcinoma. Acta radiol diagnosis 1981; 22: 625-633.
21. Plainfosse MC, Delecoeullerie G, Vital JL, Paty E, Merran S. 165 renal carcinomas: accuracy of imaging for diagnosis and spreadcost efficiency. Eur J Radiol 1983; 3: 132-137.
22. Elder DD, Orell SR, Sage MR, Sinclair GR, Marshall VR. The diagnosis and local staging of renal cancer-an appraisal. Aus NZ J Surg 1984; 54: 219-221.
23. Levine E, Maklad NF, Rosenthal SJ, Lee KR, Weigel J. Comparison of computed tomography and ultrasound in abdominal staging of renal cancer. Urology 1980; 16: 317-322.
24. Ellis JH, Bies JR, Kopecky KK, Klatte EC, Rowland RG, Donohue JP. Comparison of NMR and CT imaging in the evaluation of metastatic retroperitoneal lymphadenopathy from testicular carcinoma. J Comput Assist Tomogr 1984; 8: 709-719.
25. Lee JKT, Heiken JP, Ling D, Glazer HS, Balfe DM, Levitt RG, Dixon WT, Murphy WA. Magnetic resonance imaging of abdominal and pelvic lymphadenopathy. Radiology 1984; 153: 181-188.
26. Dooms GC, Hricak H, Moseley ME, Bottles K, Fisher M, Higgins CB. Characterization of lymphadenopathy by magnetic resonance relaxation times: preliminary results. Radiology 1985; 155: 691-697.
27. McClennan BL. Balfe DM. Oncologic imaging: kidney and ureter. Int J Rad Oncol Biol Phys 1983; 9: 1683-1704.
28. Stigsson L, Ekelund L, Karp W. Bilateral concurrent renal neoplasms: report of eleven cases. AJR 1979; 132: 37-42.

Chapter VI

MAGNETIC RESONANCE IMAGING (MRI) OF RENAL TRANSPLANTS

L. te Strake[1], L.J. Schultze Kool[1], L.C. Paul[2], A.M. Tegzess[3], J.J. Weening[4], J. Hermans[5], J. Doornbos[1], R.G. Bluemm[1], J.L. Bloem[1].

Departments of Radiology[1], Nephrology[2], Pathology[4], Medical Statistics[5] University Hospital Leiden, The Netherlands; Department of Nephrology[3], University Hospital Groningen, The Netherlands.

VI.1 Abstract

Purpose of this study was to determine the value of MRI in the differentiation of acute rejection and cyclosporin-A (CsA) nephrotoxicity in renal transplant kidneys. Fifty six MR examinations in 46 patients were prospectively and independently evaluated by 2 radiologists (O1 and O2). MRI was performed with a 0.5T superconducting MR scanner (Gyroscan S5, Philips) applying both T1 and T2 weighted pulse sequences. Biopsies were performed in 22 cases and histology was reviewed. Fifteen normally functioning transplant kidneys and 41 kidneys with graft dysfunction due to CsA nephrotoxicity, acute rejection, chronic rejection or acute tubular necrosis (ATN) were studied. Cortex-medulla demarcation (CMD) proved to be a sensitive, but non specific indicator of parenchymal disease.
In cases of CsA nephrotoxicity the allograft was diagnosed as being normal in 90% (O1) and 100% (O2). The MR appearance of acute rejection may be very similar to that of the combination of acute rejection and CsA nephrotoxicity, chronic rejection or ATN. However, differentiation between acute rejection and CsA nephrotoxicity was possible according to the following statistical data (O1-O2): sensitivity 97%-93%, specificity 80%-95%, positive predictive value 88-96%, negative predictive value 94%-90%, accuracy 90%-94%.

Clinical Radiology, accepted for publication; revised version submitted.

VI.2 Introduction

The differentiation between acute rejection and functional cyclosporin nephrotoxicity in renal transplant patients treated with CsA is both clinically and histologically a problem (1). Magnetic Resonance Imaging (MRI) is capable to show the normal anatomy of the transplant kidney and displays the cortex and medulla in a noninvasive way without the use of ionizing radiation (2). Previous studies have shown that MRI in acute rejection shows a swollen allograft with a prolonged T1 which is attributable to tissue edema (3). These early findings were confirmed by later investigations and it was shown, that the normal cortex-medulla demarcation (CMD) may be decreased or absent in case of acute or chronic rejection (4,5,6). The objective of the present study was to determine the value of MRI in the differentiation of acute rejection and CsA nephrotoxicity.

VI.3 Material and Methods

Fifty six MR examinations were performed in 46 adult renal transplant patients. The patients were selected by the nephrologists and referred for MRI without clinical information. The interval between transplantation and MRI varied from 6 days to 8 years. Eight patients were examined twice, and one patient had three MR examinations. Three patients received a kidney from a living related donor and 43 allografts came from a cadaveric donor. Twenty seven patients were treated with cylosporin-A (CsA).
CsA blood and serum levels were determined using a Radio Immuno Assay (RIA) method; CsA blood levels below 1000 ng/ml or serum levels below 400 ng/ml were considered normal. Since there is a linear relationship between CsA levels and degree of nephrotoxicity, the clinical diagnosis of CsA nephrotoxicity was based on the effect of lowering the CsA dose on graft function (7). The CsA blood levels in cases of CsA nephrotoxicity in this study varied from 1069-1670 ng/ml (mean 1401 ng/ml; n=6) or from 170-510 ng/ml (mean 391 ng/ml) in serum (n=4).

A graft biopsy was performed in conjunction with MRI in 22 patients with the following diagnoses: acute rejection (n=12), CsA nephrotoxicity (n=2), acute rejection with simultaneous CsA nephrotoxicity (n=2), and chronic rejection (n=6). In one patient MRI was performed while the graft function was normal; a biopsy was performed in this patient 2 days later and showed acute rejection. The 22 biopsies were reviewed and the histologic changes graded as normal, moderately abnormal or severely abnormal. Histologically, CsA nephrotoxicity was suspected if only few cellular infiltrates were present in as-

sociation with arteriolar constriction and degenerative changes of the tubular epithelium.

The final diagnosis at the time of MRI was based on histological and/or clinical findings, and included: normally functioning allograft (n=15), acute rejection (n=12), CsA nephrotoxicity (n=10) and acute rejection with simultaneous CsA nephrotoxicity (n=4). The latter diagnosis was based on the presence of histological and clinical signs of rejection together with a low filtration fraction, while the renal function improved after lowering of the CsA dosage only. Furthermore, 9 cases of chronic rejection and 1 case of acute tubular necrosis (ATN) were included in the study. Another 5 patients were examined with MRI while the renal function was still abnormal but improving during treatment for acute rejection (n=4) or ATN (n=1).

MRI-methods.

MRI was performed with a 0.5 T superconducting MR scanner (Gyroscan S5, Philips) applying both T1 and T2 weighted pulse sequences. Slice thickness was 1 cm, matrix size 256x256. Initially, 5 slices, 1 cm apart, were obtained in the transverse plane (TR=550 msec, TE=30 msec). From these images sagittal planes were selected and imaged twice (TR=550 msec, TE=30 msec and TR=900 msec, TE=30 msec) with contiguous slices. Then a T2 weighted pulse sequence (TR=2000 msec, TE=50 msec and 100 msec, multiecho technique) was applied in the transverse plane. In 36 MR examinations also a combined Spin Echo (TR=1000 msec, TE=50 msec, 4 echo's) and Inversion Recovery (TR=1400 msec, TI=400 msec, TE=50 msec) sequence were performed in the sagittal plane for T1 and T2 calculation. The signal intensities (SI) of cortex and medulla were measured on the sagital scans (TR=550 msec, TE=30 msec) and the cortico-medullary contrast (CMC) was calculated (8):

$$CMC = \frac{SI\ (cortex) - SI\ (medulla)}{SI\ (cortex) + SI\ (medulla)} \times 100\%$$

The MR examinations were evaluated by 2 radiologists, L.t.S (O1) and L.J.S.K. (02), independently and without knowledge of the clinical data. The cortex-medulla demarcation (CMD) on the T1 weighted images was graded as normal, decreased or absent. CMD on the T2 weighted images was graded as absent or increased, if visible.

Measurements of renal size or volume were not considered to be useful since baseline studies for comparison were not available. However, the shape of the kidney, normal or globular in appearance, was taken into account when establishing the MRI diagnosis.

The size of the pyramids was graded as normal, increased or not visible in ca-

ses of absent CMD. The signal intensity of the renal sinus fat was graded as normal or decreased. The size of the collecting system and the presence of focal parenchymal changes were assessed. MRI was considered to be normal, abnormal or slightly abnormal. In the latter case only a slightly decreased CMD was noted in an otherwise normal allograft and no specific diagnosis was possible since a decreased CMD can be found in a normally functioning kidney (5) or could also be expected during the initial stage of e.g. acute rejection and during or after treatment for acute rejection or ATN.

In this study the diagnosis of CsA nephrotoxicity was not made at MRI because no specific MR appearances are known or expected based on the histologic findings in CsA nephrotoxicity. The diagnosis of acute rejection was made if CMD was decreased or absent and if one or more of the following signs of rejection were noted: globular shape of the kidney due to swelling, enlarged pyramids and decreased SI of the renal sinus fat.

VI.4 Results

1. **Cortex-medulla demarcation** *(CMD), (Table 1).*

a. *Normally functioning transplant kidney.*

The CMD was considered to be normal in 47% (O1) and 60% (O2) of all 15 normally functioning allografts (Fig. 1a,1b). In four examinations on 3 pa-

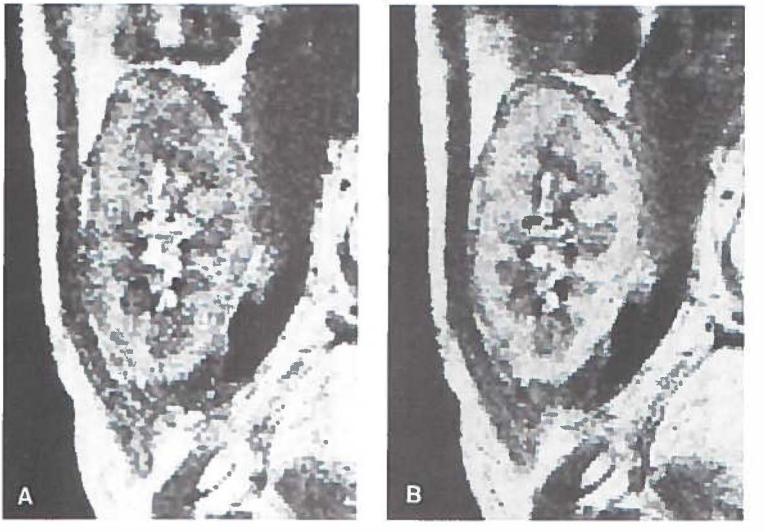

Fig. 1. Normally functioning allograft. Identical sections.
a. SE (TR=450 msec, TE=30 msec).
b. SE (TR=900 msec, TE=30 msec). Normal CMD. Bright renal sinus fat and patent hilar vessels.

tients with a normally functioning allograft both O1 and O2 graded CMD as decreased.

Table 1

Correlation between final clinical diagnosis and CMD (56 examinations).

		CMD normal			CMD decreased			CMD absent		
	n	O_1	O_2	both O_1/O_2	O_1	O_2	both O_1/O_2	O_1	O_2	both O_1/O_2
Normally functioning allograft	15	7	9	6	8	6	5	0	0	0
CsA nephrotoxicity	10	6	7	6	4	3	3	0	0	0
Acute rejection	12	1	1	0	10	9	8	1	2	1
Acute rejection and CsA nephrotoxicity	4	0	0	0	4	4	4	0	0	0
Chronic rejection	9	0	0	0	5	4	4	4	5	4
Improving dysfunction of allograft during treatment for acute rejection or ATN	5	0	1	0	3	2	2	2	2	2
ATN	1	0	0	0	1	1	1	0	0	0

The first patient was examined twice, 11 and 16 months after transplantation, and both O1 and O2 found twice a decreased CMD (Fig. 2). The diagnosis based on MRI findings was considered to be chronic rejection. The patient had on both occasions a normally functioning allograft, but was suffering from hypertension.

The second patient was examined on two occasions, the first time eleven days after transplantation with graft dysfunction due to ATN. MRI showed a decreased CMD and this case was our only example of ATN mimicking acute rejection. Eleven days later the same patient was re-examined after the renal function became normal. CMD was still decreased and both O1 and O2 found the allograft to be slightly abnormal. The MRI diagnosis suggested early or treated rejection.

The third patient was examined 9 days following transplantation. After an initial period of slowly improving renal function due to ATN, at the time of

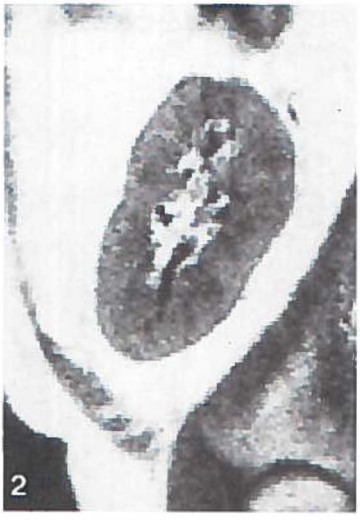

Fig. 2. Normally functioning allograft. SE (TR=450 msec, TE=30 msec). CMD decreased, probably due to hypertensive parenchymal changes.

Fig. 3. Normally functioning allograft. SE (TR=450 msec, TE=30 msec). Decreased CMD. Globular appearance of the transplant kidney. Residual changes after ATN.

MRI the allograft was functioning normally. CMD in this patient was however, decreased (Fig. 3). Thus all 3 patients had a normally functioning graft at the time of MRI and would not have been sent for this investigation under routine circumstances.

b. *CsA nephrotoxicity.*

CMD was considered to be normal by O1 in 6 and by O2 in 7 of the 10 examinations in CsA nephrotoxicity (Fig. 4). One patient was treated for a combination of acute rejection and CsA nephrotoxicity 19 days after transplantation. Three weeks later, while the patient was still on anti-rejection treatment, again impairment of renal function occurred, this time due to CsA nephrotoxicity. CMD was decreased and the diagnosis at MRI was acute (O1) and chronic rejection (O2). This patient definitely suffered from CsA nephrotoxicity but residual histologic changes due to previous acute rejection could very well have attributed to the abnormal appearance of the allograft at MRI. The statistical data will be presented both including this examination and the four examinations described under a, and after a correction which excluded the data of these 5 examinations.

c. *Acute rejection.*

CMD was considered to be decreased or absent in 92 % (O1 and O2) in acute rejection (Fig. 5, 6). When acute rejection and CsA nephrotoxicity

were present simultaneously, a decreased CMD was always noted (Fig. 7). The MRI diagnosis in these cases was acute rejection.

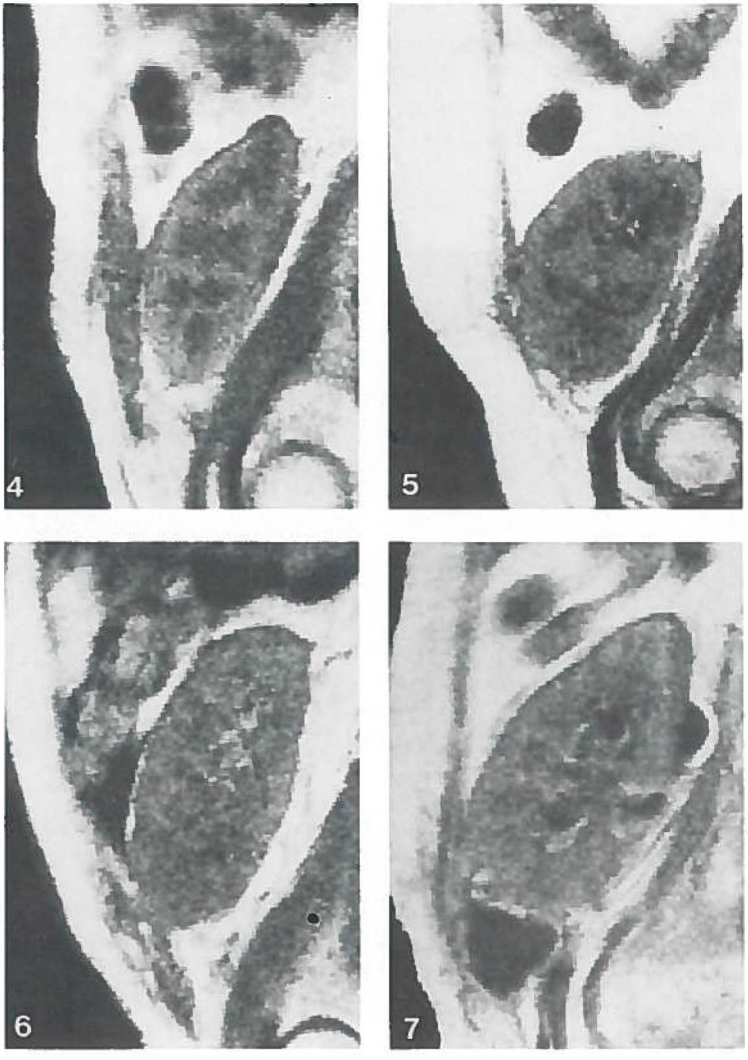

Fig. 4. Cyclosporin A nephrotoxicity. SE (TR=450 msec, TE=30 msec). Normal shape of the transplant kidney. Preservation of CMD.

Fig. 5. Acute rejection. SE (TR=450 msec, TE=30 msec). CMD is decreased. The allograft is globular in appearance.

Fig. 6. Acute rejection. SE (TR=450 msec, TE=30 msec). CMD is absent.

Fig. 7. Combination of acute rejection and CsA nephrotoxicity. SE (TR=450 msec, TE=30 msec). CMD decreased. MR appearance of allograft similar to that of acute rejection. Note perirenal fluid collection.

d. *Chronic rejection.*

In all 9 cases of chronic rejection a decreased or absent CMD was observed, while the shape of the kidney was relatively normal and renal sinus fat appeared bright on both T1 and T2 weighted pulse sequences (Fig. 8). In one case of chronic rejection a segmental area of low signal intensity was noted on the T2 weighted image and probably related to fibrotic changes secondary to previous acute rejection (Fig. 9).

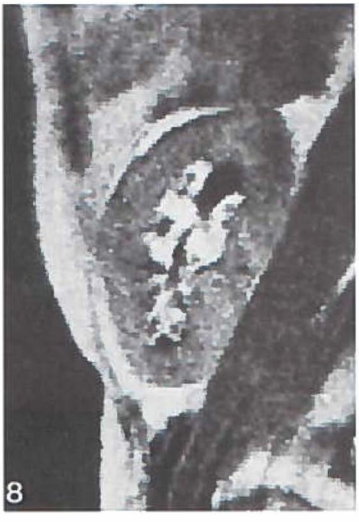

Fig. 8. Chronic rejection. SE (TR=900 msec, TE=30 msec). Complete loss of CMD. Normal shape of transplant kidney, Bright renal sinus fat.

Fig. 9. Chronic rejection. SE (TR=2100 msec, TE=100 msec). Note segmental area of low signal intensity and irregular contour of transplant kidney, most likely due to fibrotic changes following previous episodes of acute rejection.

e. *ATN.*

In the only one case of ATN the CMD was decreased and the MR appearance could not be differentiated from acute rejection (Fig. 10). Since only one patient with ATN was included in this study, this case will be excluded from further statistical analysis.

Fig. 10. ATN. SE (TR=550 msec, TE=30 msec). CMD decreased. MR appearance similar to that of acute rejection.

2. **Correlation between CMD and histology** *(Table 2).*
In order to determine the histologic changes that accounted for a loss of CMD, the histologic findings in 22 biopsies were correlated with the CMD. A loss of CMD appeared to be the result of predominantly tubulo-interstitial edema and mononuclear cell infiltration, and to a lesser extent vascular changes. Tubulo-interstitial fibrosis as a cause of decreased or absent CMD, was found only in chronic rejection.

3. **Statistical analysis** *(Table 3).*
When the MRI diagnosis was compared with the clinical and histological diagnosis it appeared that 53 (O1) and 67 % (O2) of all normally functioning transplant kidneys, and 80 (O1) and 90 % (O2) of all cases of CsA nephrotoxicity were diagnosed as being normal allografts at MRI. If the 4 patients (5 examinations) described under 1a and 1b are excluded, 73 (O1) and 91 % (O2) of normally functioning allografts, and 89 (O1) and 100 % (O2) of cases of CsA nephrotoxicity are diagnosed as being normal. Only 3 (O1) and 7 % (O2) of all cases with acute rejection only, with the combination of acute rejection and CsA nephrotoxicity or with chronic rejection were diagnosed as being normal at MRI.

Table 2

Correlation between histologic findings and CMD (22 examinations).

			CMD normal			CMD decreased			CMD absent		
		n	O_1	O_2	both O_1/O_2	O_1	O_2	both O_1/O_2	O_1	O_2	both O_1/O_2
Glomerular changes	- absent	18	3	4	2	13	11	10	2	3	2
	- mild	4	1	0	0	2	2	1	1	2	1
	- severe	0	0	0	0	0	0	0	0	0	0
Vascular changes	- absent	15	3	3	1	9	8	6	3	4	3
	- mild	7	1	1	1	6	5	5	0	1	0
	- severe	0	0	0	0	0	0	0	0	0	0
Tubulo-interstitial fibrosis	- absent	17	5	5	2	11	10	8	1	2	1
	- mild	2	0	0	0	1	0	0	1	2	1
	- severe	3	0	0	0	2	2	2	1	1	1
Tubulo-interstitial edema	- absent	4	2	2	2	2	2	2	0	0	0
	- mild	13	1	2	0	10	7	6	2	4	2
	- severe	5	1	0	0	3	4	3	1	1	1
Tubulo-interstitial cellular infiltrates	- absent	4	2	2	2	2	1	1	0	1	0
	- mild	12	0	2	0	10	7	7	2	3	2
	- severe	6	2	0	0	3	5	3	1	1	1
Medullary changes	- absent	11	3	2	2	7	6	5	1	3	1
	- mild	11	1	2	0	8	7	6	2	2	2
	- severe	0	0	0	0	0	0	0	0	0	0
Parenchymal bleeding	- absent	20	3	4	2	14	11	10	3	5	3
	- mild	2	1	0	0	1	2	1	0	0	0
	- severe	0	0	0	0	0	0	0	0	0	0

Table 3

Correlation between final clinical diagnosis and MRI diagnosis

		MRI Normal allograft			MRI Acute rejection			MRI Chronic rejection			MRI Slightly abnormal allograft, no specific diagnosis		
	n	O_1	O_2	both O_1/O_2	O_1	O_2	both O_1/O_2	O_1	O_2	both O_1/O_2	O_1	O_2	both O1/O2
Normally functioning allograft	15	8	10	7	0	1	0	2	2	2	5	2	1
CsA nephrotoxicity	10	8	9	8	1	0	0	0	1	0	1	0	0
Acute rejection	12	1	1	0	4	4	3	2	4	1	5	3	1
Acute rejection and CsA nephrotoxicity	4	0	0	0	3	2	2	0	1	0	1	1	1
Chronic rejection	9	0	0	0	0	3	0	7	5	4	2	1	0
Improving dysfunction of allograft during treatment for acute rejection or ATN	5	0	1	0	3	2	2	0	0	0	2	2	1
ATN	1	0	0	0	1	1	1	0	0	0	0	0	0

For statistical analysis the examinations were classified accordingly into two groups:
Group 1 included the normally functioning allografts and kidneys with CsA nephrotoxicity. Group 2 included acute rejection, the combination of acute rejection and CsA nephrotoxicity and chronic rejection. The MR findings regarding the size of the pyramids, renal sinus fat and the CMD on a T2 weighted image, are listed in table 4. When a CMD was noted on a T2 weighted image, the cortex was always of higher signal intensity than the medulla (Fig. 11).
Concerning the interobserver variations, the following results for the agreement between O1 and O2 were obtained on the 55 examinations:
CMD (T1 weighted pulse sequence) 82%, CMD (T2 weighted pulse sequence) 77%, size of renal pyramids 80%, SI renal sinus fat 62%.
The MRI diagnoses of O1 and O2 were in agreement with each other in 58% of cases if the clinical conditions and diagnoses were considered separately, and in 85% of cases if group 1 and group 2 were considered separately. The MRI diagnosis of both O1 and O2 was in agreement with the final clinical diagnosis in 38% of cases. However, if again group 1 and group 2 are considered as separate groups, the agreement improves considerably: 82% (O1) and 87% (O2). If a further correction is made for the 5 examinations described under 1a and 1b, the agreement between final clinical diagnosis and MRI becomes 90% (O1) and 96% (O2). MRI was found to differentiate between group 1 and

Table 4

MRI findings in Group 1* and Group 2**

	Group 1		Group 2	
	O_1	O_2	O_1	O_2
Pyramids: normal size	76%	92%	60%	66%
enlarged	24%	8%	20%	13%
not visible	0%	0%	20%	21%
Renal sinus fat: decreased signal intensity	4%	4%	7%	10%
Presence of CMD (T_2 weighted image)	50%	60%	26%	8%

Group 1* : normal allograft CsA nephrotoxicity
Group 2** : acute rejection, acute rejection and CsA nephrotoxicity, chronic rejection, allograft dysfunction during treatment acute rejection or ATN.

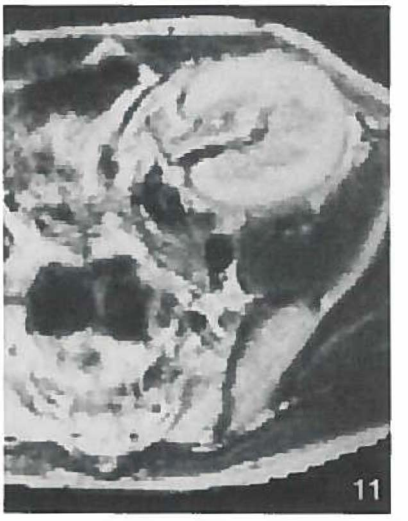

Fig. 11. Normally functioning allograft. SE (TR=2100 msec, TE=50 msec). Preservation of CMD on this T2 weighted image.

group 2 according to the following statistical data (O1-O2), (table 5, derived from table 3): sensitivity 97%-93%, specificity 64%-76%, positive predictive value 76%-82%, negative predictive value 94%-90%, accuracy 82%-85%. After correction, i.e. excluding five cases, the sensitivity became 97%-93%, specificity 80%-95%, positive predictive value 88%-96%, negative predictive value 94%-90%, accuracy 90%-94%.

Table 5

Correlation between final clinical diagnosis and MRI diagnosis

	n	MRI Normal Allograft Group 1			Abnormal Allograft Group 2		
		O_1	O_2	both O_1/O_2	O_1	O_2	both O_1/O_2
Group 1*	25	16	19	15	9	6	3
Group 2**	30	1	2	0	29	28	15

Group 1* : normal allograft, CsA nephrotoxicity.
Group 2** : acute rejection, acute rejection and CsA nephrotoxicity, chronic rejection, allograft dysfunction during treatment for acute rejection or ATN.

CMC was calculated from the signal intensity values of cortex and medulla. No statistically significant difference was found between the different groups of patients. Furthermore, the calculated T1 and T2 values of cortex and medulla obtained in the different groups were not significantly different.
The histologic diagnosis was in agreement with the final clinical diagnosis in 21 of the 22 patients who underwent renal biopsy (95%).
In one case of a combination of acute rejection and CsA nephrotoxicity, histology revealed only acute rejection.

VI.5 Discussion

An intact cortex medulla demarcation (CMD) on a T1 weighted MR image can be regarded as a hallmark for the integrity of the intrarenal anatomy.

Therefore, preservation of CMD should be expected in a normally functioning renal allograft. A normal CMD has also been described by Hricak et al. as a consistent finding in five cases of CsA nephrotoxicity (9). In our study CMD was decreased in 53% (O1) and 40% (O2) of all normally functioning allografts, and in 40% (O1) and 60% (O2) of CsA nephrotoxicity. Several factors may influence the cortico-medullary junction at MRI. Firstly, the CMD may vary with the hydration state. Increased hydration following a period of dehydration, shows a swelling of the medulla and therefore, a more prominent CMD at MRI (10). Furthermore Geisinger et al. have observed that CMD in certain cases of living related allografts is well preserved in the first 15 days following transplantation but may become less distinct as the polyuric phase subsides (5). The same authors described a normally functioning cadaveric transplant that had no detectable CMD (5). Hricak et al. did not observe any difference in CMD between the cadaveric and living related kidneys (9). The limited number of living related transplants in our study does not allow any conclusions as to possible differences in CMD between cadaveric and living related kidneys. In the present study four normally functioning allografts showed a decreased CMD as observed by both observers. The abnormal CMD may have been attributable to hypertensive changes of the renal parenchyma in two cases, and to residual histologic changes after previous ATN in two other cases. In one further case of CsA nephrotoxicity, the abnormal CMD may have been the result of residual parenchymal changes after previous acute rejection.

Leung et al. described a similar case of a normally functioning allograft and a decreased CMD due to previous episodes of rejection (11). It, therefore, appears that an abnormal CMD is a sensitive finding that may be attributable to residual histologic changes of previous ATN or acute rejection episodes even after the renal function has returned to normal. In 92% (O1 and O2) of pa-

tients suffering from acute rejection, an abnormal CMD was found. These findings are in agreement with the observations of Lipuma, who noted a decreased CMD in 92% of cases with transplant rejection (12). Also Baumgartner et al. observed a normal CMD in only 8% of the cases of acute and/or chronic rejection (13). Changes in CMD are, however, nonspecific and do not allow further differentiation between ATN, acute rejection, the combination of acute rejection and CsA nephrotoxicity, and chronic rejection. The appearance of CMD in ATN is variable. Leung at al. found a normal CMD in case of ATN (11). Geisinger et al. described a decreased CMD in ATN similar to acute rejection (5). Hricak et al. found a normal CMD in three out of four cases of ATN and a decreased CMD in one case (9). An experimental study in the mongrel dog also showed that MRI could not differentiate between ATN and acute rejection in all cases (14). The MR appearance of the allograft in the only case of ATN that we examined was similar to that of acute rejection.

The clinical and histologic findings may become even more complicated if allograft dysfunction is due to a combination of acute rejection and CsA nephrotoxicity (1,15). In the four cases that we examined, the MRI appearance of the allograft was similar to that of acute rejection. In chronic rejection, all cases showed a decreased or absent CMD.

The objective of our study was to determine the ability of MRI to differentiate between CsA nephrotoxicity and acute rejection. The normally functioning transplant kidney and the kidney with functional CsA nephrotoxicity tend to show a normal CMD. In acute rejection, in the combination of acute rejection and CsA nephrotoxicity, and in chronic rejection, CMD tends to be abnormal. Therefore, the patients were classified accordingly for statistical analysis into 2 different groups. In group 1 the pyramids were considered to be enlarged in 28% (O1) and 8% (O2) of the cases, and in group 2 enlarged or not visible in 40% (O1) and 34% (O2). It appears that apart from nonvisualisation of the pyramids, an increase in size of the pyramids may be helpfull as a parameter for the diagnosis of acute rejection. The signal intensity of the renal sinus fat on the other hand, was of little value as an indicator of rejection.

An unexpected finding was the presence of CMD on a T2 weighted image (TR=2000 msec, TE=50 msec), observed in 50% (O1) and 60% (O2) in group 1, and in 26% (O1) and 8% (O2) of cases in group 2. Lipuma noted a strong CMD on a relatively T2 weighted image with a long TE (TR=1000 msec, TE=60 msec) in four cases of ATN (12). We do not have a definite explanation for this observation although T1 effects cannot be excluded since the CMD tended to decrease or disappear on the more T2 weighted sequence (TR=2000 msec, TE=100 msec). Hricak et al. did not find any CMD on the T2 weighted images (9). Calculated T1 and T2 values, and CMC were not significantly different between the various groups. Geisinger et al. using a two-point method,

considered calculated T1 and T2 values unreliable and of no real benefit, possibly due to field inhomogeneities, partial-volume averaging, sampling errors and patient motion (5).

Hricak et al. only found statistically different values for CMC and T1 of the cortex in case of acute rejection.

The agreement between the various observations by O1 and O2 was rather good: CMD 82%, size of pyramids 80%, MRI diagnosis (group 1 v.s. group 2) 85%.

The agreement between the final clinical diagnosis and the MRI diagnosis concerning the differentiation between group 1 and group 2 was 82% (O1) and 87% (O2). Our statistical results were in the same range as those of Hricak et al., who found a sensitivity of 93% and a specificity of 94% in the differentiation of allografts with acute rejection from normally functioning allografts and those with ATN and CSA nephrotoxicity (9).

MRI in our study certainly compares favorably with other diagnostic techniques for the differentiation of acute rejection and CsA nephrotoxicity. The results of serial radionuclide studies using both Tc-99m DTPA (filtration) and I-131 hippuran (tubular function) suggest a sensitivity of 80% (16). Individual CsA blood levels are of no value for the differentiation between acute rejection and CsA nephrotoxicity; normal CsA blood levels may be found in case of CsA nephrotoxicity (1). One of our patients with CsA nephrotoxicity also had normal CsA serum levels (170 ng/ml).

Although in our study there was a good correlation between the final clinical diagnosis and the diagnosis based on histologic examination of graft dysfunction (95%), the place of renal biopsy is still subject to discussion. The histologic findings in CsA nephrotoxicity and acute rejection are often aspecific and show considerable overlap (1,16). In conclusion it appears from the results of our prospective study that MRI is a useful technique for the differentiation between acute rejection and CsA nephrotoxicity.

However, at the same time we also believe, taking into account the high cost and availability of MRI, that this modality at this moment cannot be considered as the primary imaging modality in renal transplantation and should be reserved for those cases only in which conventional examinations are insufficient or inconclusive (9,17).

VI.6 References

1. Taube DH, Williams DG, Hartley B, Rudge CJ, Neild GH, Cameron JS, Ogg CS, Welsh KI. Differentiation between allograft rejection and cyclosporin nephrotoxicity in renal transplant recipients. Lancet 1985; ii: 171-174.
2. Young IR, Boiles DR, Burl M, Collins AG, Smith DT, McDonell MJ, Orr JS., Bonks LM, Bydder GM, Greenspan RH, Steiner RE. Initial clinical evaluation of a whole body nuclear magnetic resonance (NMR) tomograph. J. Comput.Assist. Tomogr. 1982; 6: 1-18.
3. Smith FW, Reid R, Mallard JR, Hutchison JMS, Power DA, Catto GRD. Nuclear magnetic resonance tomographic imaging in renal disease. Diagnostic Imaging 1982; 51: 209-213.
4. te Strake L, Blickman JR, van der Hem GK, Hooykaas JAP, Poppema S, Brouwer-van Herwijnen AA. Imagerie RMN du rein. J Radiol 1984; 65: 631-635.
5. Geisinger MA, Risius B, Jordan ML, Zelch MG, Novick AC, George CR. Magnetic resonance imaging of renal transplants. AJR 1984; 143: 1229-1234.
6. Schultze Kool LJ, te Strake L, Paul LC, Tegzess AM, Bloem JL, Doornbos J, Bluemm RG. Magnetic resonance imaging renal transplants. Proc. EDTA-ERA 1985; 22: 609-613.
7. Henny FC, Kleinbloesem CH, Moolenaar AJ, Paul LC, Breiner DD, van Es LA. Pharmacokinetics and nephrotoxixity of Cyclosporin A in renal transplants. Transplantations 1985; 40: 261-265.
8. Thickman D, Kundel H, Biery D Magnetic resonance evaluation of hydronephrosis in the dog. Radiology 1984; 152: 113-116.
9. Hricak H, Terrier F, Demas BE. Renal allografts: evaluation by MR imaging. Radiology 1986; 159: 435-441.
10. Hricak H, Crooks L, Sheldon P, Kaufman L. Nuclear magnetic resonance imaging of the kidney. Radiology 1983; 146: 425-432.
11. Leung AWL, Bydder GM, Steiner RE, Bryant DJ, Young IR. Magnetic Resonance Imaging of the kidneys. AJR 1984; 143: 1215-1227.
12. LiPuma JP, Magnetic resonance imaging of the kidney. Radiol Clin North Amer 1984; 22: 925-941.
13. Baumgartner BR, Nelson RC, Ball TI, Wyly JB, Bourke E, Delany V, Bernardino ME. MR imaging of renal transplants. AJR 1986; 147: 949-953.
14. Terrier R, Hricak H, Revel D, Alpers C, Bretan P, Ehman RL, Feduska NJ. Magnetic Resonance Imaging in the diagnosis of acute renal allograft rejection and its differentiation from acute tubular necrosis. Experimental study in the dog. Invest. Radiol. 1985; 20:617-625.
15. Sibley RK, Rynasiewicz J, Ferguson RM, Fryd D, Sutherland DER, Simmons RL, Najarian JS. Morphology of cyclosporine nephrotoxicity and acute rejection in patients immuno-suppressed with cyclosporine and prednisone. Surgery 1983; 94:225-234.
16. Kim EE, Pjura G, Lowry P, Verani R, Sandler C, Flechner S, Kahan B. Cyclosporin-A nephrotoxicity and acute cellular rejection in renal transplant recipients: correlation between radionuclide and histologic findings. Radiology 1986; 159: 443-446.
17. Halasz NA. Differential diagnosis of renal transplant rejection: Is MR imaging the answer? AJR 1986; 147: 954-955.

Chapter VII

MRI: QUO VADIS?

VII.1 Introduction

When in 1984 the imaging protocols for this thesis were set up, spin echo (SE) pulse sequences were considered most suited for MR imaging of the kidney.

Conventional SE technique has some limitations as outlined in chapter III. The main problems are the long acquisition times with subsequent movement artefacts, and inaccurate T1 and T2 measurements.

The lack of specificity regarding tissue characterization is at present a major drawback of any imaging modality. MRI is still in a state of development. A number of current and new developments aiming at improved MR performance are discussed in this chapter.

VII.2 Contrast agents

The administration of contrast agents in MRI may be useful for the differentiation between iso-intense tissues, the evaluation of tissue function and perfusion, as well as for the study of metabolic pathways (1). A number of different contrast agents have been studied. Paramagnetic substances are the most commonly evaluated.

Paramagnetic contrast agents alter their local magnetic environment and shorten the relaxation times of tissues (1,2). After intravenous injection of the contrast material, the signal intensity of tissue on a T1 weighted image may become very bright as opposed to the low signal intensity on the nonenhanced image. Excellent delineation of poorly vascularized tissue from well perfused tissue is possible within a short acquisition time. Several nitroxide stable free radicals (TES and TCA) have shown to be effective in the study of ischaemic conditions in animal kidneys (3,4). For human studies, Gadolinium-DTPA (Gd-DTPA) has proven to be a safe and effective contrast agent. Gd-DTPA is administered at a dose of 0.1-0.5 mmol/kg and is excreted mainly, 90% within 24 hours after injection, through the kidneys (5,6,7). The toxicity of Gd-DTPA appears lower than that of iodinated contrast agents, e.g. the neural tolerance is several times better than for diatrizoate. The first report on the clinical application of Gd-DTPA, was in a patient with a renal cyst (8). Animal experiments

showed a good correlation between changes of T1 and T2 following the injection of Gd-DTPA and renal function (9). Gd-DTPA is also an effective oral contrast agent for the enhancement of the gastro-intestinal tract (11).

Recently we have studied some of the results of the clinical applications of a new paramagnetic contrast agent, Gd-DOTA (personal communications with B. Bonnemain, Laboratoire Guerbet). Like Gd-DTPA, Gd-DOTA is administered intravenously at a dose of 0.1 mmol/kg. Gd-DOTA appears to be at least as affective as Gd-DTPA. However, detailed comparative studies are needed before a statement can be made as to the differences between both contrast agents. A most exciting development is the use of immunospecific superparamagnetic contrast agents. Superparamagnetic contrast agents (e.g. magnetite Fe_2O_4) can be coupled to monoclonal antibodies and have shown in the mice a specific binding to a neuroblastoma specific cell surface antigen (12). This technique offers great potential for increased specificity of MRI in cancer diagnosis.

VII.3 Fast Imaging

An important improvement, which may in the short term drastically alter the impact of MRI in the evaluation of the upper abdomen, is the implementation of fast imaging techniques. The hybrid fast-scan technique reduces the imaging time by a factor 4 (13). More revolutionary is the Fast-Field-Echo (FFE) or Flash (fast low-angle shot) technique (14,15). This pulse sequence uses a short TR, e.g. 25 msec, and the RF excitation is done with a pulse angle much smaller than 90°. The RF energy absorption in the body is low.

An acquisition time of 2 seconds for a single slice is possible (14). Using 3-D technique extremely thin contiguous slices can be obtained with high S/N ratio and spatial resolution (15,16). The advantages are obvious: the acquisition time is shortened, resulting in a reduction or absence of motion artefacts, and patient throughput is increased considerably. Fast imaging techniques can be used in combination with i.v. administration of Gd-DTPA allowing the assessment of renal perfusion and qualitative evaluation of glomerular filtration rate (17,18). Since the acquisition time of FFE is short, the S/N ratio will be relatively poor. The initial results with FFE at 0.5 T at the University Hospital of Leiden, indeed indicated that a high field magnet (1.5 T or higher) is needed in order to achieve proper S/N ratio and image quality (Fig. 1,2).

Noteworthy is furthermore that the contrast obtained with FFE is completely different from the contrast using conventional pulse sequences. Extensive investigations considering the relation between SI, TR, pulse angle and tissue parameters are needed in order to determine proper pulse sequence optimization for fast MR imaging.

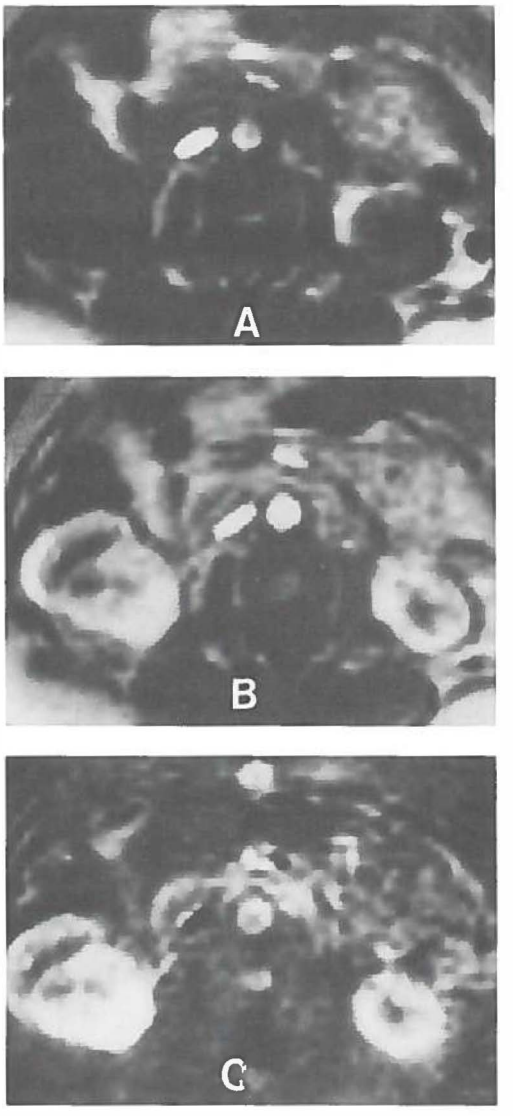

Fig. 1 Renal cell carcinoma right kidney.

a. FFE (flip angle 35°, scantime 3.2 sec.). Tumor of low signal intensity.

b. FFE (flip angle 35°, scantime 3.2 sec., scan interval 4 sec.). Twenty seconds following i.v. bolus injection of 0.1 Gd-DTPA. Note enhancement of tumor and normal cortex of right and left kidney.

c. Subtraction image.

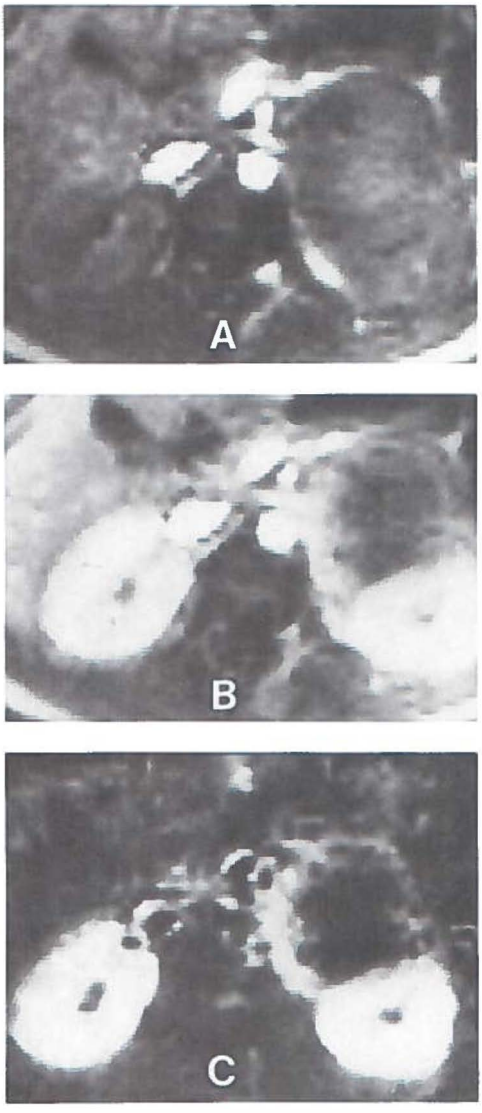

Fig. 2 Retroperitoneal metastasis of ovarium carcinoma.

a. FFE (flip angle 35°, scantime 3.2 sec., scan interval 4 sec.). Note indistinct border between isointense tumor and left kidney.

b. FFE (flip angle 35°, scantime 3.2 sec.). Forty eight seconds following i.v. bolus injection of 0.1 Gd-DTPA.
Note enhancement of renal parenchyma as opposed to low intensity partly necrotic metastasis.

c. Subtraction image.
(Fig. 1 and 2: Courtesy of Dr. R.G. Bluemm)

VII.4 Flow

The complex relation between the appearance of blood flow on a MR image, different flow patterns, flow velocities and different ways to acquire the data has been studied and described extensively (19,20,21,22,23). Blood flow velocity (cm/sec) can be measured in vivo and flow rates (ml/sec) calculated (24). Quantitative data on blood flow can be obtained in several ways. Phase-sensitive imaging allows the measurement of flow velocity by determining phase shifts in the MR image (25,26). Using this technique good general agreement has been observed between flow measurements of the carotid arteries obtained with MRI and Doppler ultrasound (25). The time-of-flight method represents a more direct means of imaging profiles of velocity distribution (27). Although it has been demonstrated that qualitative and quantitative blood flow measurements are possible, much more research and experience is needed before reliable and reproducible data in a clinical setting on a routine basis will be feasible.

VII.5 Chemical shift imaging

The first chemical shift images in vivo in a normal volunteer were published in 1983 and it was stated that chemical shift imaging would be potentially useful for tissue characterization (28). The technique is based on the difference in resonance frequency (3.5 ppm) for hydrogen and lipid protons. This difference in resonance frequency can be detected by conventional whole body MR scanners and can be used to display specifically the water or lipid protons instead of the composite image. The first chemical shift images in a patient showing bone marrow involvement of chronic myeloid leucaemia were obtained at 0.17 T and published in 1984 (29). Dixon has described the phase contrast technique which uses 2 acquisitions displaying water only, fat only or the difference between water and fat intensity (30). This method proved to be useful for the investigation of red and white bone marrow disease and is capable of detecting liver metastases as small as 1 cm, which are not visible on conventional MRI or CT (31,32).

Joseph described a selective spin echo technique which uses one acquisition to obtain a water or lipid image (33). Chemical shift selective (CHESS) MRI is another way to selectively display water or fat (34). The water, fat and the composite image can be recorded simultaneously by using multi-CHESS imaging in combination with STEAM (stimulated-echo acquisition mode)(35). Recently a fast chemical shift imaging technique has been presented allowing the acquisition of 16 images in 3.5 minutes (36). Chemical shift imaging has not

only shown to be useful for the study of bone marrow and liver disease but appears to be also useful for better delineation of water containing tumors in regions of high lipid content, e.g. the breast (37,38).

It is to be expected that a more accurate assessment can be made in selected cases of perirenal extension of renal cell carcinomas.

Interesting is the superior display of synovial structures in the hip joint compared to the conventional composite image (34).

VII.6 MR diffusion imaging

A shortened T2 relaxation time of simple fluids, at least tenfold shorter than T1, has been observed and attributed to molecular self-diffusion (39). The effect and calculation of self-diffusion on the attenuation of NMR signals was first described by Hahn in 1950 (40).

The random Brownian motion of molecules in a magnetic field gradient causes random phase shifts, resulting in a decreased echo amplitude (41). By applying two SE sequences which eliminate the effects of T1, T2 and proton density, the diffusion coefficient can be calculated and shown on a calculated image (41). Early experiments on phantoms with the stimulated-echo acquisition mode(STEAM) already demonstrated the feasibility of producing images, which display the self-diffusion coefficient (42). In patients with brain tumors the diffusion coefficient of tumor tissue is lower than that of the surrounding edema because of the restricted diffusion in the tumor tissue (41). Using this method, self-diffusion and perfusion (the microcirculation of blood in the capillary network) can be imaged and calculated separately extending the potential of tissue characterization and functional studies (41,43). In the transplant kidney the demonstration of edema and reduced perfusion may be useful in the diagnosis of acute rejection.

VII.7 Spectroscopy

Spectroscopy is commonly used as a general term for NMR experiments other than simple proton imaging, including proton chemical shift imaging (30), ^{31}P spectroscopic imaging (44) and the investigation of spectra of elements including ^{1}H (45). Spectroscopy deals with chemical shifts, which may be different for a single nucleus depending on its magnetic environment(45). An example is the different resonance frequency and chemical shift for protons in water, lipids and lactate. Elements other than ^{1}H are less abundant in the human body than ^{1}H and produce a very much weaker signal than protons. The-

refore S/N ratio in experiments involving these nuclei will be relatively poor and need to be maximized by using a high static magnetic field, surface coils and for imaging often long acquisition times. Differences in chemical shift may be very small, requiring a highly homogeneous magnetic field for detection. The homogeneity of the magnetic field can be increased over a larger volume by selecting a strong static magnetic field of at least 1.5 T.

The relaxation times of other elements may be either shorter or longer than those of ^{1}H. Sodium(^{23}Na) has a short T1, phosphorus (^{31}P) has a long T1 compared to protons. Therefore sodium images with a spatial resolution of 4 mm can be acquired within the same time as and even simultaneously with proton images (46,47,48). The clinical potential and use of sodium MRI has to be determined yet.

Phosphorus (^{31}P) imaging at 1.5 T on the other hand requires much longer acquisition times of at least one hour at a much lower spatial resolution of 1-2 cm, indicating the need for an even higher magnetic field strength (44,45). A more practical application of ^{31}P spectroscopy at the moment is the investigation of ^{31}P-spectra, which can be acquired within 5 minutes in combination with proton MRI for localization (50). ^{31}P-spectroscopy combined with proton imaging has been succesfully used to monitor in vivo the effects of radiotherapy in brain tumors (51). In vitro experiments on renal cell carcinomas already indicated earlier the possible application of ^{31}P NMR imaging to assess the therapeutic response during regional perfusion of malignant tumors in man (52). ^{31}P spectroscopy is a promising tool for the study of in vivo metabolism. It has been applied for in vivo studies not only of the brain but also of other areas in the body including the transplant kidney (53,54). The determination of the monophosphate to inorganic phosphate(MP/Pi) ratio appears to be a useful parameter for the determination of allograft viability (52). Furthermore ^{31}P spectroscopy could possibly be applied to study renal function and metabolism in patients with renal failure (55).

Carbon (^{13}C) spectroscopy so far has shown to be effective for the evaluation of fat, glycogen and hepatic ethanol metabolism (56,57). In vivo spectroscopy is still in its infancy, but indeed is a promising tool to improve the specificity of NMR.

VII. 8 References

1. Brash RC. Work in progress: methods of contrast enhancement for NMR imaging and potential applications. A subject review. Radiology 1983; 147: 781-788.
2. Runge VM, Stewart RG, Clanton JA, Jones MM, Lukehart CM, Partain CL, James AE. Work in progress: potential oral and intraveneous paramagnetic NMR contrast agents. Radiology 1983; 147: 789-791.
3. Brash RC, London DA, Wesbey GE, Tozer TN, Nitecki DE. Williams RD, Doemeny J, Tuck LD, Lallemand DP. Work in progress: nuclear magnetic resonance study of a paramagnetic nitroxide contrast agent for enhancement of renal structures in experimental animals. Radiology 1983; 147: 773-779.
4. Lamarque JL, Almès C, Rouanet JP, Prat X, Bruel JM, Pujol J. Rodière MJ, Martin JM, Lopez P, Rossi M, Zanca M, Bonnet PA, Subra G, Suné A, Robbe Y, Boucard M, Michel A, Fernandez JP. Chapat JP. Ideal imaging in MR: contrast-enhancing pharmaceuticals. Evaluation of tempo carboxilic acid as nitroxide diagnostic agent. Europ J Radiol 1986; 6: 48-52.
5. Weinman HJ, Brasch RC, Press W-R, Wesbey GE. Characteristics of gadolineum-DTPA complex: a potential NMR contrast agent. AJR 1984; 152: 619-624.
6. Runge VM, Clanton JA, Herzer WA, Gibbs SJ, Price AC, Partain CL, James AE. Intravascular contrast agents suitable for magnetic resonance imaging. Radiology 1984; 153: 171-176.
7. Wolf GL, Fobben ES. The tissue proton T1 and T2 response to gadolineum DTPA injection in rabbits. A potential renal contrast agent for NMR imaging. Invest Radiol 1984; 19: 324-328.
8. Schoerner W, Laniado M, Felix R. Erster Klinischer Einsatz von Gadolineum-DTPA in der Kernspin Tomographischen Darstellung einer parapelvinen Nierencyste. Röfo 1984; 141: 227-228.
9. Weininger J, Abrashkin S. Renal function correlated with proton magnetic resonance (MR) measurements in rats. Fifth annual meeting SMRM 1986; 4: 1547(ab).
10. Kaude JV, Ackerman N, Yancey JM, Googe RE, Hackett RL, Mancuso AA, Hagen DA, Caballero J, Scott KN. Improvement of MRI diagnosis of renal cell carcinoma by gadolineum-DTPA. An experimental study in rabbits. Fifth annual meeting SMRM 1986. WIP, Vol 1: 275-276(ab).
11. Kornmesser W, Hamm B, Laniado M, Clauss W. First clinical use of Gd-DTPA for gastrointestinal contrast enhancement. Society of magnetic resonance in medicine. Book of abstracts 1986; 4: 1522-1523.
12. Renshaw PF, Owen CS, Evans AE, Leigh JS. Immunospecific NMR contrast agents. Magn Res Imag 1986; 4: 351-357.
13. Haacke EM, Bearden FH, Clayton JR, Linga NR. Reduction of MR imaging time by the hybrid fast-scan technique. Radiology 1986; 158: 521-529.
14. van der Meulen P, Groen JP, Cuppen JJM. Very fast MR imaging by field echoes and small angle excitation. Magn Res Imag 1985; 3: 297-299.
15. Matthaei D, Frahm J, Haase A, Hänicke W, Merbolt KD. Three-dimensional flash MR imaging of thorax and abdomen without triggering or gating. Mag Res Imag 1986; 4: 381-386.
16. Frahm J, Haase A, Matthaei D. Rapid three-dimensional MR imaging using the FLASH technique. J Comput Assist Tomogr 1986; 10: 363-368.
17. Bluemm RG, Doornbos J, van der Meulen P, Cuppen J, Clauss W. First clinical results of fast-field echo(FFE) MR imaging: a very fast imaging technique. Radiology 1985; 157(P): 335(ab).
18. Pettigrew RI, Avruch L, Dannels W, Coumans J, Bernardino ME. Fast-field-echo MR imaging with Gd-DTPA: physiologic evaluation of the kidney and liver. Radiology 1986; 160: 561-563.

19. Bradley WG, Waluch V, Lai KS, Fernandez EJ, Spalter C. The appearance of rapidly flowing blood on magnetic resonance images. AJR 1984; 143: 1167-1174.
20. George CR, Jacobs G, MacIntyre WJ, Lorig RJ, Go RT, Nose Y, Meany TF. Magnetic resonance signal intensity patterns obtained from continuous and pulsatile flow models. Radiology 1984; 151: 421-428.
21. Axel L. Blood flow effects in magnetic resonance imaging. AJR 1984; 143: 1157-1166.
22. Bradley WG, Waluch V, Blood flow: Magnetic resonance imaging. Radiology 1985; 154: 443-450.
23. Crooks LE, Kaufman L. NMR imaging of blood flow. Br Med Bull 1984; 40: 167-169.
24. Singer JR. Nuclear magnetic resonance blood flow measurements. Cardiovasc Intervent Radiol 1986; 8: 251-259.
25. Bryant DJ, Payne JA, Firmin DN, Longmore DB. Measurement of flow with NMR imaging using a gradient pulse and phase difference technique. J Comput Assist Tomogr 1984; 8: 588-593.
26. Valk PE, Hale JD, Crooks LE, Kaufman L, Roos MS, Ortendahl DA, Higgins CB. MRI of blood flow: correlation of image appearance with spin-echo phase shift and signal intensity. AJR 1986; 146: 931-939.
27. Axel L, Shimakawa A, MacFall J. A time-of-flight method of measuring flow velocity by magnetic resonance imaging. Magn Res Imag 1986; 4: 199-205.
28. Pykett IL, Rosen BR. Nuclear magnetic resonance: in vivo proton chemical shift imaging. Radiology 1983; 149: 197-201.
29. Sepponen RE, Sipponen JT, Tanttu JI. A method for chemical shift imaging: demonstration of bone marrow involvement with proton chemical shift imaging. J Comput Assist Tomogr 1984; 8: 585-587.
30. Dixon WT. Simple proton spectroscopic imaging. Radiology 1984; 153: 189-194.
31. Wismer GL, Rosen BR, Buxton R, Stark DD, Brady TJ. Chemical shift imaging of bone marrow: preliminary experience. AJR 1985; 145: 1031-1037.
32. Lee JKT, Heiken JP, Dixon WT. Detection of hepatic metastases by proton spectroscopic imaging. Work in progress. Radiology 1985; 156: 429-433.
33. Joseph PM. A spin echo chemical shift MR imaging technique. J Comput Assist Tomogr 1985; 9: 651-658.
34. Frahm J, Haase A, Hänicke W, Mattthaei D, Bomsdorf H, Helzel T. Chemical shift selective MR imaging using a whole-body magnet. Radiology 1985; 156: 441-444.
35. Matthaei D, Frahm J, Haase A, Merboldt KD. Hänicke W. Multipurpose NMR imaging using stimulated echoes. Magn Res Med 1986; 3: 554-561.
36. Ströbel B, Ratzel D. Fast chemical shift imaging. Fifth annual meeting SMRM 1986; 3: 664-665(ab).
37. Rosen BR, Carter EA, Pykett IL, Buchbinder BR, Brady TJ. Proton chemical shift imaging: an evaluation of its clinical potential using an in vivo fatty liver model. Radiology 1985; 154: 469-472.
38. Brateman L. Chemical shift imaging: a review. AJR 1986; 146: 971-980.
39. Wesbey GE, Moseley ME, Ehman RL. Translational molecular self-diffusion in magnetic resonance imaging. 1. Effects on observed spin spin relaxation. Invest Radiol 1984; 19: 484-490.
40. Hahn EL. Spin echoes. Phys Rev 1950; 80: 580-594.
41. Le Bihan D, Breton E, Lallemand D, Grenier P, Cabanis E, Laval-Jeantet M. MR imaging of intra-voxel incoherent motions: application to diffusion and perfusion in neurologic disorders. Radiology 1986; 161: 401-407.
42. Merboldt KD. Hänicke W, Frahm J. Self-diffusion NMR imaging using stimulated echoes. J Magn Reson 1985; 64: 479-486.

43. Le Bihan D, Breton E, Guéron M. Separation of perfusion and diffusion in intra-voxel incoherent motion (IVIM) MR imaging. Fifth Annual Meeting SMRM 1986; WIP: 7-8(ab).
44. Maudsley AA, Hilal SK, Simon HE, Wittekoek S. In vivo MR spectroscopic imaging with P-31. Radiology 1984; 153: 745-750.
45. Kushmerick MJ. Spectroscopic applications of magnetic resonance to biomedical problems. Cardiovasc Intervent Radiol 1986; 8: 382-389.
46. Feinberg DA, Crooks LA, Kaufman L, Brant-Zawadzki M, Posin JP, Arawaka M, Watts JC, Hoenninger J. Magnetic resonance imaging performance: a comparison of sodium and hydrogen. Radiology 1985; 156: 133-138.
47. Hilal SK, Maudsley AA, Ra JB, Simon HE, Roshmann P, Wittekoek S; Cho ZH, Mun SK. In vivo NMR imaging of sodium-23 in the human head. J Comput Assist Tomogr 1985; 9: 1-7.
48. Lee SW, Hilal SK, Cho ZH. A multi nuclear magnetic resonance imaging technique-simultaneous proton and sodium imaging. Magn Res Imag 1986; 4: 343-350.
49. Radda GK, Bore PJ, Rajagopalan B. Clinical aspects of ^{31}P NMR spectroscopy. Br Med Bull 1984; 40: 155-159.
50. Bottomley PA, Hart HR, Edelstein WA, Schenck JF, Smith LS, Leue WM, Mueller OM, Redington RW. Anatomy and metabolism of the normal human brain studied by magnetic resonance at 1,5 T. Radiology 1984; 150: 441-446.
51. den Hollander JA, Arnold DA, Baleriaux D, Segebarth C, Luyten PR. Phosphorus-31 MR spectroscopic evaluation of treatment of human brain tumors in situ. Radiology 1986; 161(P): 92.
52. Ross B, Marshall V, Smith M, Bartlett S, Freeman D. Monitoring response to chemotherapy of intact human tumors by ^{31}P nuclear magnetic resonance. Lancet 1984; 1(8378): 641-646.
53. Bore PJ. Principles and applications of phosphorus magnetic resonance spectroscopy. Magnetic Resonance Annual 1985: 45-69. Ed. H.Y. Kressel, Raven Press, New York, 1985.
54. Ross BD, Radda GK, Gadian DG, Rocker G, Esiri M, Falconer-Smith J. Examination of a case of suspected McArdle's Syndrome by ^{31}P Nuclear magnetic resonance. N Eng J Med 1981; 304: 1338-1342.
55. Bretan PN, Vigneron DB, Hricak H, Collins GM, Price D, Tanagho EA, James TL. Human cadaveric renal viability assessed by ^{31}P MRS before transplantation. Fifth Annual Meeting SMRM 1986; 3: 1025-1026(ab).
56. Weimer MW, Adam WR. Magnetic resonance spectroscopy for evaluation of renal function. Semin Urol 1985; 3: 34-42.
57. Alger JR, Shulman RG. Metabolic applications of high-resolution ^{13}C nuclear magnetic resonance spectroscopy. Br Med Bull 1984; 40: 160-164.
58. Irving MG, Simpson SJ, Brooks WM, Holmes RS, Doddrell . Application of the reverse dept polarization-transfer pulse sequence to monitor in vitro and in vivo metabolism op ^{13}C-ethanol by ^{1}H-NMR spectroscopy.
Int J Bioch 1985; 17: 471-478.

Chapter VIII

SUMMARY OF RESULTS: MRI OF THE KIDNEY, CURRENT STATUS AND FUTURE DIRECTIONS

VIII.1 Introduction

The results of our pilot study (chapter II) were in agreement with early reports in literature concerning the application of MRI in renal disease. MRI appeared to be a very sensitive modality with excellent contrast resolution and tissue differentiation. However, at the same time it also appeared that MRI was not any more specific as to tissue characterization than the existing imaging modalities. In the summary of the results of our pilot study we made a positive statement concerning the value of MRI in the staging of renal cell carcinoma. On the other hand no prediction was made in 1984 regarding the value of MRI in the diagnosis of diffuse renal parenchymal disease.

VIII.2 Technical aspects

In chapter III and VII of this thesis a review of the literature up to December 1986 and a description of our own observations concerning the technical aspects of MRI are presented. The aspects of MR technology with regard to conventional spin echo (SE) pulse sequences are discussed.

On the one hand SE technique is very sensitive and can be optimized in order to show the relevant details of renal anatomy. On the other hand acquisition times are long resulting in motion artefacts. Respiratory movements of the diaphragm and organs in the upper abdomen, bowel peristalsis and pulsatile blood flow not only generate visible artefacts such as blurring and ghosting, but also lead to inaccurate measurements of T1 and T2 values. In addition, instrumental and biological factors not related to the pulse sequence used account for the erroneous and nonspecific quantitative data obtained with MRI. One has to be very cautious with the interpretation of qualitative information since the observed signal intensities may not relate to the actual tissue properties but can be falsely low or high as a result of technical imperfections and artefacts.

The main goal of current MR research is to improve the image quality and specificity of MRI. Image quality can be improved by the development of fast

imaging techniques, which allow a shortening of the acquisition time and better soft tissue contrast resolution. Up to now the use of paramagnetic contrast agents in MRI seems limited and comparable to that of iodinated contrast material in CT. At this stage spectroscopy appears to be one promising tool to increase the specificity of MRI regarding tissue characterization and could also provide significant insight in in-vivo metabolism. Monoclonal antibodies coupled to superparamagnetic contrast agents may become another important tool to improve specificity. Both qualitative and quantitative MRI of flow could eventually replace some of the current applications of X-ray angiography and provide relevant functional information on tissue perfusion.

VIII.3 Diffuse renal parenchymal disease

MRI showed to be very sensitive in detecting renal parenchymal changes. A number of histological changes such as fibrosis, vascular abnormalities and glomerular changes may account for a loss of cortex medulla demarcation (CMD). A decreased CMD may also be found in the absence of histological changes at light microscopy in case of nephrotic syndrome due to minimal change disease as a result of generalized edema. The MR findings proved not to be conclusive for a particular renal disease. Therefore, MRI can not replace renal biopsy. It is not to be expected that in the near future any of the new developments will change the impact of MRI in the diagnosis of diffuse renal disease.

VIII.4 Renal transplants

The statistical analysis of our study revealed that MRI is an acceptable investigation test for the differentiation between acute rejection and cyclosporin A nephrotoxicity. Distinction between acute rejection and other causes of allograft failure such as ATN or chronic rejection, appeared to be not possible. Theoretically, there are three options to improve the MR performance in the examination of transplant kidneys: improved and detailed qualitative and quantitative analysis of blood flow, water content and metabolism of the allograft. Flow-sensitive fast imaging pulse sequences and diffusion-perfusion imaging could provide useful information about vascular changes even at capillary level. Chemical shift imaging, diffusion imaging and Na^+ imaging are all suitable to image water changes within the kidney. These techniques could be useful to study edema and intra- and extracellular Na^+ shift. Spectroscopy and the use of monoclonal antibodies coupled with superparamagnetic contrast

agents are potential possibilities to directly study the rejection process and subsequent changes in cell metabolism. At present there is little or no place for MRI in the diagnosis of rejection or cyclosporin A nephrotoxicity on a routine basis. This is because of the high cost of MRI and the similar results that are currently obtained with much cheaper Doppler ultrasound.

VIII.5 Renal masses

The protocol on the diagnosis and staging of renal masses was not designed in such a way that a statistical conclusion could be made as to the sensitivity of MRI in the detection of renal masses. Nevertheless in our series of 40 patients with suspected renal masses, a small transitional cell carcinoma of the right renal pelvis was diagnosed with CT and remained undetected by MRI. Our study has shown that MRI is definitely not more specific as to tissue characterization than CT. In the staging of renal cell carcinoma CT was slightly superior to MRI because of better delineation of perinephric extension of a tumor. This is mainly caused by blurring of the MR image and subsequently unsharp tumor boundaries due to respiratory movement artefacts. The ability of MRI to detect enlarged lymph nodes and its inability to differentiate metastatic lymph node involvement from benign hyperplasia are comparable to CT. Fast imaging pulse sequences will reduce movement artefacts and may also increase the accuracy of MRI in the staging of renal cell carcinoma because of different soft tissue contrast resolution. It cannot be excluded that spectroscopy in the future will improve tissue characterization and allow further differentiation of primary and secondary renal masses.

VIII.6 Conclusion

MRI at 0.5 T using conventional pulse sequences has little to offer over existing, cheaper imaging modalities in the diagnosis of kidney disease. However, a number of new developments are on the horizon or already available. In the short term fast imaging techniques will drastically increase patient throughput and improve image quality. The currently available fast imaging techniques are only effective at high magnetic field strength. The need for higher magnetic field strength also applies to spectroscopy. Spectroscopy is still in its infancy, and a large number of technical problems will have to be solved. The development and application of superparamagnetic contrast agents coupled to monoclonal antibodies has just started. Much more investments and research on improved methods of tissue characterization and functional studies are needed

before a definite statement can be made as to the eventual role of MRI in the diagnosis of diseases of the kidney and the upper abdomen in general. It will take many more years, possibly more than a decade, before the full potential of NMR will have been exploited.

Chapter IX

SUMMARY

This thesis reflects our experience with Magnetic Resonance Imaging (MRI) in the diagnosis of kidney disease. Initial results were obtained on a 0.15 T resistive and a 0.5 T superconducting prototype MR scanner (Philips, Best, the Netherlands).

Further clinical trials on the application of MRI in the diagnosis of kidney disease were performed at the University Hospital Leiden, The Netherlands, with a 0.5 T superconducting MR scanner (Philips, Gyroscan S5). A protocol on MRI of diffuse parenchymal disease was carried out in cooperation with the Departments of Radiology and Nephrology, Free University Hospital Amsterdam, The Netherlands (Technicare, 0.6 T Teslacon).

CHAPTER I The historical aspects of NMR are reviewed. The objective of this study is defined as:
'to determine the value of MRI in:
1. the diagnosis of diffuse parenchymal renal disease;
2. the diagnosis and staging of kidney tumors;
3. the evaluation of transplanted kidneys'.

CHAPTER II This pilot study describes our initial experience with MRI of the kidney. Compared to CT a superior contrast resolution of MRI was noted. However, MRI did not appear to be more specific as to tissue characterization. The need for prospective studies in order to assess the value of MRI in the diagnosis of renal disease was stressed.

CHAPTER III The objective of this chapter is to put into perspective the interactions between tissues, instrumental MR parameters and the diagnostic information obtained with MRI. Image quality and pulse sequence optimization are discussed in general and in relation to MR imaging of the kidney. The abundance of artefacts in MRI studies of the upper abdomen as well as the limited value of quantitative T1 and T2 information obtained from in vivo MRI studies are stressed. It is demonstrated that artefacts may cause severe degradation of image quality and might occasionally lead to erroneous interpretation of parenchymal disease.

CHAPTER IV The purpose of this study was to investigate the correlations between MRI, and clinical and histologic findings in patients with diffuse renal parenchymal diseases, and to determine the possible application of MRI as an adjunct to renal biopsy. Ten healthy volunteers and 38 patients with acute or chronic renal failure were studied at 2 different institutions with 2 different (0.5T and 0.6T) MR scanners applying a T1 weighted spin echo pulse sequence. Patients were classified into 3 categories according to MRI findings of a normal cortex-medulla demarcation (CMD; group 1), decreased CMD (group 2) or absent CMD (group 3). Patients with nephrotic syndrome due to minimal change disease were not found in group 3. Although an abnormal CMD is highly indicative of the presence of diffuse renal disease, MRI will not replace renal biopsy since the MR findings are not conclusive for a particular renal disease.

However, MRI appears to be a useful technique to select those cases with nephrotic syndrome and selective proteinuria due to minimal change disease that can be treated with corticosteroids without previous biopsy, particularly children and adults with a contraindication for percutaneous renal biopsy, e.g. the existence of a solitary kidney. Further experience in a larger group of patients with nephrotic syndrome and selective proteinuria is needed before definite statements can be made. Generalized edema, also present in the kidneys of patients with minimal change disease, is at present difficult to assess and may disturb the correlation between a normal CMD and the absence of mild or severe histological changes.

CHAPTER V Purpose of this prospective study was to compare the accuracy of MRI and CT in the diagnosis and staging of renal masses. MRI was performed with a 0.5T superconducting MR scanner using conventional T1 and T2 weighted spin echo pulse sequences. The results of MRI and CT were compared in thirty one patients with a renal mass. Comparable information was obtained by MRI and CT in the diagnosis of benign tumors. One transitional carcinoma was not shown by MRI. CT appeared to be slightly more accurate in the determination of perinephric extension (Stage I v.s. Stage II). Similar results were obtained in Stage III and Stage IV tu-

mors. MRI and CT showed the same limitations which may result in inaccurate staging or renal cell carcinoma: the assessment of tumor extension into the intrarenal vein, the differentiation between lymphadenopathy due to reactive hyperplasia and metastatic involvement and the differentiation between tumor extension into adjacent organs and adhesions without tumor spread beyond the renal capsule. It is concluded that CT remains the method of choice in the diagnosis and staging of renal masses as long as no substantial improvements in MRI performance have been achieved.

CHAPTER VI Purpose of this study was to determine the use of MRI in the differentiation between acute rejection and cyclosporin-A (CsA) nephrotoxicity in renal transplant kidneys. Fifty six MR examinations in 45 patients were prospectively and independently evaluated by 2 radiologists (O1 and O2). MRI was performed with a 0.5T superconducting MR scanner (Gyroscan S5, Philips) applying both T1 and T2 weighted pulse sequences. Biopsies were performed in 22 cases and histology was reviewed. Fifteen normal grafts and 41 cases of allograft dysfunction due to CsA nephrotoxicity, acute rejection, chronic rejection or ATN were studied. Cortex-medulla demarcation (CMD) proved to be a sensitive, but non specific indicator of parenchymal disease. The MR appearance of acute rejection may be very similar to that of the combination of acute rejection and CsA nephrotoxicity, chronic rejection or ATN. However, differentiation between acute rejection and CsA nephrotoxicity was possible according to the following statistical data(O1-O2): sensitivity 97%-93%, specificity 80%-95%, positive predictive value 88-96%, negative predictive value 94%-90%, accuracy 90%-94%.

CHAPTER VII In terms of providing clinically relevant additional or unique information in the diagnosis of kidney disease, MRI at 0.5 T using conventional spin echo pulse sequences has little to offer over existing, less expensive modalities. Given the current limitations of conventional MRI in the diagnosis of renal disease, new and future developments are discussed which most likely will improve MRI performance. In the short term fast imaging techniques might dramatically

change the impact of MRI in the study of the upper abdomen in general. In the longer term, spectroscopy appears to be a promising technique to improve the specificity of MRI. However, it may take more than a decade from now before the full potential of NMR will have been exploited.

Chapter IX

SAMENVATTING

In dit proefschrift worden onze ervaringen met Magnetic Resonance Imaging (MRI) bij de diagnostiek van nierziekten beschreven. De eerste resultaten werden verkregen met behulp van een prototype 0.14 T en 0.5 T MR scanner, uitgerust met respectievelijk een weerstands en supergeleidende magneet (Philips, Best).

Verder klinische toepassingen van MRI bij de diagnostiek van nierziekten werden onderzocht in het Academisch Ziekenhuis Leiden met behulp van een 0.5 T supergeleidende MR scanner (Philips, Gyroscan S5). Het protocol voor MRI van diffuse nierafwijkingen werd uitgevoerd in samenwerking met de afdelingen Radiodiagnostiek en Nierziekten, Academisch Ziekenhuis Vrije Universiteit, Amsterdam (Technicare, 0.6 T Teslacon).

Hoofdstuk I Historisch overzicht van NMR.
Het doel van het onderzoek wordt als volgt gedefinieerd:
'het bepalen van de waarde van MRI bij:
1. de diagnostiek van diffuse parenchymateuze nierafwijkingen;
2. de diagnostiek en stagering van niertumoren;
3. het onderzoek van de getransplanteerde nier'.

Hoofdstuk II Deze pilot studie beschrijft onze eerste ervaringen met MRI van de nier. Het contrast oplossend vermogen van MRI bleek aanmerkelijk beter dan dat van CT. Echter de specificiteit van MRI, het vermogen om onderscheid te maken tussen weefsels op basis van histologische samenstelling, scheen niet wezenlijk te verschillen van die van CT. Dit onderzoek leidde tot het opstellen van een aantal protocollen voor prospectief onderzoek om de waarde van MRI bij de diagnostiek van nierafwijkingen te kunnen bepalen.

Hoofdstuk III Doel van dit overzicht is de interactie tussen MR eigenschappen van weefsels en opnametechniek met behulp van MRI, alsmede de hieruit voortkomende diagnostische informatie

met elkaar in verband te brengen. De factoren welke van invloed zijn op de beeldkwaliteit en het optimaliseren van puls sequenties worden in het algemeen, en in relatie tot het MR onderzoek van de nier in het bijzonder, beschreven. Gewezen wordt op de veelvuldige artefacten die kunnen optreden bij het MRI onderzoek van de bovenbuik, alsmede op de betrekkelijke waarde van gekwantificeerde in vivo T1 en T2 bepalingen. Aangetoond wordt dat artefacten de beeldkwaliteit in ernstige mate nadelig kunnen beïnvloeden en zelfs tot foutieve beoordeling van diffuse parenchymateuze orgaanafwijkingen kunnen leiden.

Hoofdstuk IV Dit onderzoek beschrijft de relatie tussen MRI en de klinische en histologische bevindingen bij patiënten met diffuse parenchymateuze nieraandoeningen en de mogelijke toepassingen van MRI als methode naast de nierbiopsie. Tien gezonde vrijwilligers en 38 patiënten met acute of chronische nierinsufficiëntie werden onderzocht met behulp van 2 verschillende MR scanners (0.5 T en 0.6 T) en T1 gedomineerde puls sequenties. De patiënten werden onderverdeeld in 3 groepen overeenkomstig de MR bevindingen van een normaal schorsmerg onderscheid (CMD; groep 1), afgenomen CMD (groep 2) of afwezig CMD (groep 3). Patiënten met nefrotisch syndroom op basis van 'minimal change disease' werden niet aangetroffen in groep 3. Hoewel een abnormale CMD een sterke aanwijzing blijkt te vormen voor de aanwezigheid van diffuse nierafwijkingen, kan MRI de nierbiopsie niet vervangen aangezien de MR bevindingen niet specifiek zijn voor een bepaalde nieraandoening. Echter, MRI zou van nut kunnen zijn om die patiënten met nefrotisch syndroom en selectieve proteinurie op basis van minimal change disease te selecteren, die in aanmerking komen voor een behandeling met corticosteroïden zonder voorafgaande nierbiopsie. Met name kan gedacht worden aan kinderen en volwassen patiënten bij wie een contraïndicatie bestaat voor percutane nierbiopsie zoals het (congenitaal) ontbreken van een nier. Deze laatste voorzichtige conclusie dient echter in verdere studies getoetst te worden aan de resultaten van MR onderzoek bij een grotere groep patiënten met 'nefrotisch syndroom en selectieve proteinurie'.

Gegeneraliseerd oedeem, ook aanwezig in de nieren bij patiënten met minimal change disease, is een op dit moment moeilijk te objectiveren parameter, welke de correlatie tussen een normaal CMD en afwezigheid van matige of ernstige histologische veranderingen kan verstoren.

Hoofdstuk V De betrouwbaarheid van MRI en CT bij de diagnostiek en stagering van niertumoren werd in een vergelijkende prospectieve studie onderzocht. MRI werd uitgevoerd met behulp van T1 en T2 gedomineerde spin echo puls sequenties. De resultaten van MRI en CT werden vergeleken bij 31 patiënten met een niertumor. Vergelijkbare informatie werd verkregen bij MRI en CT ten aanzien van de diagnostiek van goedaardige tumoren. Een overgangsepitheel carcinoom werd niet gediagnostiseerd met behulp van MRI. CT bleek in geringe mate betrouwbaarder te zijn dan MRI bij het vaststellen van tumoruitbreiding buiten het nierkapsel (stadium I v.s. stadium II). Vergelijkbare resultaten werden verkregen bij stadium III en IV tumoren.
Dezelfde beperkingen bleken te gelden voor MRI en CT t.a.v. een juiste stagering van het niercelcarcinoom: het vaststellen van tumoruitbreiding in de vena renalis, het onderscheid tussen lymphkliervergroting als gevolg van reactieve hyperplasie en metastatische activiteit en het onderscheid tussen tumordoorgroei in omliggende structuren en verkleving zonder tumordoorgroei buiten het nierkapsel. De conclusie van het onderzoek is dat CT beschouwd dient te blijven als het onderzoek van keuze bij de diagnostiek en stagering van niertumoren zolang er geen aanzienlijke verbeteringen in MRI techniek en resultaten zijn gerealiseerd.

Hoofdstuk VI De waarde van MRI bij de differentiatie van acute rejectie en cyclosporine-A (CsA) nefrotoxiciteit in de transplantatie nier wordt beschreven aan de hand van 56 MR onderzoeken bij 45 patiënten welke prospectief en onafhankelijk van elkaar werden beoordeeld door 2 radiologen (O1 en O2). MRI werd uitgevoerd met behulp van zowel T1 als T2 gedomineerde puls sequenties. Bij 22 patiënten werd een biopsie verricht en de histologische bevindingen werden opnieuw beoordeeld en gecorreleerd aan MRI. Vijftien normale getransplanteerde nieren en 41 gevallen van verminderde nierfunctie op basis van

CsA nefrotoxiciteit, acute rejectie, chronische rejectie of acute tubulus necrose (ATN) werden onderzocht.
Schors-merg onderscheid (CMD) bleek een gevoelige, maar niet specifieke graadmeter te zijn voor parenchymateuze veranderingen. Het MR beeld van de acute rejectie kon niet onderscheiden worden van dat van de combinatie van acute rejectie en CsA nefrotoxiciteit, chronische rejectie of ATN.
Differentiatie tussen acute rejectie en CsA nefrotoxiciteit was echter mogelijk overeenkomstig de volgende statische gegevens (01-02): sensitiviteit (97%-93%), specificiteit (80%-95%), positief voorspellende waarde (88%-96%), negatief voorspellende waarde (94%-90%), betrouwbaarheid (accuracy)(90%-94%).

Hoofdstuk VII MRI biedt bij een veldsterkte van 0.5 T en toepassing van conventionele spin echo puls sequenties weinig voordelen boven bestaande, goedkopere methoden wat betreft het verschaffen van klinisch relevante, aanvullende of nieuwe informatie bij de diagnostiek van nierafwijkingen. Gegeven de huidige beperkingen van conventionele MRI worden nieuwe en toekomstige ontwikkelingen belicht welke naar alle waarschijnlijkheid uiteindelijk zullen leiden tot aanzienlijke verbeteringen in de informatie die met behulp van NMR in algemene zin verkregen kan worden. Op korte termijn zullen nieuwe, snelle opnametechnieken de toepassingsmogelijkheden van MRI in de bovenbuik kunnen verbeteren. Op langere termijn is spectroscopie een interessante mogelijkheid om de specificiteit van MRI te verhogen. Het zal echter nog vele jaren, mogelijk een decennium, van intensief onderzoek vergen voor alle mogelijkheden van NMR ten volle onderzocht en bekend zijn.